Politecnico di Milano
School of civil, environmental and land management engineering

Graduation project

Designing an experimental test on a reinforced concrete frame with polystyrene infill

Presented by:

Cristian Sotela Sobrado

Supervisor:

Prof. Ing. Liberato Ferrara

Italy September, 2016

ABSTRACT

Frame structures are one of the most common type of structural schemes currently used to resist both gravitational and lateral loading. Façade walls are, in many cases, not needed for the lateral resistance, and hence not detailed accordingly. It is not strange to encounter frame structures with infill walls (typically infilled with unreinforced masonry) which have been conceived by the designer as just frames with added weight. This topic has been widely studied in the case of masonry, and it has been concluded that, in many cases, it leads to non-conservative results, due to the fact that the masonry infill will unavoidably tend to stiffen up the structure if no special detailing is carried out. An interesting new option to use as infill has been developed, which consists of polystyrene foam. This product works as insulation, with only a fraction of the weight of masonry, making it ideal to use as infill in façade walls. As any new product, its structural behavior must be properly studied and tested, in order to develop design guidelines that comply with design codes and pre-defined limit states. Masonry infilled frames were studied as a starting point, and the methods of analysis were suitably adopted for polystyrene infilled frames. A simplified analytical method was carried out for one infilled frame. Then, a finite element analysis was carried out for the same infilled frame, by means of both a static non-linear analysis (pushover analysis) and an elastic analysis. Results were then compared amongst each other in order to quantify the difference between all approaches. Results show that no significant error is made when assuming the polystyrene infill as a non-structural element, regarding low damage limit states. However, there is a significant gain of strength of the structure when considering post-elastic behavior. The results obtained during this research are meant to be compared with the experimental values obtained during the testing of the specimen.

ACKNOWLEDGEMENTS

The author wishes to thank in particular all those people whose friendly assistance and wise guidance supported him throughout the duration of this research project. Thanks to the Professors of the Department of Structural Engineering at Politecnico di Milano. Thanks particularly to Professor Ing. Liberato Ferrara, for the proposition of the topic, and supervision during the research project. The author would also like to thank Marko Djuranovic, who assisted in the elaboration of this document, and will continue to carry out the testing phase. The author would like to thank his family for an unconditional support throughout this challenge. Also, special thanks to Juan Carlos Sotela, who has been a role model as a structural engineer and father. Finally, the author would like to thank his wife, Rocio Ulate, for always supporting him during this new experience, and the many more yet to come.

TABLE OF CONTENTS

LIST OF FIGURES

LIST OF TABLES

1 INTRODUCTION

In current structural engineering practice, one of the most used types of structural systems is frame system with infill walls. Traditionally, masonry was present as an infill material and was regarded as the best choice for it. Nowadays, since optimization of costs and quality is a major concern, new materials are being invented and new ways of using them are being patented constantly.

Trying to overcome some of the drawbacks of masonry (large weight when used in big amounts, and influence on the stiffness of the whole structure) which are giving problems to engineers when designing structures, especially for earthquake resistance, this research will assess the use of polystyrene panels covered with a thin mortar layer interconnected with glass fibers as the infill material. Polystyrene was selected knowing that it has low weight, would not alter the stiffness in great amount and can act as an insulation by itself.

1.1 OBJECTIVE AND SCOPE

In this thesis an investigation will be performed on how reinforced concrete (RC) frames behave when polystyrene panels are used as the infill. In order to achieve this, finite element modeling of several different models were carried out, also with the aim of designing a laboratory test on a full scale mockup.

This project intends to demonstrate what are the effects of polystyrene panels on post elastic behavior of an RC frame, comparing those effects with the ones coming from a masonry infill, and formulating recommendations for the design of this type of frames.

1.2 IMPORTANCE AND SIGNIFICANCE OF THIS STUDY

As mentioned before, masonry used as infill material has some drawbacks that affect the whole structure. Polystyrene panels can avoid some of these inconveniences, but with this new way of using polystyrene, a lot of uncertainties arise. These unknowns will be explained in order to have a clear understanding of the response of a structure when using polystyrene as infill in everyday constructions. Several possible failure modes may occur and each one of them must be properly investigated, in order to determine what they are dependent on.

1.3 POSSIBLE CONNECTION BETWEEN MASONRY AND POLYSTYRENE INFILL

Since not many (if any) studies like this have been performed, a familiar starting point has to be determined. In this case, a logical starting point is to study masonry infills, for which a lot of experiments have been done and countless papers have been written.

This analogy between polystyrene and masonry can be justified by the fact that both of the materials can be considered to have brittle behavior compared to a RC frame's one. For the masonry infill, several "common" failure modes have been determined, and those modes will be adopted for polystyrene also. Although, it cannot be said that these modes are the same for both cases, it is a reasonable starting point. Also, some analytical methods exist which were used when more refined methods are unavailable. These solutions will have to be calibrated to suit the case of using polystyrene instead of masonry.

2 REVIEW OF LITERATURE

In the following chapter some of the key aspects and results from previous studies on masonry-infilled RC frames are presented. Particular attention is given to single story – single bay frames. Different cases are considered regarding infill reinforcement, which influences the behavior, modeling and expected failure modes.

2.1 INTRODUCTION

Masonry infilled frames represent a common construction technique employed in buildings all over the world. However, it is a common mistake to consider these infills as "non-structural components", and consider just the bare frame for the analysis of the structural response. Although the masonry is not detailed accordingly to act as a shear wall, if it's in contact with the frame, it will tend to prevent the RC frame to deform as it would normally do if there was no infill present. For this reason, the infill will have a non-negligible stiffness (and energy dissipation contribution) under the dynamic response of the structure, especially under low intensity excitations. Maximum displacements and energy dissipation demands for the frame elements are also expected to reduce. (Decanni, et al., 2004)

If the structure is modeled as a bare frame, with "added mass" due to the "nonstructural infills", the fundamental period of the structure will be overestimated (the structure will be more flexible in the model), and thus, the seismic forces will be, in some cases, underestimated, resulting in different seismic response than the one anticipated by the designer. Needless to say, neglecting the infill rigidity is, in many cases, not a conservative approach and should be avoided. In general, according to (Decanni, et al., 2004), the overall response of the structure can be significantly improved by the presence of the infills, even after accounting for the added mass for the inertial loads. Different types of models have been developed to study the behavior of these structures, and the most typical failure modes have been outlined in several research papers.

Masonry is a much stiffer and stronger material than polystyrene, and therefore, it is expected for the two systems to behave differently. However, in the absence of any previous studies done specifically on polystyrene infilled frames, studying the behavior of masonry infilled frames gives a good starting point as to what to expect.

2.2 BARE FRAME BEHAVIOR

Reinforced concrete frame structures are a well-known type of lateral load resisting system, which has been studied thoroughly in the past. These types of structures are known

to have a very ductile behavior, with large hysteresis loops under cyclic loading (Figure 2.1), which means they are able to dissipate a great amount of energy. Another big advantage of frame structures is their great flexibility under seismic actions. Due to this feature, they usually have longer fundamental periods, and hence, reduced inertial loads. Figure 2.1 shows the expected plastic hinges that form on the structure (at top and bottom of columns and at the faces of the beam) under cyclic loading. The experimental results are usually in very good agreement with the numerical predictions for this type of structure, which can be estimated, e.g., by means of a non-linear cyclic analysis.

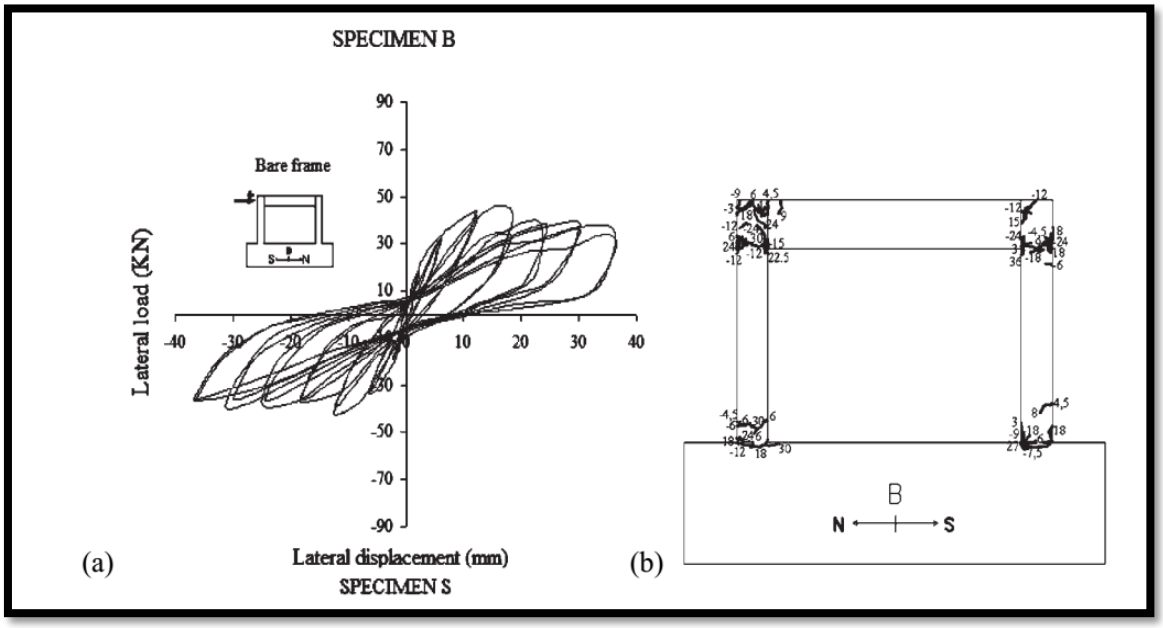

Figure 2.1. Bare frame behavior under cyclic loading **(Kakaletsis & Karayannis, 2008)**

2.2.1 Modeling

The bare frame model is fairly simple. Classical structural mechanics is sufficient to model a frame structure, considering Euler-Bernoulli frame elements for both beams and columns (neglecting shear deformation in the kinematic model).

Boundary conditions at the base of the columns should be suitably accounted for. This is one of the modelling approximations, namely, since in a real structure, only in a very few cases, an edge which is completely restrained (no rotation at all) can be achieved. The use of fully fixed restraints at element ends in structural models is always questionable. It is well known that for different rigidities of a connection, different distribution of internal forces in the structure will be obtained. This issue can be overcome by careful examination of the structure and proper calibration of the model.

Both steel and concrete material properties should be adequately accounted for. Steel distribution in the RC elements needs to be defined, in order to plot a moment-curvature diagram, due to the non-linear nature of the problem.

2.2.2 Failure modes

The single frame depicted in Figure 2.1 is a 3 times statically indeterminate structure. Therefore, a total of 4 plastic hinges are needed in order to obtain the collapse mechanism. Since frame structures are usually slender, their failure is governed by a flexural behavior. These plastic hinges are expected to form at the portions of the members where the highest moment concentrations are located (top and bottom of columns and at beam ends), as seen from the figure.

2.3 RC FRAME WITH UNREINFORCED MASONRY INFILL

Some masonry infill panels have absolutely no reinforcement, since they are conceived as "non-structural elements" by the designer. The behavior of panels that have no reinforcement differs greatly from the one of slightly reinforced panels, as it will be discussed later.

2.3.1 Modeling

Two types of models can be differentiated for simulating the in-plane behavior of infilled RC frames subjected to a lateral force:

- Micro-models: Sophisticated analysis such as Finite Element Method are used to model in detail the behavior of masonry infilled RC frames. Several types of elements need to be used (continuum elements, for the frame and infill, interphase elements between frame and infill, and sometimes even additional elements for the mortar joints). Usually, non-linear finite elements are needed to model the behavior appropriately. The data input, and also the computational time, are much more complex than those required when a macro model is employed.
- Macro-models: The simplest case is the so called "simplified model", which uses a single strut to model the masonry infill. This approach is suitable for global effects of the structural behavior (stiffness, period, drifts) but is not able to capture the failure modes of the individual frames or the infills. Variations to this approach are the so called "multi strut models", which are a more refined version of the latter one. Different layouts are illustrated in *Figure 2.2*. These models are used to describe the local behavior, and are able to predict the typical failure modes of the

infilled RC frame. Multi strut models are a popular way to proceed, and give acceptable results.

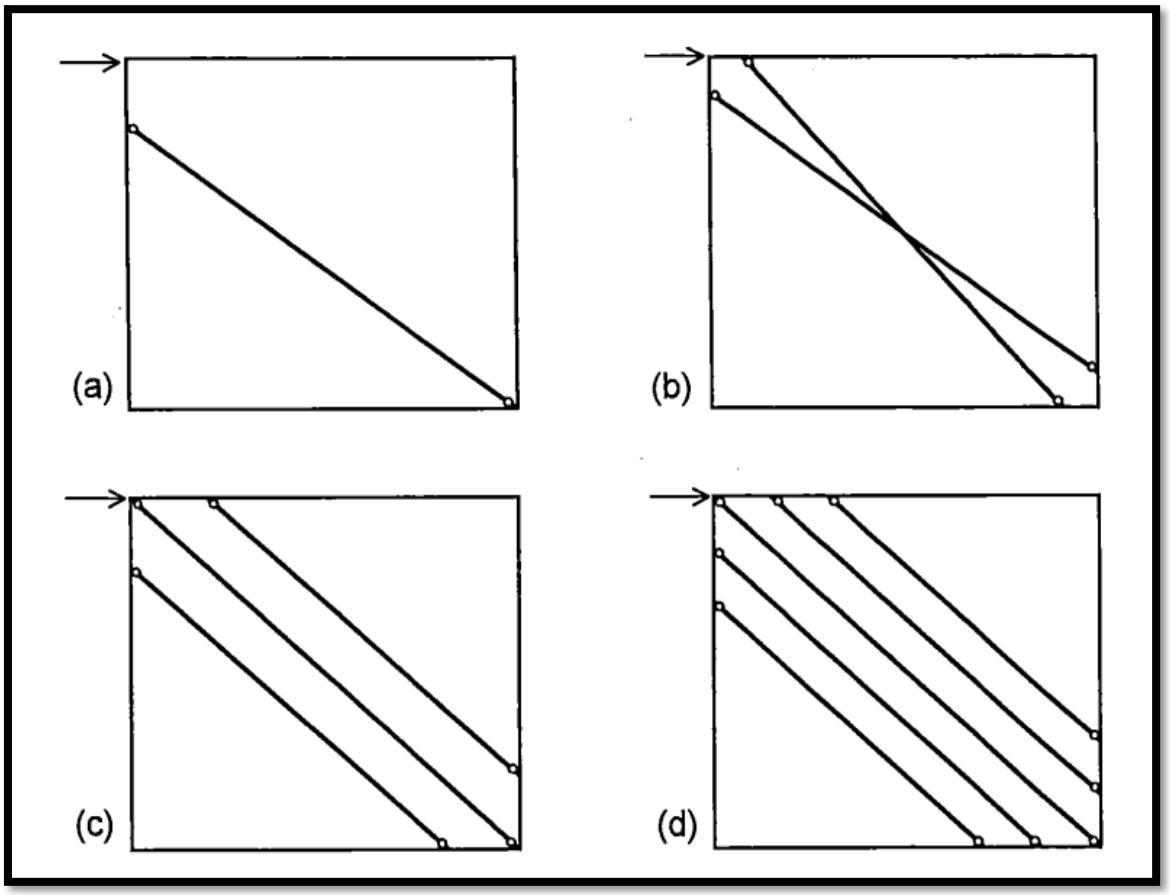

Figure 2.2. Macro models: Single strut (a) and multi strut (b), (c), (d) **(Crisafulli, 1997)**

Masonry is a material that works mainly under compression, and has a negligible tensile strength. For this reason, the panel separates from the frame at the tension areas. *Figure 2.3* shows a mechanism that occurs after the separation. So, many authors agree that a suitable model to approximate the effect of having a masonry infill is achieved by adding a compression strut to the bare frame structure, having the same thickness as the wall. A topic of interest is the width "w" of such strut which is the basic parameter for defining its axial stiffness. Several values and formulas can be found in the literature, typically depending on the compressive strength of masonry, and the relative stiffness between frame and infill. Usual values for "w" are shown below.

$$\frac{L}{4} \leq w \leq \frac{L}{3} \qquad \textbf{(2-1)}$$

Where:

- L = Length of compression strut
- w = width of compression strut

Figure 2.4 shows the variation of "w/L" ratio as a function of the relative stiffness between the frame and infill (λ_h), according to several researchers. Other characteristic properties for strut are considered equivalent to the masonry infill. The stress distribution along the masonry, before and after separation of the frame-infill has occurred, can be seen in Figure 2.5, from a Finite Element Analysis.

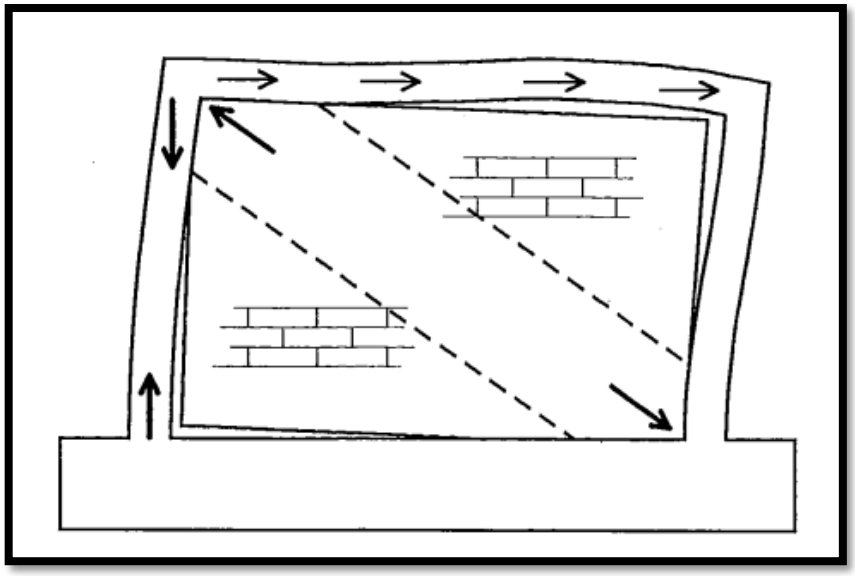

Figure 2.3. Equivalent truss mechanism for infilled frame structure **(Crisafulli, 1997)**

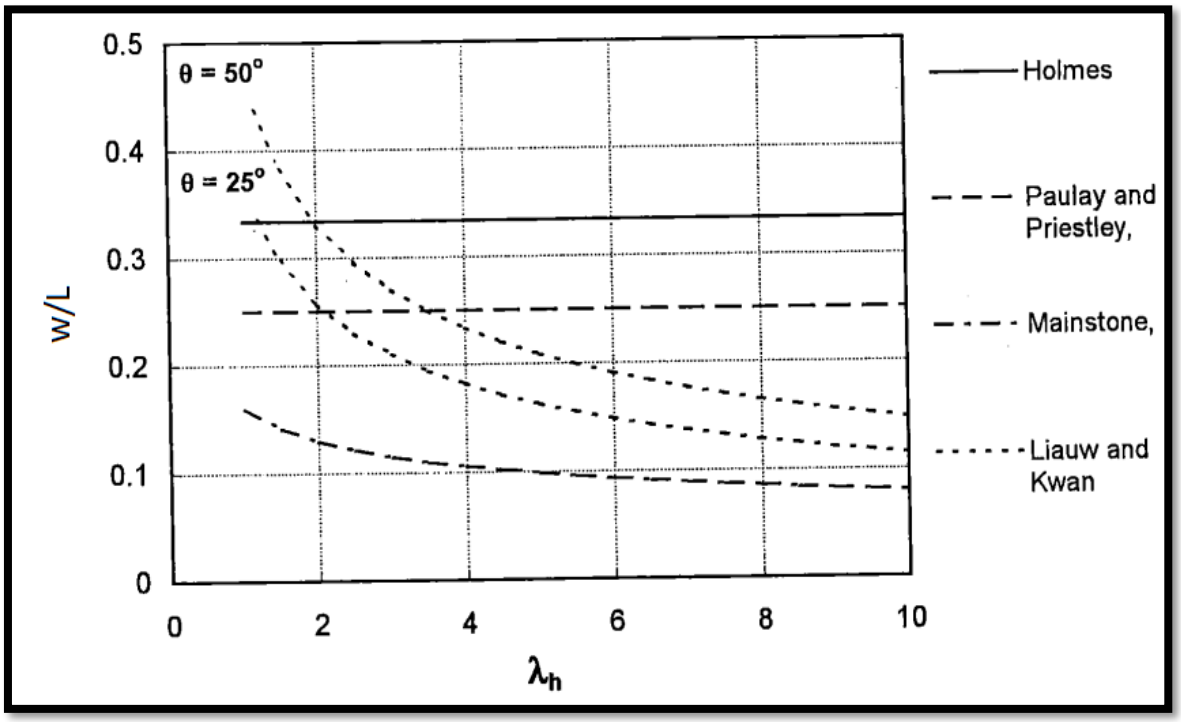

Figure 2.4. Variation of the w/L ratio as a function of λ_h **(Crisafulli, 1997)**

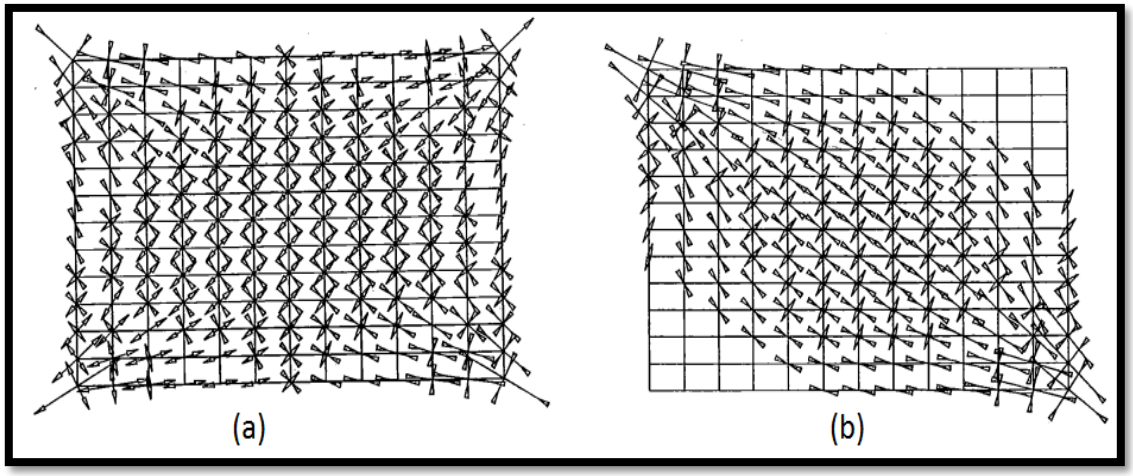

Figure 2.5. Stress distribution in masonry before separation (a) and after separation occurs (b) **(Crisafulli, 1997)**

2.3.2 Behavior of infilled RC frames under monotonic loading

Initially, under low stresses, the frame and masonry act together as a monolithic element, and behave elastically, similar to a cantilever wall. From Figure 2.5 (a) it can be observed that the stress concentrations occur at the corners, while the panel exhibits mainly shear stresses.

As the load increases, due to increase of stress in masonry panel, and incompatibility between the panel and the frame because of their different deformability properties, cracking occurs at the frame/panel interface, and the panel separates from the frame, except at the diagonally compressed corners. This results in a decrease of the structure stiffness (strength is not significantly affected), and an overload of compression stresses at the compressed corners, which experience a biaxial compression state, as depicted in Figure 2.6. Since only a limited portion of the frame is compressed at the corners, the idea of the equivalent compression strut was proposed by Polyakov in 1958, and later improved by several authors.

Internal action diagrams (bending moment, shear and axial force) can be obtained for the frame through a finite element analysis, or through a multi-strut model. Several multi-strut models have been proposed in the literature, depending on the expected type of failure. A simplified single strut model does not give realistic results for local analysis of the infilled frame, as mentioned before.

Results show that for normal infilled frames, after separation occurs, the maximum bending moments in the columns can be up to six times lesser than in the case of the bare frame (Crisafulli, 1997). However, the internal actions highly depend on the relative rigidity between the frame and the infill, as depicted in Figure 2.7 (b). It is interesting to note how

for the case of a very rigid frame (compared to the infill), the behavior tends to the one of the bare frame. In any case, the final behavior at large drifts (internal actions and global stiffness) always tends towards the one of the bare frame, as the infill panel will be completely cracked and its load carrying capacity will be quite low.

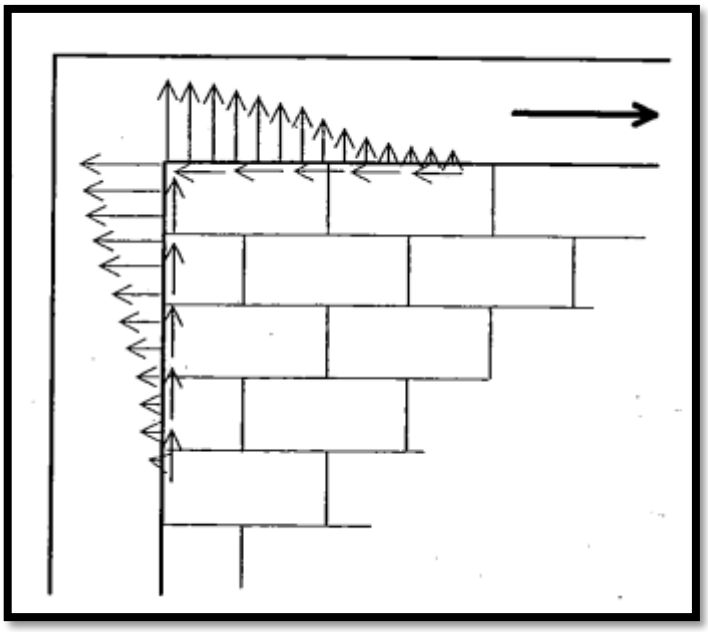

Figure 2.6. Normal and shear stresses acting on a loaded corner of the frame **(Crisafulli, 1997)**

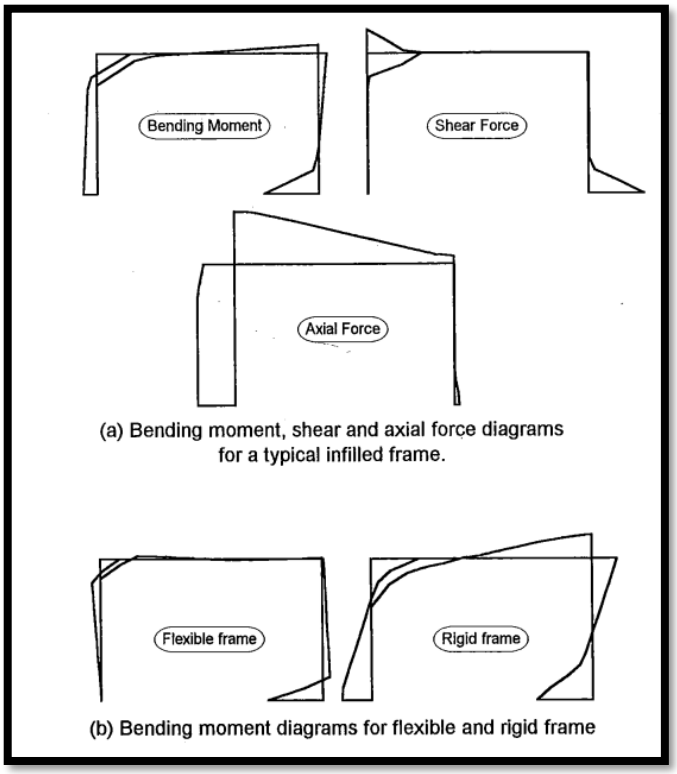

Figure 2.7. Typical bending moment, shear and axial forces diagrams obtained from and infilled RC frame, after separation occurs **(Crisafulli, 1997)**

For the case of non-integral infilled frames (when the infill is placed after casting the frame) the behavior is similar to the one described previously. However, some differences could arise due to unwanted gaps between frame and masonry (if no expansive mortar is used to prevent them). This results in a low initial stiffness, until the frame deforms enough to close the gaps between itself and the masonry panel. Then there is a significant increase of stiffness, as both members start to work together.

In general, four different stages can be distinguished during monotonic loading of masonry infilled RC frame structures, according to Crisafulli (1997):

1. During the initial stage the structure behaves as a monolithic cantilever wall until separation occurs.
2. Then the behavior is characterized by the composite interaction between the panel and the frame, although the materials remain mainly uncracked.
3. The induced state of stress into the panel produces different cracking patterns, with significant damage until the maximum lateral resistance is achieved.
4. Finally, the lateral strength decreases and the response is mainly controlled by the frame.

2.3.3 Failure modes

The failure type of infilled RC frames depends on several factors (relative rigidity between frame and infill, dimensions of the structure, mechanical properties of components, mortar joint thickness, frame reinforcing steel, vertical loads, amongst others). Several types of failure are defined conventionally, however, the real failure will generally be a combination of the failure modes described in this section. Failure can occur either in the masonry panel, or in the RC frame, and for each of these two different modes have been defined.

2.3.3.1 Failure in masonry panel

"*The failure of the masonry panel can develop by debonding of the mortar joints, cracking or crushing of the masonry units or a combination of these. The occurrence of the different types of failure depends on the material properties and the stress state induced in*

the panel"[1]. Figure 2.8 shows a diagram summarizing the different types of failure modes observed for the masonry infills.

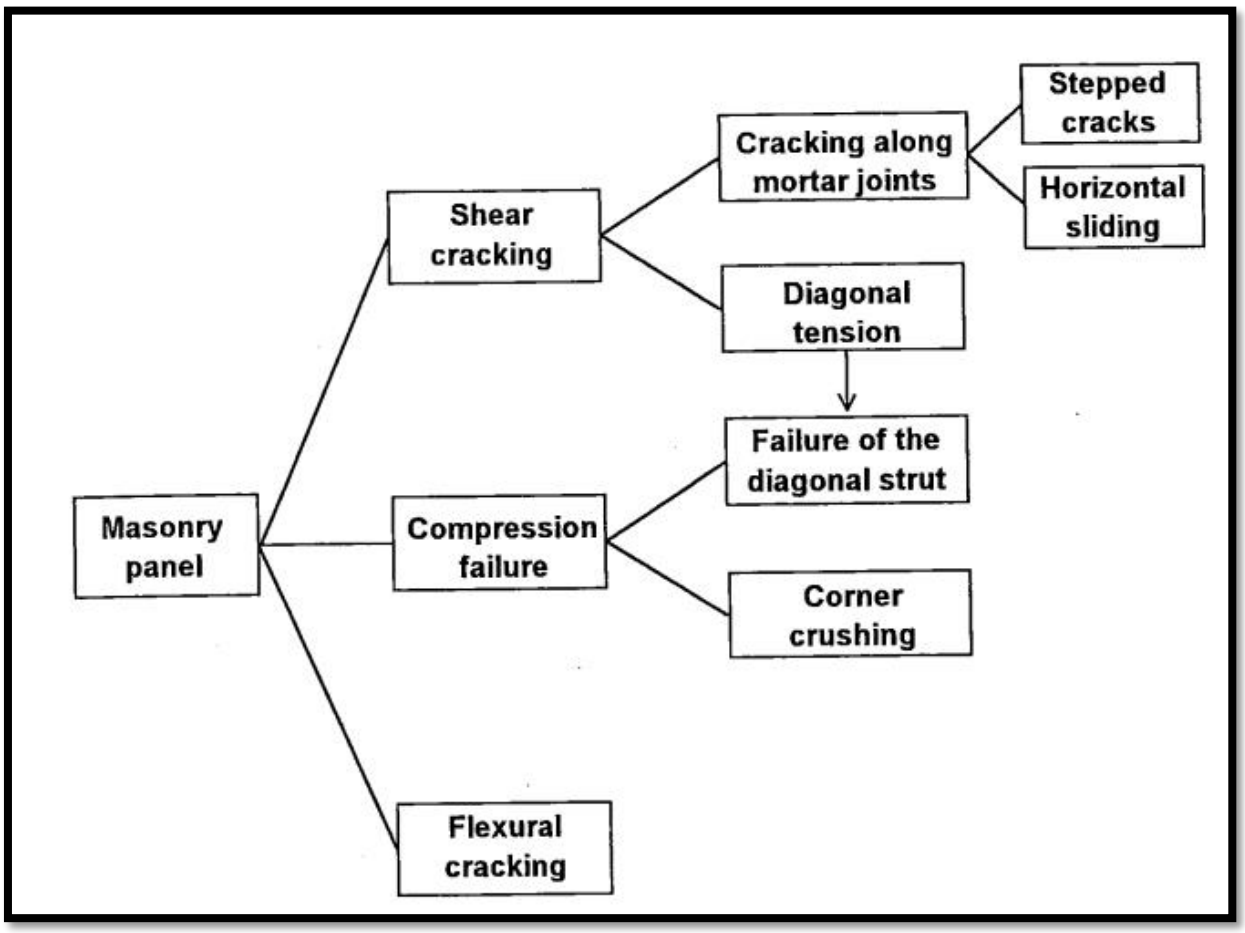

Figure 2.8. Modes of failure observed in masonry infills **(Crisafulli, 1997)**

- Shear Cracking

This is the most common type of failure according to experimental observations and affected panels in existing buildings. It mainly depends on the bond strength and friction coefficient of the mortar joints, tensile strength of masonry, and the relative values between normal and shear stresses. Depending on the stress ratio, the failure can be along the mortar joints, or cracks that cross the masonry units. The stress ratio can be directly related with the aspect ratio (height/length) of the infill. Cracks along the mortar joints could take place along a horizontal plane, or follow a stepped pattern, as observed in Figure 2.9. According to (Mehrabi & Shing, 2003), this is the most common type of failure for a relatively weak panel with respect to the surrounding frame. Also, cracking due to diagonal tension (Figure 2.11) has been defined in the literature, which occurs along the diagonal of

[1] (Crisafulli, 1997)

the infill panel, due to a biaxial tension-compression state, as seen in Figure 2.10. Generally, for high shear stresses (low aspect ratios), cracking along mortar joints is more common. However, when mortar joints are very strong, or the wall has medium to high aspect ratios, diagonal tension could be expected. Diagonal tension is regarded as a very dangerous type of failure, since after the formation of cracks along both diagonals, expulsion of the masonry units becomes imminent.

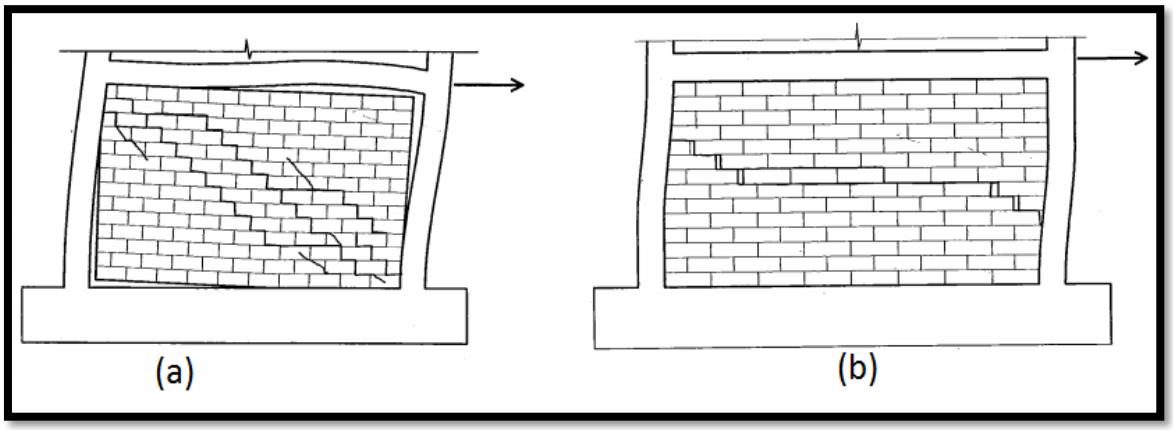

Figure 2.9. Typical failure modes for shear cracking. Stepped cracking pattern (a) or horizontal sliding (b) **(Crisafulli, 1997)**

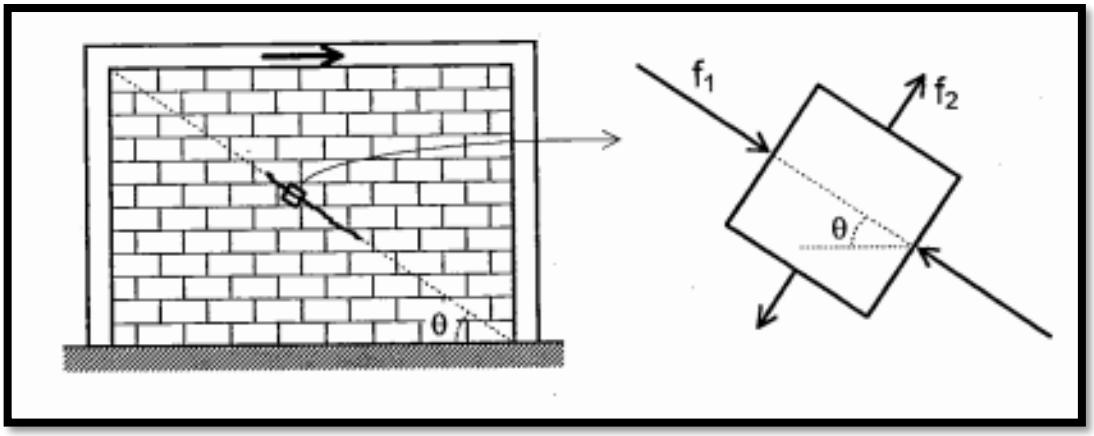

Figure 2.10. Biaxial tension – compression stress state in the infill panel. **(Crisafulli, 1997)**

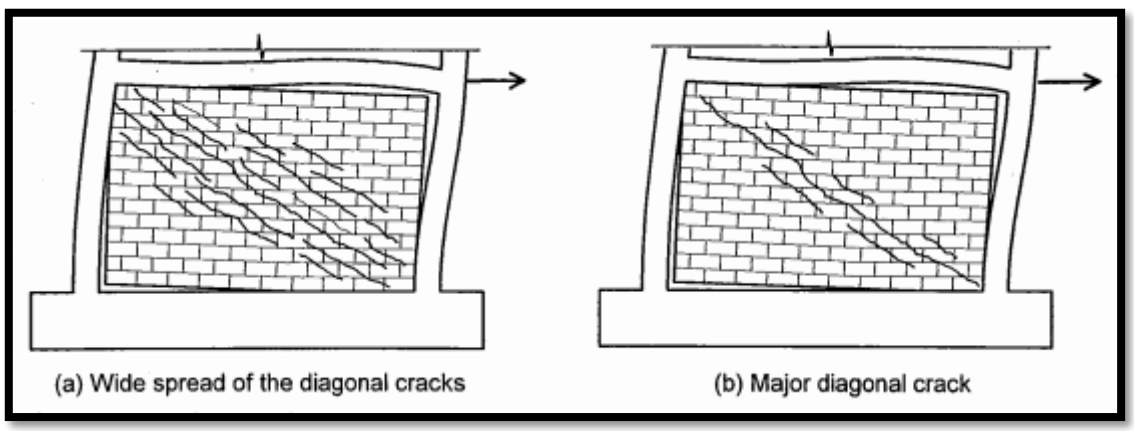

Figure 2.11. Cracking induced by diagonal tension. **(Crisafulli, 1997)**

- Compressive Failure

Two types of compressive failure have been observed in the masonry panels. The first one is the crushing of the loaded corners, where there is a biaxial compressive stress state (Figure 2.12). It could be expected to occur when the frame is very flexible, hence the contact length between frame and infill decreases, and stresses increase. The second mechanism is due to the compressive failure of the diagonal strut. After separation, as the lateral deformations increase, instability of the compressed strut is eventually reached.

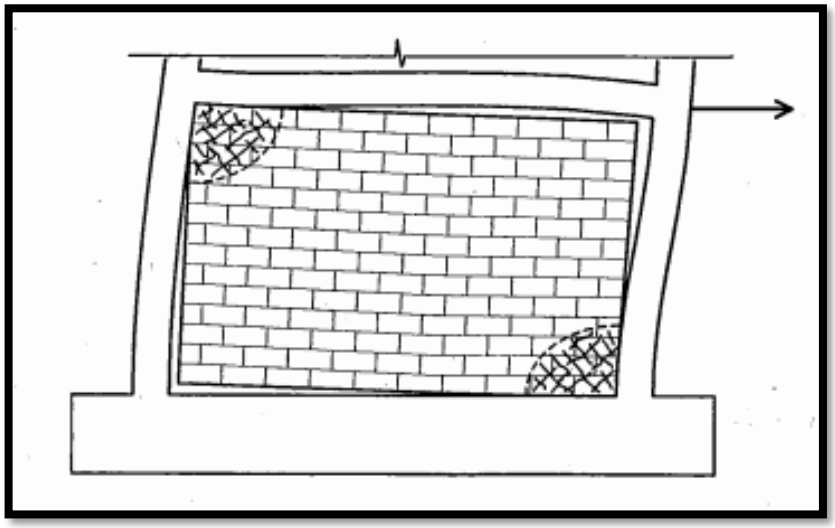

Figure 2.12. Crushing of the loaded corners. **(Crisafulli, 1997)**

- Flexural Cracking

This type of failure can be observed where flexure effects are predominant (as in multistory, slender infilled frames). Cracks develop on the tension side of the infilled frame, in the masonry infill. However, this type of failure is rarely seen, since separation of the frame-infill usually occurs before flexural cracking, and the horizontal actions are resisted through truss mechanism.

2.3.3.2 Failure in the RC frame

Different failure mechanisms have also been observed on the surrounding RC frame during horizontal actions. "*Damage in the frame members usually occurs from flexural plastic hinges, shear failure, yielding under axial forces, compression failure or a combination of these*"[2]. Similar to the previous section, Figure 2.13 shows the different failure modes for the RC frame, which are explained below.

[2] (Crisafulli, 1997)

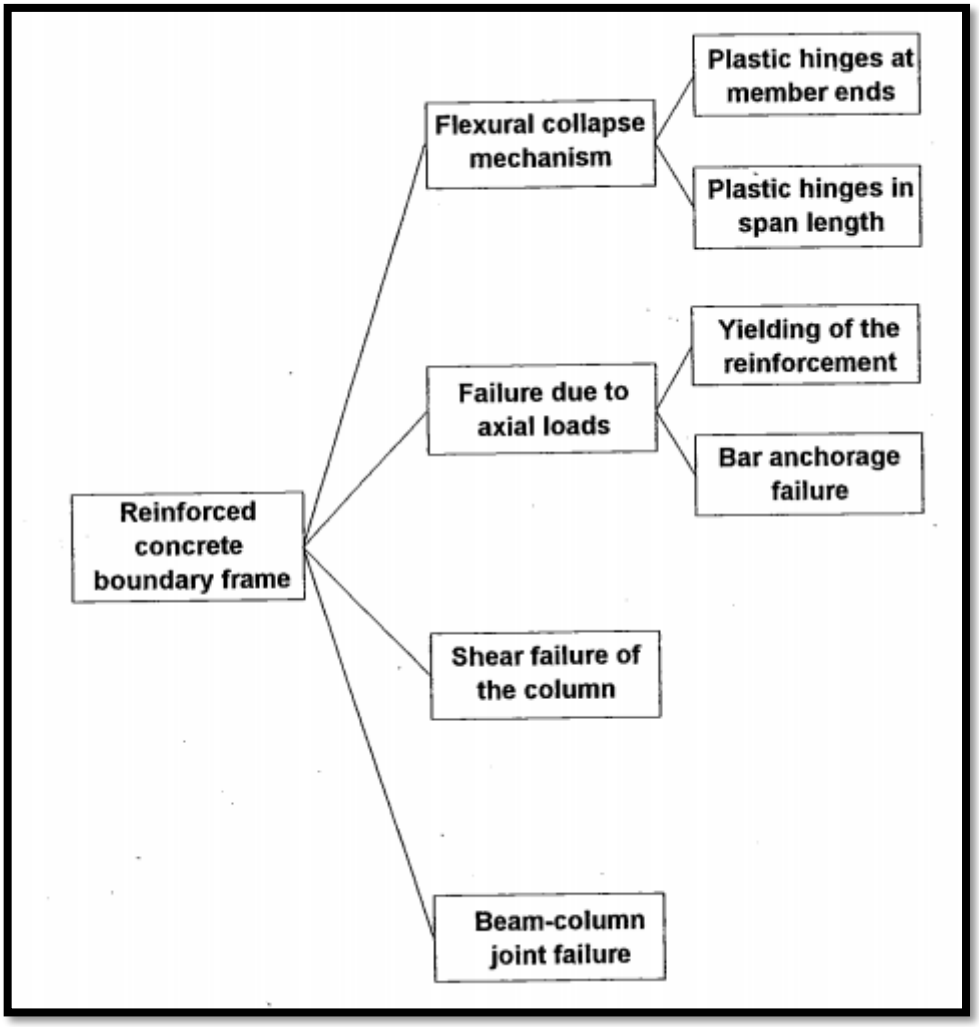

Figure 2.13. Modes of failure observed in RC boundary frames. **(Crisafulli, 1997)**

- Flexural Collapse Mechanism

This mechanism usually develops after the masonry panel has failed. It is characterized by the formation of plastic hinges at the column ends, where expected maximum bending moments occur. However, when sliding shear in the panel occurs, plastic hinges could form within the span of the column (Figure 2.14b), inducing an undesirable increase of shear forces.

- Failure Due to Axial Loads

Under lateral loading, columns work as a truss mechanism, under axial forces (tension and compression). After concrete cracks, because of its intrinsic low tensile strength, if the load is further increased, yielding in tension members can be reached. Two types of mechanisms of this nature have been observed. The first one is known as the "flexural failure", and can be observed in slender frames (high aspect ratios), generally multi story frames. Horizontal flexural cracks develop along the tension element because of the high plastic deformations of the longitudinal reinforcement (Figure 2.15a). Beams also tend to undergo some plastic

elongation, and hence, the interaction between the frame and infill can be significantly degraded or completely lost during this process. The other mechanism is the bar anchorage failure (Figure 2.15b), which can be avoided by providing proper development length for the longitudinal bars.

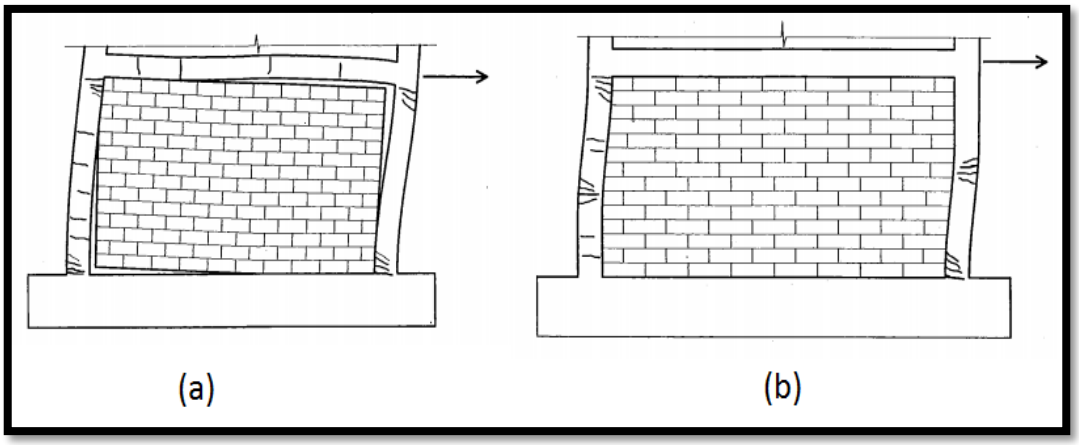

Figure 2.14. Flexural collapse mechanism with formation of plastic hinges at column ends (a) or at the column span length (b) **(Crisafulli, 1997)**

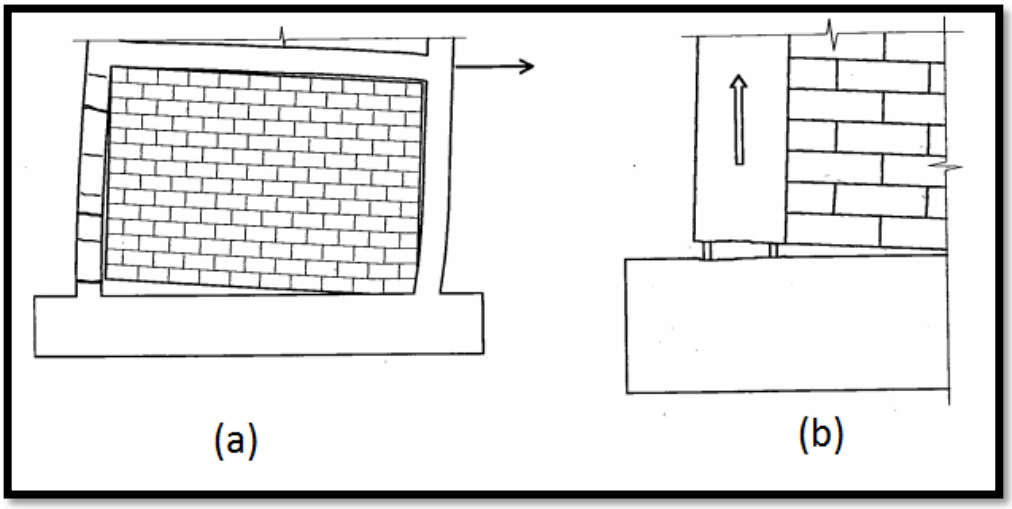

Figure 2.15. Tension failure of the column (a) and bar anchorage failure (b). **(Crisafulli, 1997)**

- Shear Failure of the Columns

As seen in Figure 2.6, there is a concentration of shear stresses at the loaded corners of the columns, along the contact length, due to the interaction with the infill at these regions. Shear resistance in the columns basically depends on transversal reinforcement, concrete strength and axial load. Although the compression column will have a higher shear resistance, it will also usually have the highest shear action. Figure 2.16 shows a typical shear failure taking place in column members.

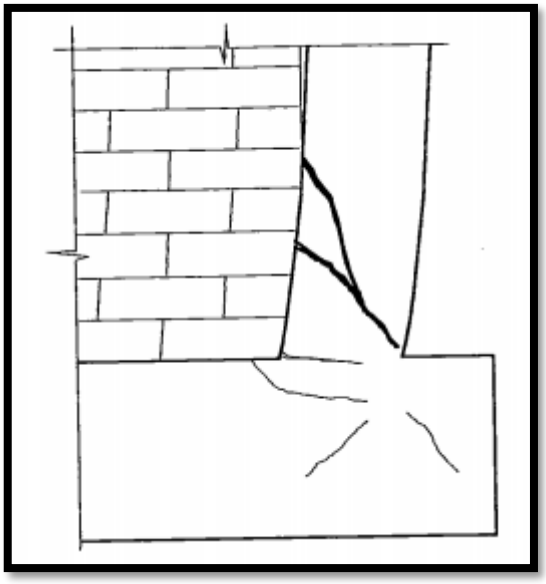

Figure 2.16. Shear failure of the column. **(Crisafulli, 1997)**

- Beam-Column Joint Failure

Concentration of normal and shear stresses develop close to the loaded corners (Figure 2.6), hence inducing large shear and bending moments. Failure of the joint is a highly unfavorable situation, since it decreases the contact length, and therefore decreases the effective strut width, which results in an increase of the stresses on the masonry. It also decreases the effectiveness of load transfer between the floor beam and the columns and infill. During this failure, a diagonal crack appears at the beam column joint (Figure 2.17).

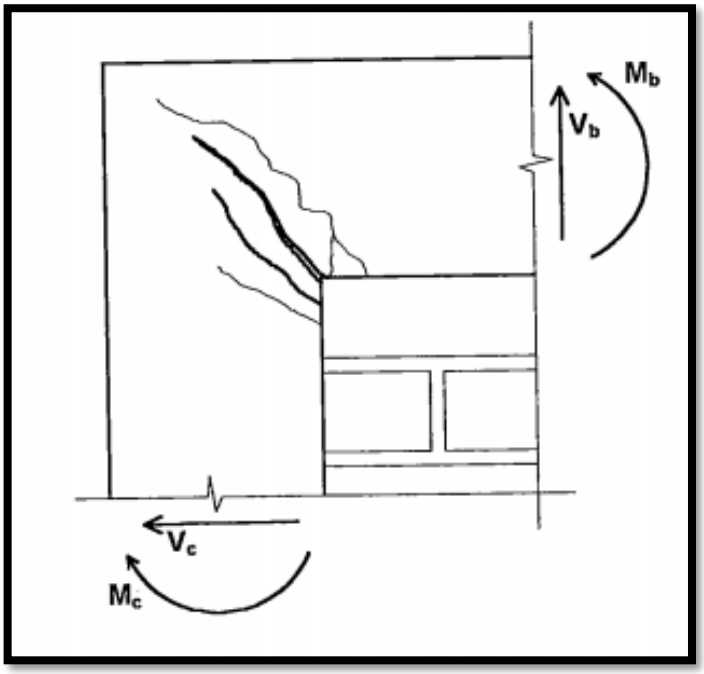

Figure 2.17. Beam-Column joint failure. **(Crisafulli, 1997)**

2.3.4 Analytical prediction of lateral resistance and stiffness

A simple analytical approach to quantify the lateral resistance of infilled frames without openings, in the absence of more refined experimental data, was proposed by (Mehrabi & Shing, 2003). From all the failure mechanisms previously described, this method chooses 5 of them as the most probable ones, as shown in Figure 2.18. For each failure mode, the lateral resistance is obtained by analytical equations developed by (Mehrabi, et al., 1994). Finally, the mechanism that results in the lowest lateral resistance value is considered to be the predominant failure mechanism, and hence is considered the lateral load resistance value. This method is briefly described below. It is interesting to point out that, from the research carried out for several masonry infilled RC frames, the most common type of failure mechanism observed in experimental tests for weak infills corresponds to mechanism 5, where large slips along the bed joints and plastic hinges in the columns govern. On the other hand, for strong infills, mechanism 2 is the most common one, which is governed by the diagonal/sliding shear failure of the infill and the shear failure of the windward column.

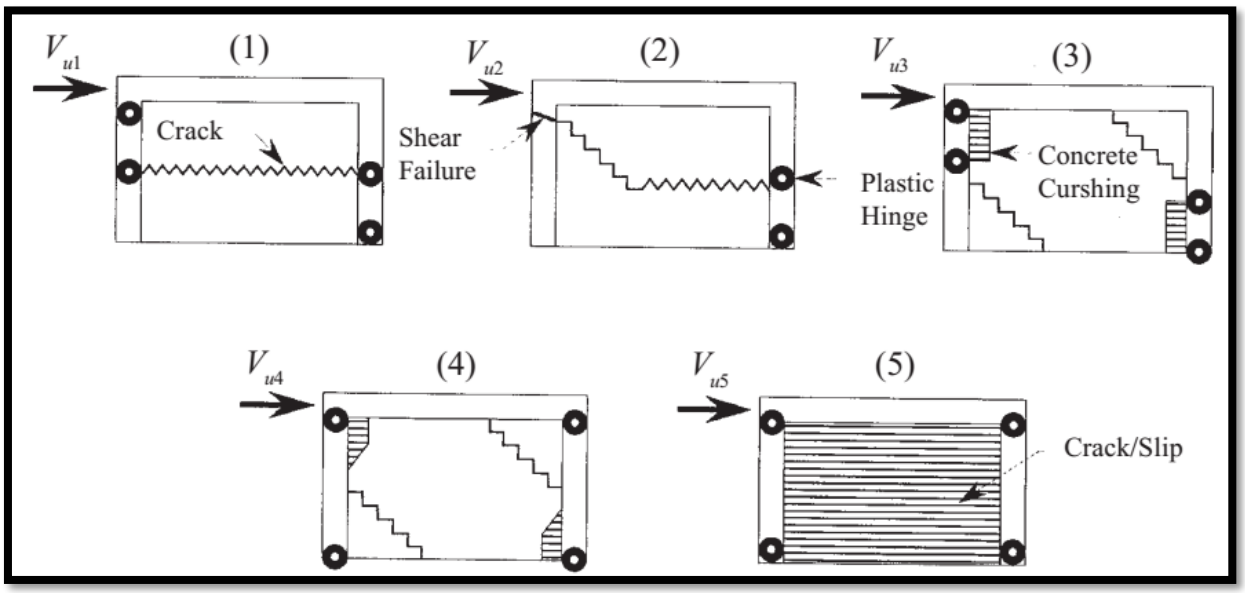

Figure 2.18. Selected failure mechanisms **(Mehrabi & Shing, 2003)**

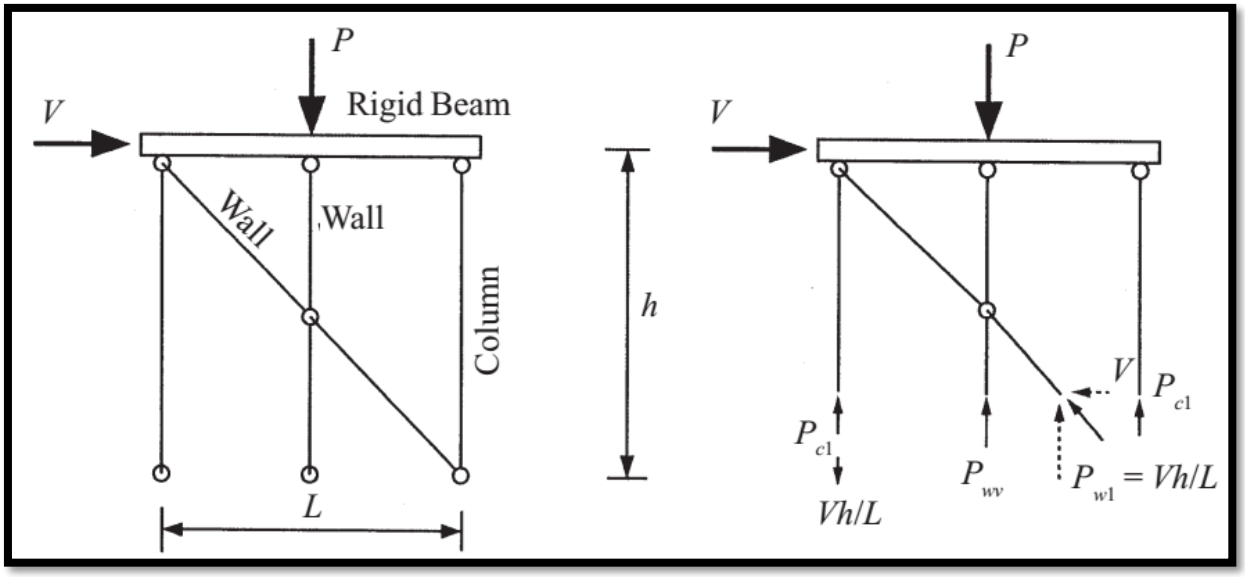

Figure 2.19. Vertical load distribution model **(Mehrabi & Shing, 2003)**

2.3.4.1 Residual shear strength of cracked wall

The cracking load is evaluated through the model proposed by (Fiorato, et al., 1970) shown in Figure 2.19. The beam is rigid and the wall is represented by a diagonal and a vertical strut, which are connected by a hinge. P is the total vertical load, and V the total lateral load. As observed in Figure 2.19, P_{cl} corresponds to the axial force in the columns, due to P, P_{wv} is the axial load in the vertical strut due to P, and P_{wl} is the vertical component of the axial force in the diagonal strut due to P. Hence, for equilibrium, it must be:

$$P = 2P_{cl} + P_{wv} + P_{wl} \quad \textbf{(2-2)}$$

The cracking load is estimated by means of the Mohr-Coulomb criterion:

$$V_{wcr} = CA_w + \mu_0 P_w \quad \textbf{(2-3)}$$

Where C is a cohesion factor, A_w the cross sectional area of the wall, μ_0 is the initial friction coefficient of masonry mortar joints, and P_w is the total axial load due to P on the wall.

$$P_w = P_{wv} + P_{wl} \quad \textbf{(2-4)}$$

It is assumed that the two columns and the infill panel act as two springs in parallel, hence the total axial load is distributed according to their own axial stiffness.

$$P_{wv} = \frac{PA_w}{A_w + 2A_{ceq}} \quad \textbf{(2-5)}$$

$$P_{wl} = V_{wcr}\frac{h}{l} \quad \textbf{(2-6)}$$

Where:

- h = story height
- L = frame span length
- A_{ceq} = equivalent area of RC columns, in masonry = $A_c \frac{E_c}{E_w}$
- A_c = cross sectional area of RC column = $h_c b_c + A_s \left(\frac{E_s}{E_c} - 1\right)$
- E_c, E_w, and E_s = Elastic moduli of concrete, masonry and steel, respectively
- h_c , b_c = Plan dimensions of RC columns
- A_s = Longitudinal rebar area in a column

By combining equations (2-3) - (2-6) the following expression can be derived for the residual shear strength of a cracked wall, V_{wr}:

$$V_{wr} = A_w \frac{\frac{\mu_r P}{A_w + 2A_{ceq}}}{1 - \mu_r \frac{h}{L}} \quad \textbf{(2-7)}$$

The residual shear strength (V_{wr}) is obtained from the cracking load (V_{wcr}), by means of eliminating the cohesion factor (C), and replacing the initial friction coefficient (μ_0) for the residual friction coefficient (μ_r).

2.3.4.2 Crushing load

The crushing lateral load, which corresponds to the crushing of the diagonal compression masonry strut, can be obtained by means of the concept proposed by (Stafford, 1962).

$$V_{crush} = wtf'_m cos\theta \quad \textbf{(2-8)}$$

Where:

- f'_m = the compressive strength of masonry
- t = The wall thickness
- w = The effective strut width, determined by means of Figure 2.4
- θ = The angle between the diagonal strut and a horizontal line

2.3.4.3 Failure Mechanism 1 (shear failure)

The lateral resistance considered in mechanism 1 is the sum of the shear forces in the columns and the shear resistance of the wall, as seen in Figure 2.20. By force equilibrium in the horizontal direction, the lateral load resistance for mechanism 1 is computed as follows:

$$V_{u1} = V_{wr} + F_{cc} + F_{ct} \quad \textbf{(2-9)}$$

Where:

- V_{u1} = Lateral load resistance for mechanism 1
- V_{wr} = Residual shear strength of wall, obtained by equation (2-7)
- F_{cc} = Shear force in leeward column
- F_{ct} = Shear force in windward column

The expression for F_{cc} and F_{ct} are derived by moment equilibrium of the free body diagram in Figure 2.20, for each individual column segment, as follows:

$$F_{ct} = \frac{4M_{pct}}{h} \quad \textbf{(2-10)}$$

$$F_{cc} = \frac{4M_{pc}}{h} \quad \textbf{(2-11)}$$

Where:

- M_{pct} = The plastic moment developed in the windward column, considering the effect of the axial force
- M_{pc} = The plastic moment developed in the leeward column, not considering the effect of the axial force

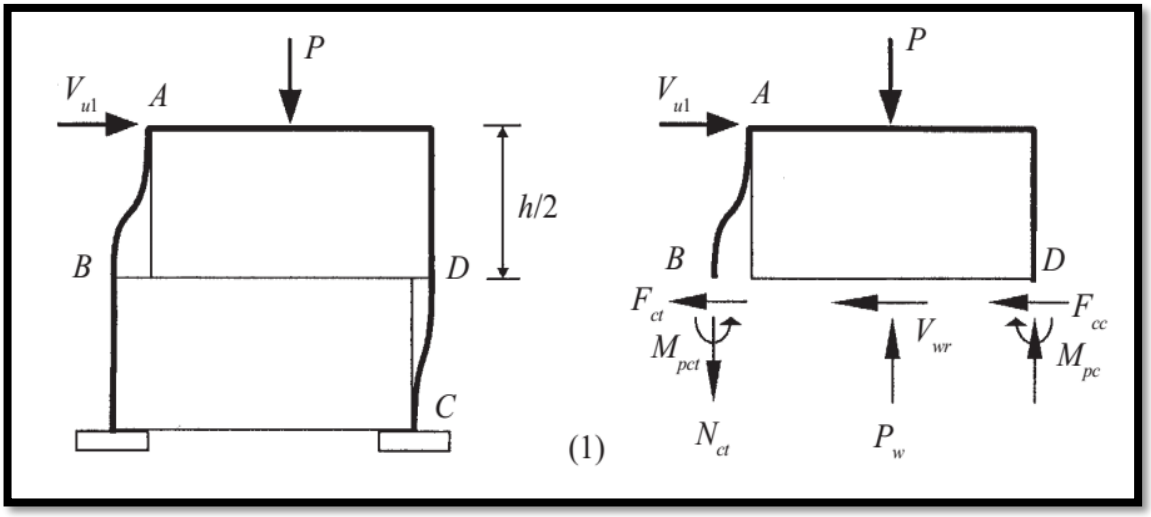

Figure 2.20. Failure mechanism 1 **(Mehrabi & Shing, 2003)**

2.3.4.4 Failure Mechanism 2 (shear failure with inclined crack)

This mechanism is similar to the first one. However, the crack in the panel is conceived as a diagonal (Figure 2.21), and therefore, the residual stress is slightly modified. Also, the ultimate shear resistance is considered for the windward column (V_{ct}) instead of F_{ct}. It follows:

$$V_{u2} = V'_{wr} + F_{cc} + V_{ct} \quad \textbf{(2-12)}$$

Where:

- V_{u2} = Lateral load resistance for mechanism 2
- V'_{wr} = Residual shear resistance provided by the horizontal crack, as expressed in equation (2-13)
- F_{cc} = Shear force in leeward column, as expressed in equation (2-11)
- V_{ct} = Ultimate shear resistance of windward column, as expressed in equation (2-14)

$$V'_{wr} = A_w \frac{\frac{\mu_r P}{A_w + 2A_{ceq}}}{1 - 0.5\mu_r \frac{h}{L}} \quad \textbf{(2-13)}$$

$$V_{ct} = 0.8V_{cs} + V_{cc} \quad \textbf{(2-14)}$$

Where:

- V_{cs} = Shear resistance provided by stirrups
- V_{cc} = Shear resistance provided by concrete

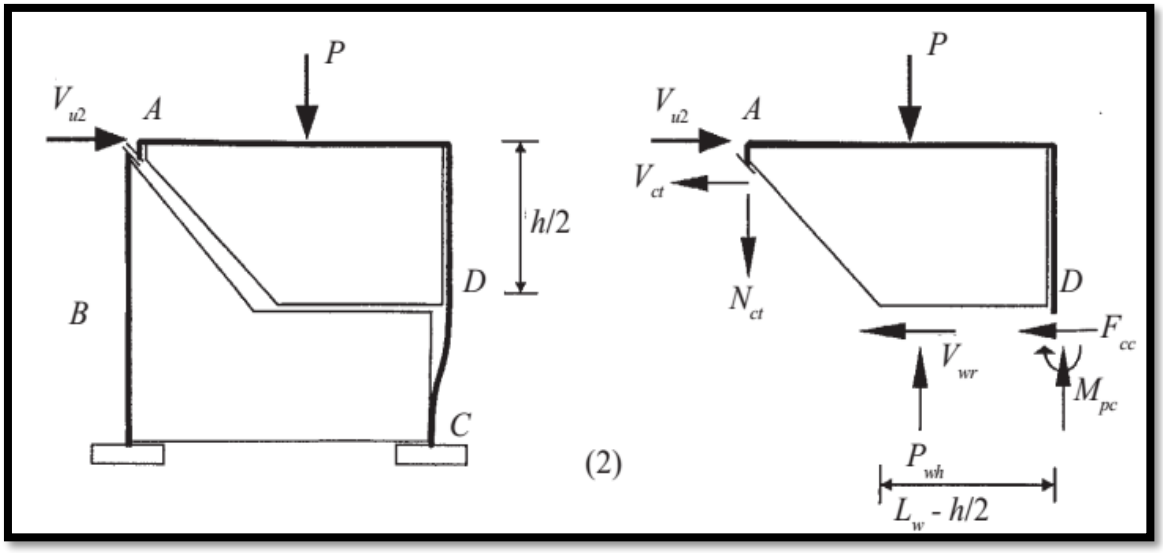

Figure 2.21. Failure mechanism 2 **(Mehrabi & Shing, 2003)**

2.3.4.5 Failure Mechanism 3 (masonry crushing and plastic hinge formation)

In this mechanism, masonry is assumed to reach the crushing strength along the contact length "y" with the frame, and plastic hinges are assumed to form in the columns (near the beam-column joint, and in point b), as depicted in Figure 2.22. The stress is uniform along "y", so the whole segment AB is under plastic state of stress. Point "B" is the point of maximum moment, and hence, zero shear force. This approach was proposed by (Liuaw & Kwan, 1985).

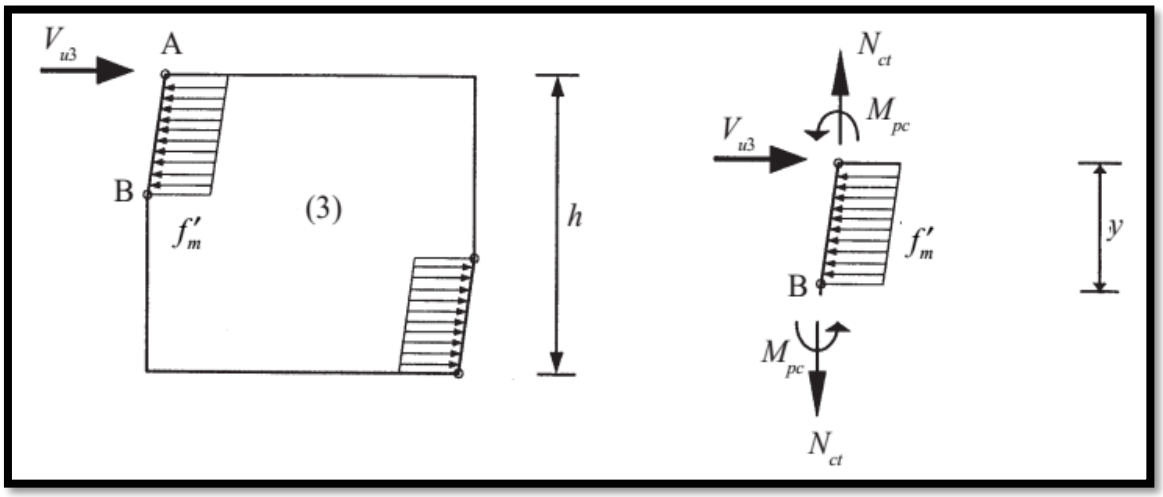

Figure 2.22. Failure mechanism 3 **(Mehrabi & Shing, 2003)**

From moment equilibrium in segment AB:

$$\frac{f'_m t y^2}{2} = 2M_{pc} \qquad \textbf{(2-15)}$$

Where:

- f'_m = Compressive strength of masonry
- M_{pc} = Plastic moment of the columns (neglecting axial force)
- t = Wall thickness

Therefore, from equation (2-15), the contact length can be derived as:

$$y = \sqrt{\frac{4M_{pc}}{f'_m t}} \qquad \textbf{(2-16)}$$

Finally, considering force equilibrium in the horizontal direction for the free body diagram of segment AB:

$$V_{u3} = y f'_m t \qquad \textbf{(2-17)}$$

2.3.4.6 Failure Mechanism 4 (masonry crushing and plastic hinge formation)

Mechanism 4 is also based on plastic theory, and is proposed, similarly to the previous mechanism, by (Liuaw & Kwan, 1985). The difference in this method is that the plastic hinges are assumed to form at the ends of the columns (Figure 2.23), and the stress on the compressed masonry corners is assumed parabolic along the contact length (αh) because of the linear variation of strains, due to the rotation of the columns. Masonry is assumed to crush at the corners, where the parabolic stress reaches its maximum value.

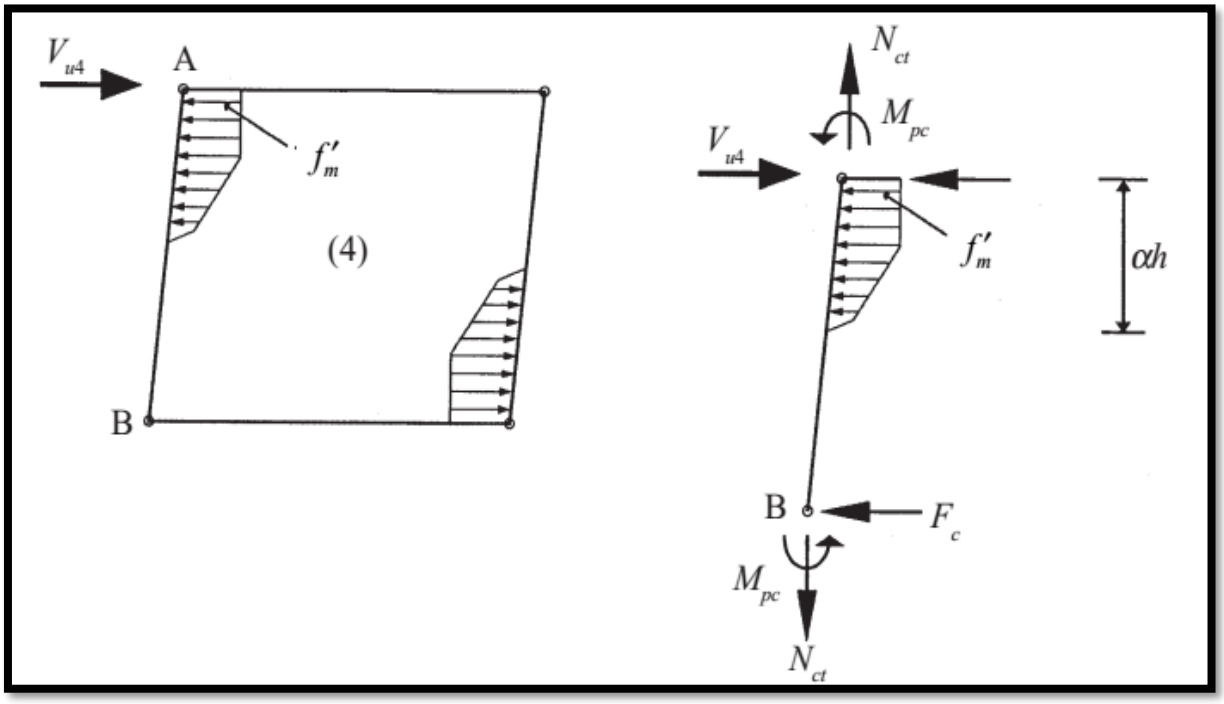

Figure 2.23. Failure mechanism 4 **(Mehrabi & Shing, 2003)**

Computing moment equilibrium about point A in column AB:

$$F_c h + 0.25 f'_m t(\alpha h)^2 = 2M_{pc} \quad \textbf{(2-18)}$$

Where

- F_c = Shear force in each column
- M_{pc} = Plastic moment of column AB, neglecting influence of axial force

Computing force equilibrium for column AB:

$$V_{u4} = 0.67 f'_m t\alpha h + 2F_c = (m_c^2 + 0.67\alpha - 0.5\alpha^2) f'_m th \quad \textbf{(2-19)}$$

$$m_c = \sqrt{\frac{4M_p}{f'_m t h_c^2}} \quad \textbf{(2-20)}$$

The contact length (αh) was proposed by *Stafford Smith* in 1966 as follows:

$$\alpha h = \pi \sqrt[4]{\frac{E_c I_c h}{4E_w t \sin(2\theta)}} \quad \textbf{(2-21)}$$

2.3.4.7 Failure Mechanism 5 (residual shear + flexure)

The last mechanism considers the frame and infill to act as two independent resistant members (Figure 2.24), working in parallel, with a displacement compatibility at the compressed corners. Therefore, the total lateral resistance is given by the sum of the residual shear resistance of the fractured wall, and the flexural resistance of the frame.

$$V_{u5} = V_{wr} + F_f \quad \textbf{(2-22)}$$

Where:

- V_{u5} = Lateral resistance of mechanism 5
- V_{wr} = Residual shear resistance of fractured wall, obtained by equation (2-7)
- F_f = Flexural resistance of the bare frame, with plastic hinges at column end sections, obtained by means of equation (2-23)

$$F_f = \frac{4M_{pc}}{h} \quad \textbf{(2-23)}$$

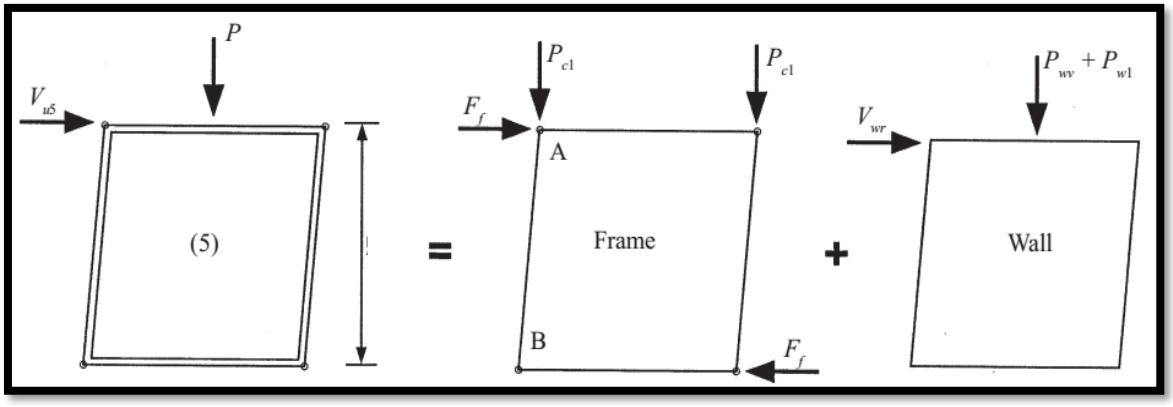

Figure 2.24. Failure mechanism 5 **(Mehrabi & Shing, 2003)**

2.3.5 Behavior of infilled RC frames under cyclic loading

According to (Kakaletsis & Karayannis, 2008) it has been shown that the total energy dissipation capacity of a masonry infilled RC frame is around 1.5 times larger than that of a bare frame subjected to the same cyclic loading. This is depicted in Figure 2.25. Another interesting fact is that the loss of strength is smaller than the corresponding loss of energy dissipation. This is due to the noticeable pinching effect.

With reference to the initial stiffness, the one of the infilled frame is approximately 2.5 times larger than the initial stiffness of the bare frame. This can be seen by comparing initial slopes in the diagrams depicted in Figure 2.25(a) and (c).

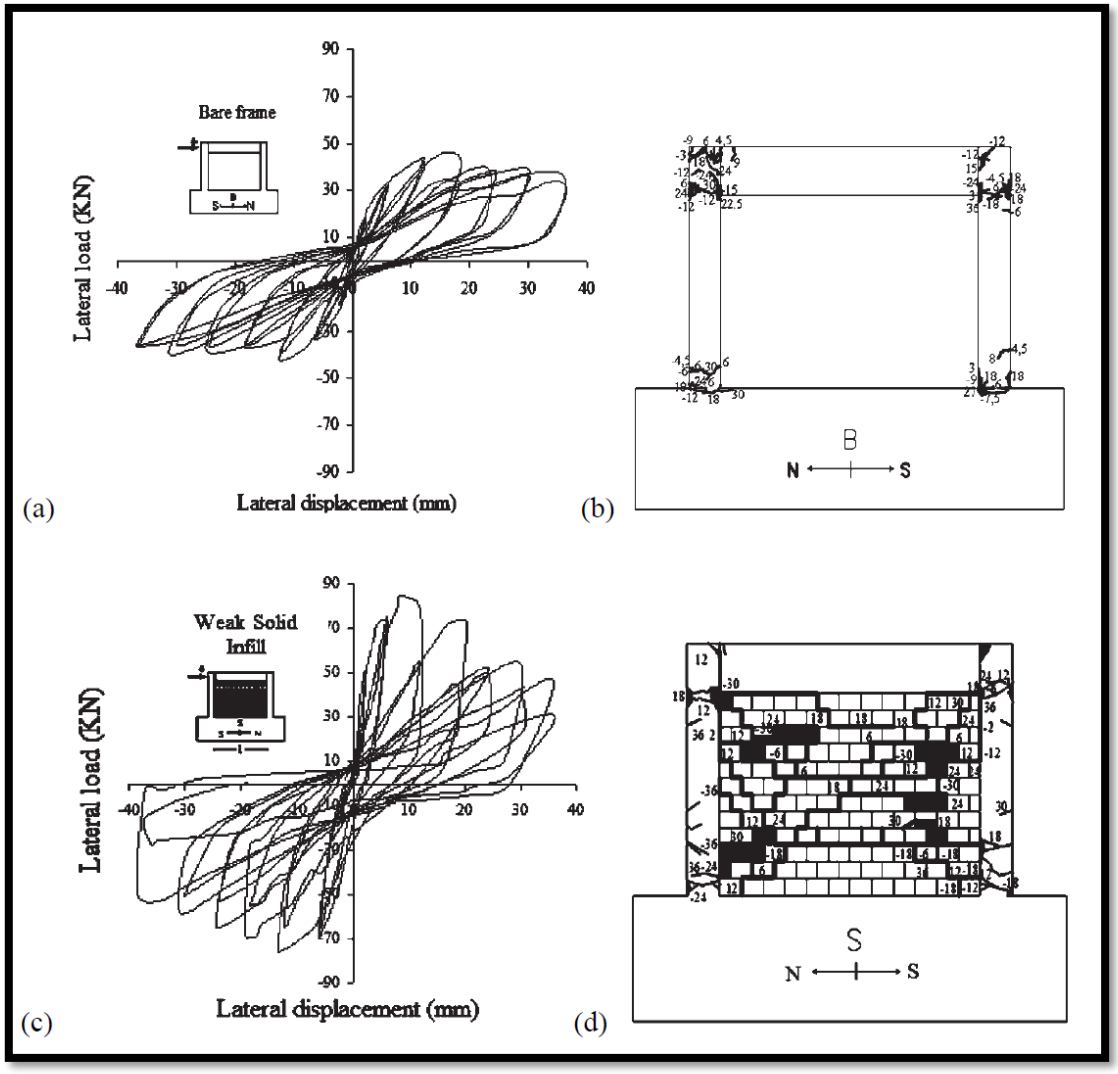

Figure 2.25. Lateral load-displacement hysteresis curves and failure modes of a bare frame (a) (b) and a masonry infilled RC frame (c) (d) **(Kakaletsis & Karayannis, 2008)**

Various methods have been used to calculate the energy dissipation capacity based on results acquired from cyclic tests. For this purpose, (Valiasis & Stylianidis, 1989) introduced a parameter which is defined as "energy dissipated by cycle divided by corresponding total displacement of the cycle". Tests were conducted on bare frames and masonry infilled ones. Results are shown in Figure 2.26. It can be seen that the energy per unit of total displacement dissipated by the bare frame grows during the whole experiment, while for the infilled frame, a sudden drop can be observed in the range of large displacements (due to masonry degradation). In other words, in the range of large lateral displacements, behavior of an infilled frame tends to be similar to the behavior of a bare frame. Regardless of this, energy dissipation of an infilled frame is still considerably larger than that of a bare frame.

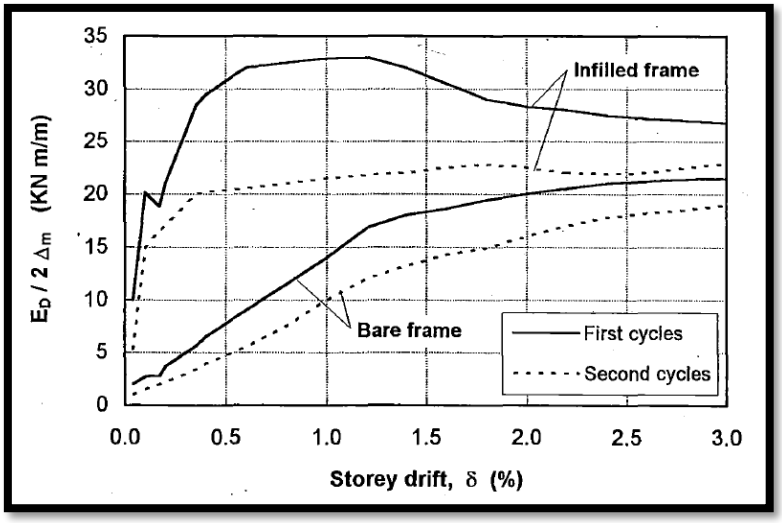

Figure 2.26. Energy dissipated per cycle **(Valiasis & Stylianidis, 1989)**

2.4 RC FRAME WITH SLIGHTLY REINFORCED MASONRY INFILL

2.4.1 Introduction

As mentioned before, since masonry infills are often conceived as non-structural elements, they are most of the times unreinforced. However, it has been shown that adding light reinforcing to the panels can dramatically improve the performance of the infilled frame (Calvi, et al., 2004).

Steel reinforcing could be placed either in the bed joints, or as a wire mesh between the infill and the plaster, with no continuity between the steel in the infill and the surrounding RC frame (Figure 2.27). The external mesh option uses roughly twice the amount of steel than the bed joint reinforcing, but gives by far the best results in terms of ductility and post-peak behavior.

Out of plane expulsion is a topic of interest for masonry infilled RC frames. Although the wall can continue to carry load after expulsion, this is considered a dangerous situation for human safety, and should therefore be considered as an Ultimate Limit State situation. Slight reinforcing of the infill greatly improves the out-of-plane resistance, and therefore, expulsion occurs at much higher values of loading.

Reinforcing of infill panels affects mostly the post-peak behavior of infilled frames. For this reason, there is not much difference in the behavior for low damage situations in comparison to the unreinforced infills. However, for significant damage limit states (at significant drift values), the slight reinforcement gives a remarkably superior behavior.

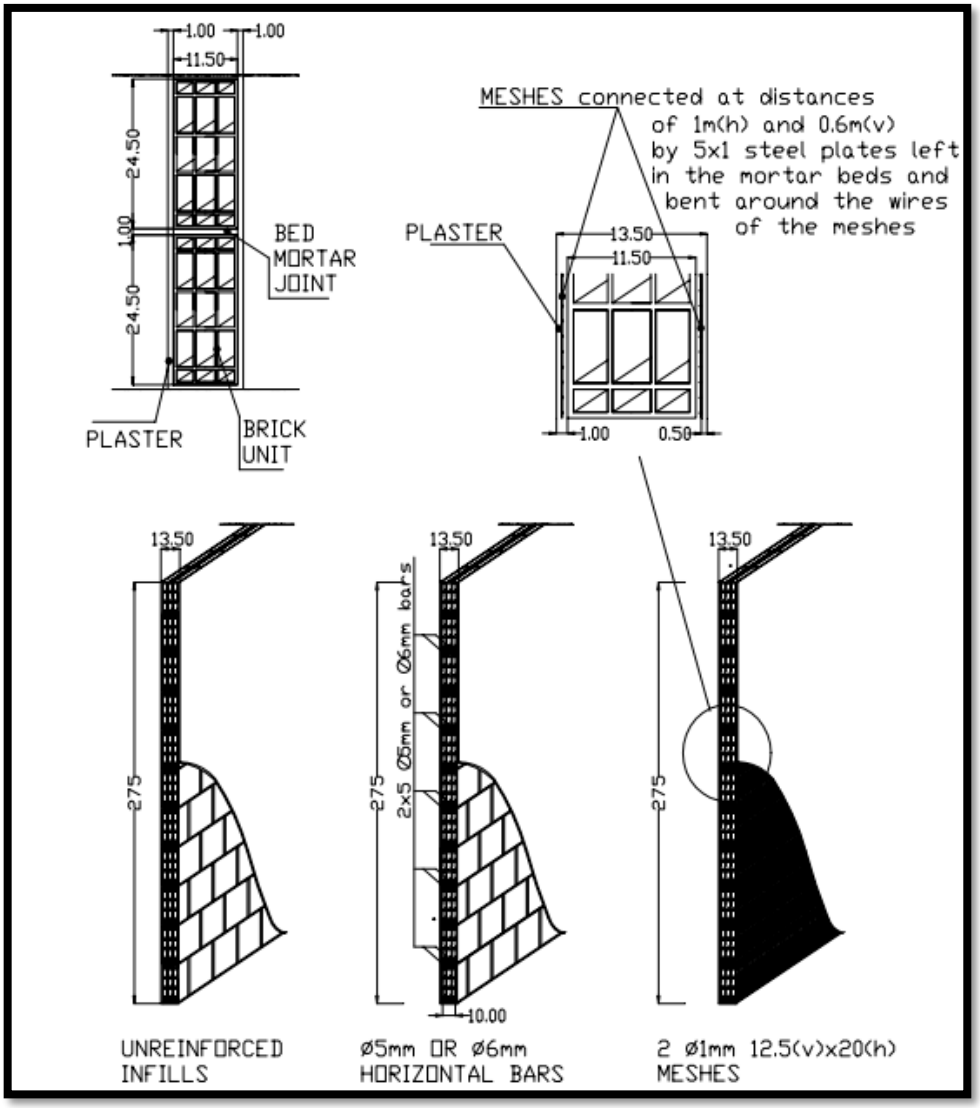

Figure 2.27. Details of reinforcing of the masonry panel **(Calvi, et al., 2004)**

2.4.2 Modeling and analysis

Modeling of the slightly reinforced infilled frames has been carried out, according to (Calvi, et al., 2004), with Takeda-type non-linear elements for beams and columns (which account for concrete cracking and yielding of steel rebars), and using an equivalent diagonal compression strut for the infill panel, with an effective width of 25% of the length of the strut, and force-displacement curves which have been derived from experimental data.

Non-linear analysis was carried out by means of a pushover analysis. Numerical results are in good agreement with the experimental ones, and show how adding a slight amount of reinforcement can have a positive impact on the overall structural response. Also, different ways of reinforcing give different responses and are characterized by different ductility level as represented in Figure 2.28.

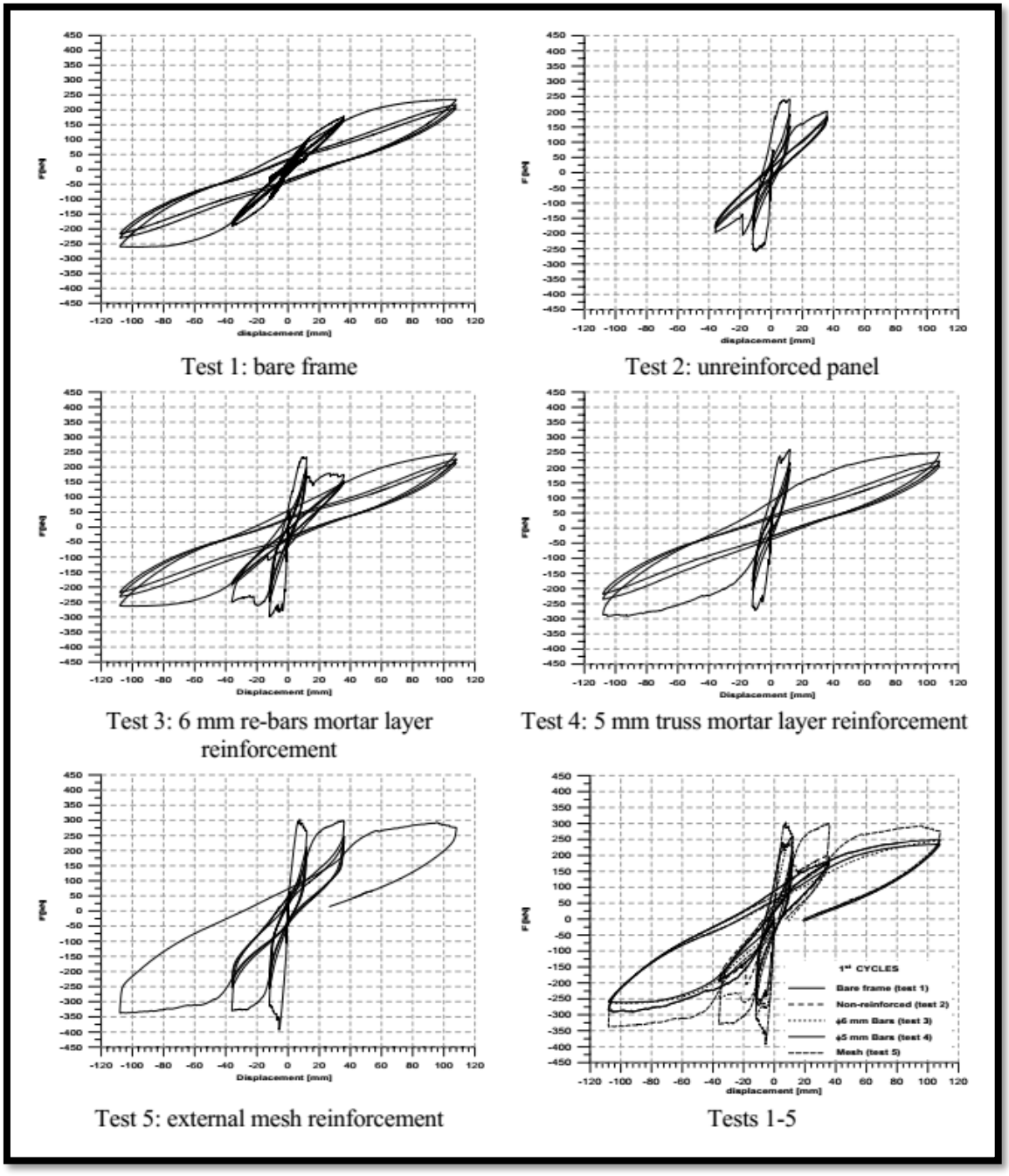

Figure 2.28. Hysteretic loops for different types of reinforcing **(Calvi, et al., 2004)**

2.5 COMPARISON OF THE BARE FRAME VS. MASONRY INFILLED FRAME BEHAVIOR UNDER MONOTONIC LOADING

Many studies have been made for the case of masonry infilled RC frames. Some common general conclusions found in the literature are discussed below.

- The masonry infill has a non-negligible influence on the overall structural response of the frame under lateral loading.
- Its influence is more relevant under low horizontal loading, when the masonry is not fully cracked.
- It can be observed from experimental cyclic tests, that the initial stiffness is always much greater for an infilled frame vs. the bare frame.
- Eventually, at large drifts, the response always tends to the one of the bare frame.
- Serious "pinching" of the hysteresis loops can occur in an infilled frame when it is not reinforced
- Adding a slight amount of steel reinforcing to the infill will help the pinching effect, the post-peak behavior, and the out-of-plane capacity.
- If adequately designed, the masonry infill is always beneficial in terms of stiffness and energy dissipation vs. the bare frame.

3 PREDICTION OF ULTIMATE LOAD VIA ANALYTICAL METHOD

A simplified analytical approach that quantifies the lateral resistance of masonry infilled frames, proposed by (Mehrabi & Shing, 2003) was described in section 2.3.4. The method was used in this research for the initial estimation of the lateral resistance of polystyrene infilled frames. It is recalled that the method foresees five different possible failure modes in which the infilled frame may fail, out of which the lowest value is the one governing the ultimate resistance (*Figure 3.1*).

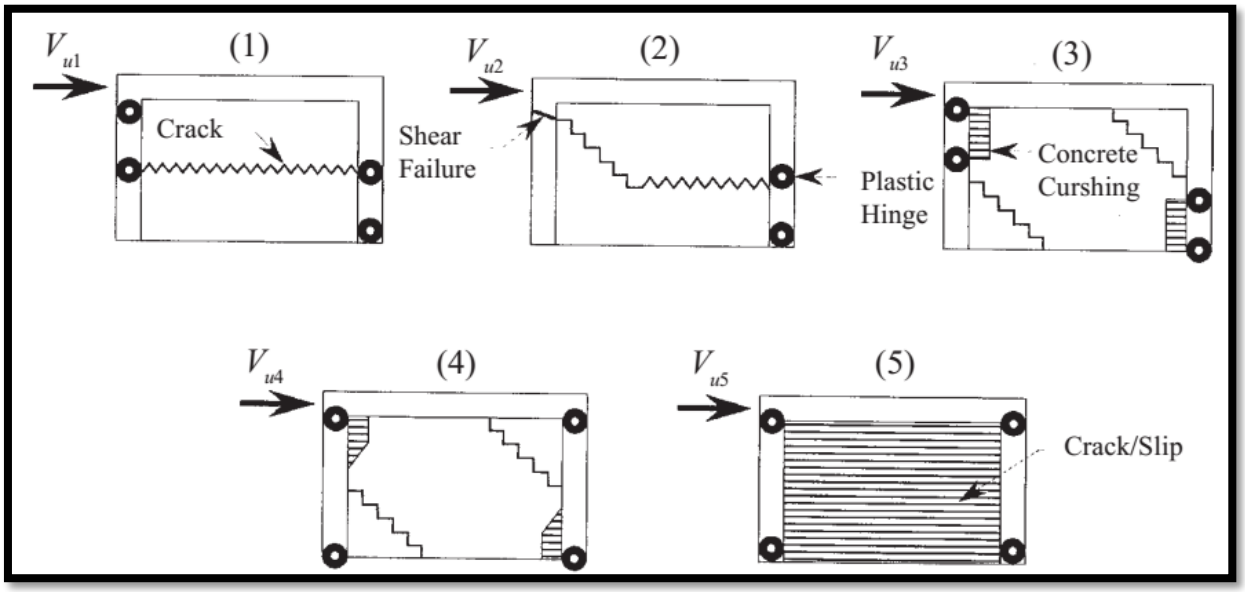

Figure 3.1. Possible failure mechanisms considered **(Mehrabi & Shing, 2003)**

3.1 DESCRIPTION OF THE EXPERIMENTAL SPECIMEN

The frame under study has the geometrical characteristics depicted in *Figure 3.2* and *Figure 3.3*. For the purpose of estimating the lateral load capacity, also some mechanical properties are required (Table 3-1 and Table 3-2). It should be noted that this particular frame has no additional vertical axial load acting on it, and therefore the axial load on columns (P_{cl}) is only due to the frame self-weight. Similarly, the axial load acting on the infill is only due to its own self-weight (P_{wv}). An iterative process was undergone in order to determine the lateral load resistance, since some of the failure modes require the total axial load on the columns, which depends on the horizontal load (V), due to frame action.

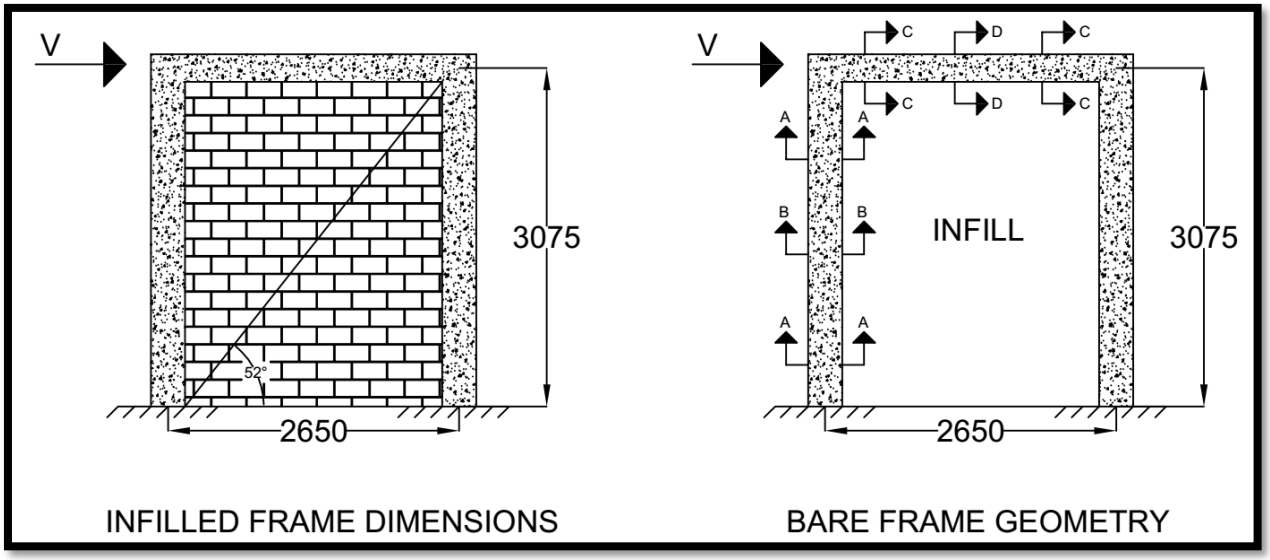

Figure 3.2. Infilled frame geometry

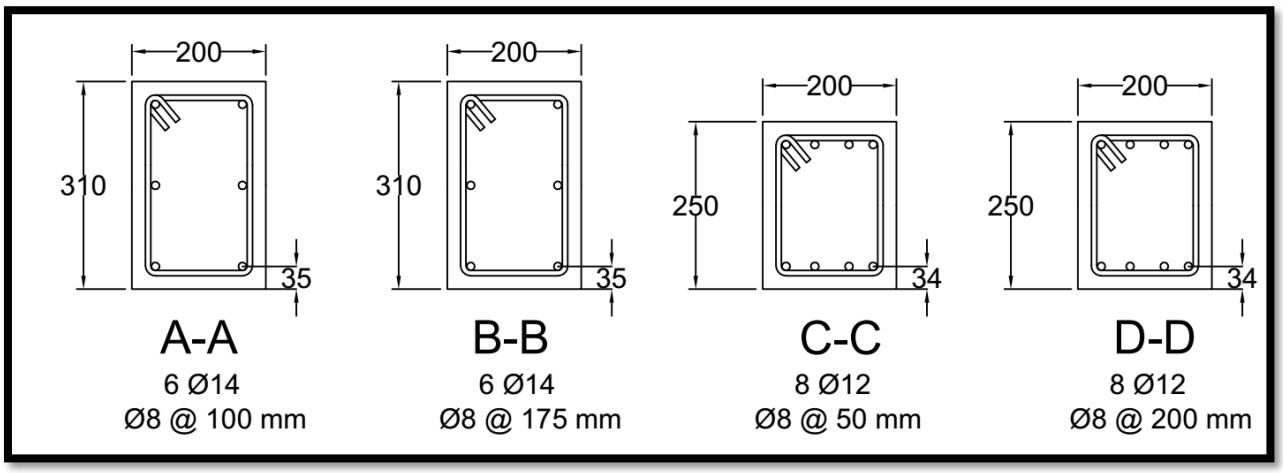

Figure 3.3. Beam and column cross sections

Material Mechanical Properties	E_c [GPa]	30	Concrete Elastic Modulus
	E_p [MPa}	4.35	Polystyrene Elastic Modulus
	E_s [GPa}	210	Steel Elastic Modulus
	f_{pk} [MPa]	0.12	Polystyrene characteristic compressive strength
	f_{ck} [MPa]	20	Concrete characteristic compressive strength
	f_{yk} [MPa]	450	Steel rebar characteristic tensile strength
	μ_0	0.5	Polystyrene initial friction Coefficient
	μ_r	0.15	Polystyrene residual friction Coefficient
	ρ_c [kN/m^3]	25	Reinforced concrete density
	ρ_p [kN/m^3]	10.4	Polystyrene density

Table 3-1. Material mechanical properties of infilled frame components

Geometry and loads	h [m]	3.075	Height
	L [m]	2.65	Length
	θ [°]	52	Strut angle
	D [m]	4.06	Diagonal length
	w/D	0.25	Assumed compression strut width ratio
	w [m]	1.01	Compression strut width
	V [kN]	70	Total Expected Horizontal Load
	P [kN]	27.20	Total Vertical Load
	h_c [m]	0.31	Column dimensions
	b_c [m]	0.2	
	d [m]	0.276	Concrete column inner lever arm
	I [m^4]	0.00050	Concrete column moment of inertia
	t_w [m]	0.2	Infill thickness
	A_s [mm^2]	1231.5	Longitudinal steel area in columns
	A_{st} [mm^2]	100.531	Transverse steel area in columns
	s [mm]	175	Stirrup spacing close to mid-height of column
	A_w [m^2]	0.468	Infill Area in horizontal plane
	A_c [m^2]	0.069	Column Area
	A_{ceq} [m^2]	1.04	Equivalent area of RC columns in polystyrene
	P_{wv} [kN]	14.36	Axial load in vertical strut due to P (self-weight)
	P_w [kN]	14.36	Total axial load due to P on the wall
	P_{cl} [kN]	6.42	Total axial load due to P on each column
	V*h/L [kN]	81.23	Total axial load due to V on the columns

Table 3-2. Frame geometry and loads

Once convergence was reached, the axial load contribution on columns due to the lateral load (V) was taken into account for the computation of the plastic moment capacity of the columns, as well as their shear capacity. For this task an interaction diagram was computed for the columns, which is depicted in *Figure 3.4*, and was used with the respective axial load for each column.

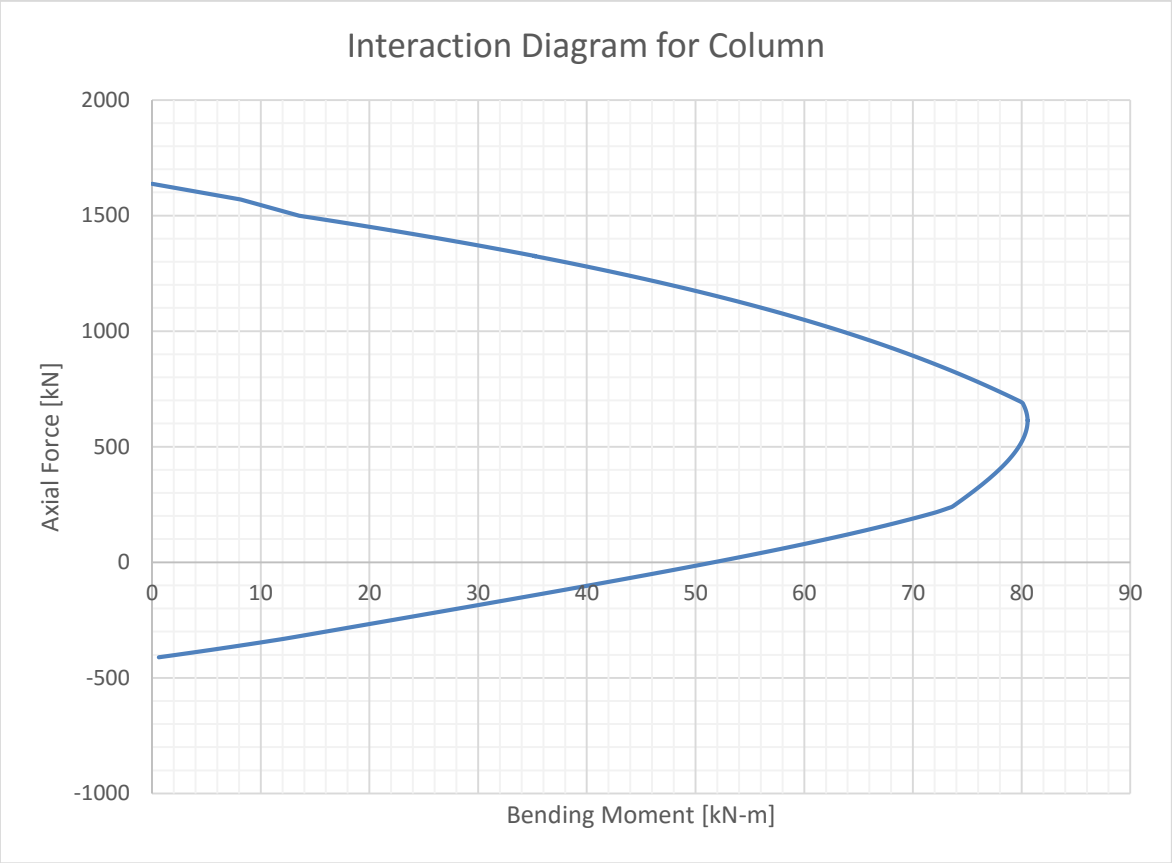

Figure 3.4. Interaction diagram for columns

3.2 FAILURE MECHANISM 1

Following the procedure explained in section 2.3.4.3, the lateral load resistance due to failure mechanism 1 corresponds to the sum of the shear forces in the columns and the shear resistance of the wall (*Figure 3.5*), and was computed as follows.

$$V_{u1} = V_{wr} + F_{cc} + F_{ct}$$

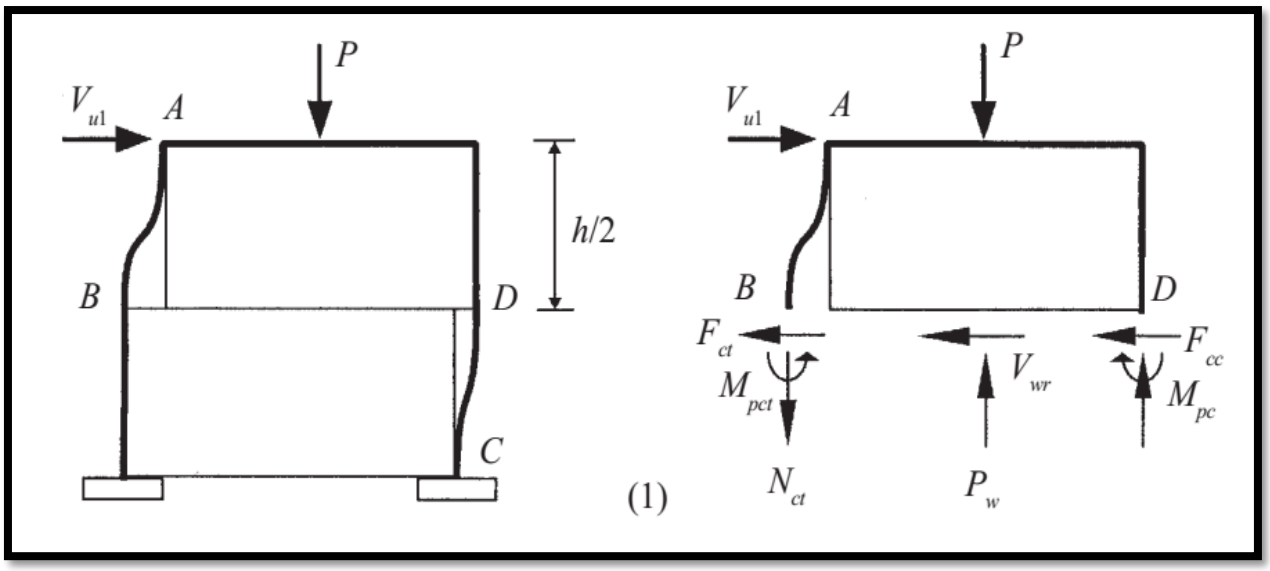

Figure 3.5. Failure mechanism 1 **(Mehrabi & Shing, 2003)**

$$V_{wcr} = CA_w + \mu_0 P_w$$

$$V_{wr} = \mu_r P_w$$

$$P_w = P_{wv} + P_{wl}$$

$$P_{wv} = 14.36\ kN$$

$$P_{wl} = V_{wcr}\frac{h}{l}$$

By combining the previous equations, substituting μ_0 for μ_r, and considering C=0, the following expression is obtained for the residual shear strength.

$$V_{wr} = \frac{\mu_r P_{wv}}{1 - \mu_r \frac{h}{L}} = \frac{0.15 \cdot 14.36}{1 - 0.15 \cdot \frac{3.075}{2.65}} = 2.61\ kN$$

It now follows to compute the shear force in windward and leeward columns.

$$F_{ct} = \frac{4M_{pct}}{h} \qquad\qquad F_{cc} = \frac{4M_{pc}}{h}$$

The plastic moment on both columns was determined from the interaction diagram in *Figure 3.4*, with the corresponding axial load on each column (neglecting axial load contribution of "V" in leeward column, and considering the contribution of "V" in windward column).

$$M_{pct} = \ 45.77\ kN \cdot m \qquad\qquad M_{pc} = 52.34\ kN \cdot m$$

$$F_{ct} = \frac{4 \cdot 45.77}{3.075} = 59.54\ kN \qquad\qquad F_{cc} = \frac{4 \cdot 52.34}{3.075} = 68.08\ kN$$

The lateral load capacity is calculated as follows.

$$V_{u1} = V_{wr} + F_{cc} + F_{ct} = 2.61 + 59.54 + 68.08 = 130.23\ kN$$

3.3 FAILURE MECHANISM 2

Following the procedure explained in section 2.3.4.4, the lateral load resistance due to failure mechanism 2 was computed. The failure mechanism corresponds to the sum of a slightly modified residual shear stress of the wall (because of the diagonal crack), the ultimate shear resistance in windward column, and the shear force in leeward column (*Figure 3.6*).

$$V_{u2} = V'_{wr} + F_{cc} + V_{ct}$$

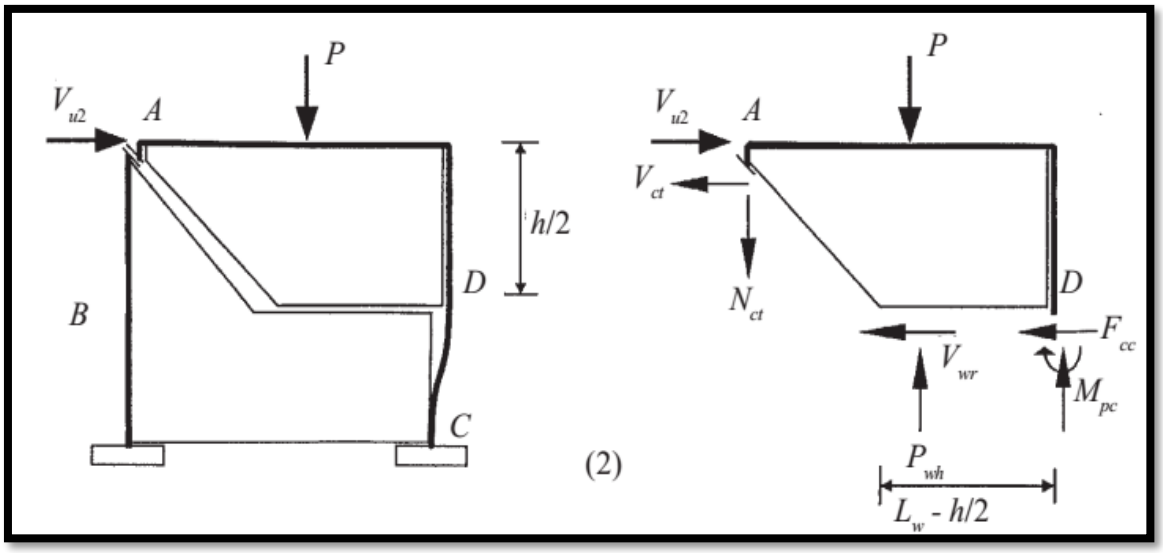

Figure 3.6. Failure mechanism 2 **(Mehrabi & Shing, 2003)**

$$V'_{wr} = \frac{\mu_r P_{wv}}{1 - 0.5\mu_r \frac{h}{L}} = \frac{0.15 \cdot 14.36}{1 - 0.5 \cdot 0.15 \cdot \frac{3.075}{2.65}} = 2.36\ kN$$

$$V_{ct} = 0.8V_{cs} + V_{cc}$$

The shear resistance of concrete was calculated according to EN 1992-1-1:2004, section 6.2.2. Calculations are presented below

$$V_{cc} = \left[C_{Rd,c} k (100\rho_1 f_{ck})^{1/3} + k_1 \sigma_{cp}\right] b_w d$$

$$= \frac{\left[0.12 \cdot 1.85 \cdot (100 \cdot 0.002 \cdot 25)^{\frac{1}{3}} - 0.15 \cdot 0.48\right] 200 \cdot 276}{1000} = 37.96\ kN$$

Where:

$C_{Rd,c}$	=	0.12	Concrete shear calculation coefficient
K	=	$1 + \sqrt{\frac{200}{d}} = 1.85$	Concrete shear calculation coefficient
k1	=	0.15	Concrete shear calculation coefficient
ρ_1	=	0.02	Longitudinal steel area ratio
σ_{cp}	=	-0.48	Axial stress due to design gravity loads (negative in tension)
v_{min}	=	0.39	Concrete shear calculation coefficient

The minimum value for the shear resistance of concrete is calculated as:

$$V_{cc,min} = \frac{(v_{min} + k_1\sigma_{cp})b_w d = (0.39 - 0.15 \cdot 0.48)200 \cdot 276}{1000} = 17.55\ kN$$

$\therefore V_{cc} = 37.96\ kN$

The shear resistance of stirrups was calculated according to EN 1992-1-1:2004, section 6.2.3. Calculations are presented below. An angle for the compression strut θ = 45° was assumed for this calculation.

$$V_{cs} = \frac{A_{st}}{s} z f_{yd} cot\theta = \frac{\frac{100.531}{175} \cdot (276) \cdot 391.3 \cdot 1}{1000} = 62\ kN$$

The maximum shear force provided by stirrups is limited by the following expression.

$$V_{Rd,max} = \frac{\alpha_{cw} b_w z v_1 f_{cd}}{cot\theta + tan\theta} = \frac{1 \cdot 200 \cdot 276 \cdot 0.6 \cdot 11.33}{\cot(45°) + \tan(45°)} \cdot \frac{1}{1000} = 187.63\ kN$$

V_{cs} is used since it is lesser than $V_{Rd,max}$.

$\therefore V_{cs} = 62\ kN$

It is now possible to compute the ultimate shear resistance of the windward column.

$$V_{ct} = 0.8V_{cs} + V_{cc} = 0.8 \cdot 62 + 37.96 = 87.60\ kN$$

It now follows to sum all the contributions together in order to determine the capacity of failure mechanism 2.

$$V_{u2} = V'_{wr} + F_{cc} + V_{ct} = 2.36 + 68.08 + 87.60 = 158.04\ kN$$

3.4 FAILURE MECHANISM 3

Following the procedure explained in section 2.3.4.5, the lateral load resistance due to failure mechanism 3, which corresponds to crushing of the infill along the contact length, and plastic hinges formation on columns, near to beam-column joint and point B (*Figure 3.7*), was computed as follows.

$$V_{u3} = y f_{pk} t$$

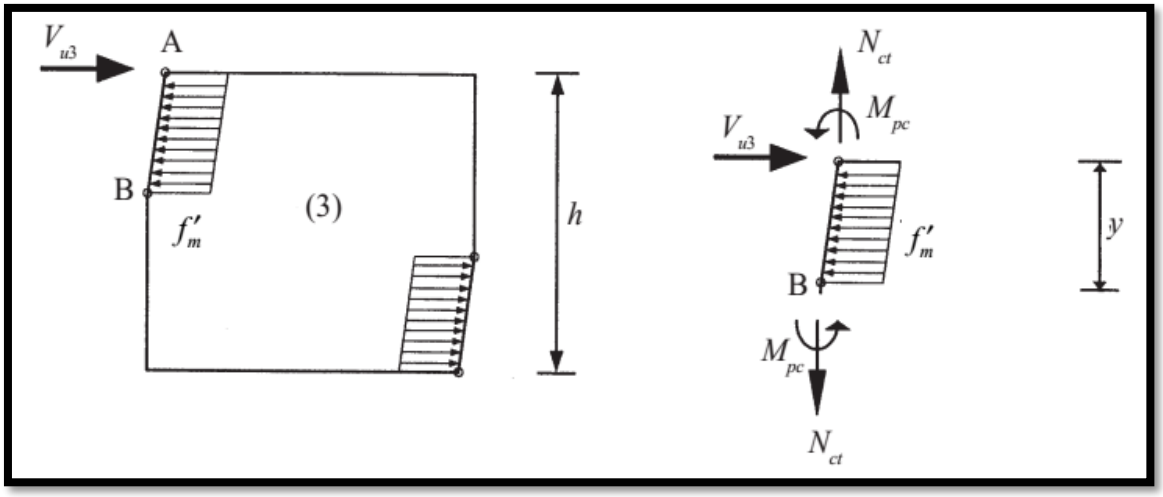

Figure 3.7. Failure mechanism 3 **(Mehrabi & Shing, 2003)**

The contact length between infill and frame is calculated first.

$$y = \sqrt{\frac{4M_{pc}}{f_{pk} \cdot t}} = \sqrt{\frac{4 \cdot 52.34 \cdot 1000 \cdot 1000}{0.12 \cdot 200}} \cdot \frac{1}{1000} = 2.95\ m$$

It now follows to compute the lateral load resistance due to failure mechanism 3.

$$V_{u3} = y f_{pk} t = \frac{2950 \cdot 0.12 \cdot 200}{1000} = 70.88\ kN$$

3.5 FAILURE MECHANISM 4

Following the procedure explained in section 2.3.4.6, the lateral load resistance due to failure mechanism 4 was computed. This failure mode is quite similar to the previous case, but the plastic hinges are assumed to occur at the base of the column (point B in *Figure 3.8*), and the distribution of stresses along the contact length is assumed to be parabolic.

$$V_{u4} = 0.67 f_{pk} t \alpha h + 2F_c$$

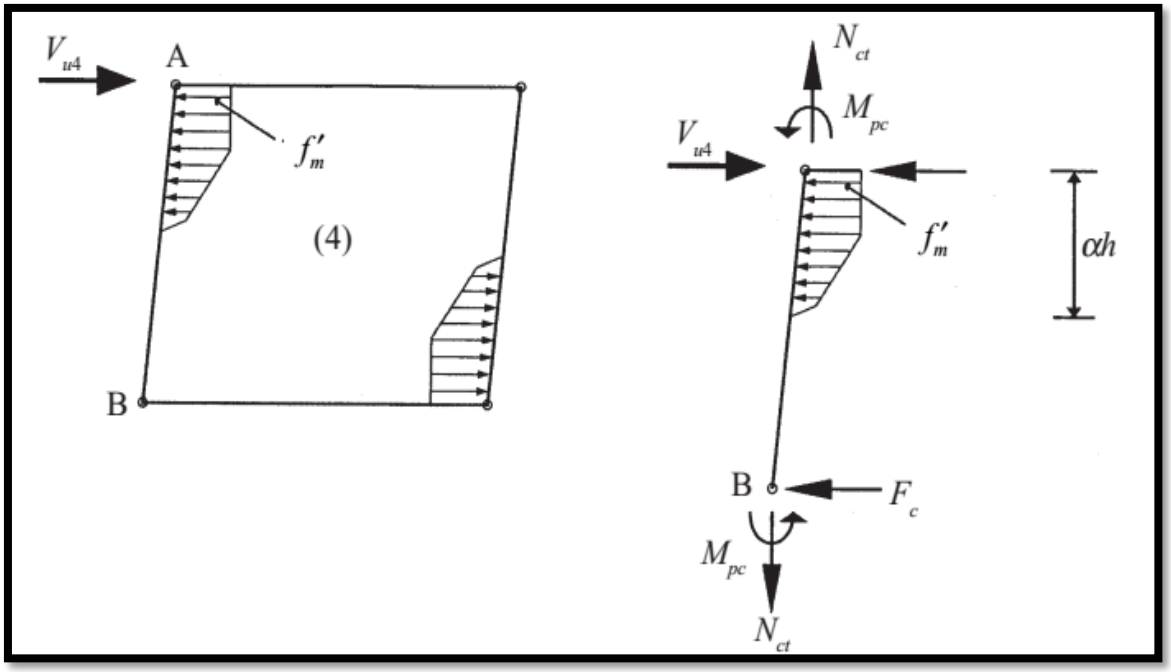

Figure 3.8. Failure mechanism 4 **(Mehrabi & Shing, 2003)**

The contact length between infill and frame is calculated first.

$$\alpha h = \pi \sqrt[4]{\frac{E_c I_c h}{4 E_w t sin(2\theta)}} = \pi \sqrt[4]{\frac{30 \cdot 0.0005 \cdot 3.075}{4 \cdot 4.35 \times 10^{-3} \cdot 0.2 \cdot sin(2 \cdot 52)}} = 6.04\ m$$

Since the computed contact length is bigger than the structure, the contact length will be limited to the height of the infill

$$\therefore \alpha h = 2.95m$$

Next, the shear force in each column is computed.

$$F_c h + 0.25 f_{pk} t (\alpha h)^2 = 2M_{pc} \quad \rightarrow \quad F_c = \frac{2M_{pc} - 0.25 f_{pk} t (\alpha h)^2}{h}$$

$$F_c = \frac{2 \cdot 52.34 - 0.25 \cdot 0.12 \cdot 1000 \cdot 0.2 \cdot 2.95^2}{3.075} = 17.06\ kN$$

It is now possible to determine the lateral resistance of the frame due to failure mechanism 4.

$$V_{u4} = 0.67 f_{pk} t \alpha h + 2F_c = 0.67 \cdot 0.12 \cdot 1000 \cdot 0.2 \cdot 2.95 + 2 \cdot 17.06 = 81.56\ kN$$

3.6 FAILURE MECHANISM 5

Following the procedure explained in section 2.3.4.7, the lateral load resistance due to failure mechanism 5 was computed. The resistance is composed by the sum of the residual shear resistance of the fractured wall and the flexural resistance of the frame (*Figure 3.9*). This is the type of failure mechanism which has been observed to occur more often in the case of weak infills. Since polystyrene is much weaker than masonry, it is expected to govern.

$$V_{u5} = V_{wr} + F_f$$

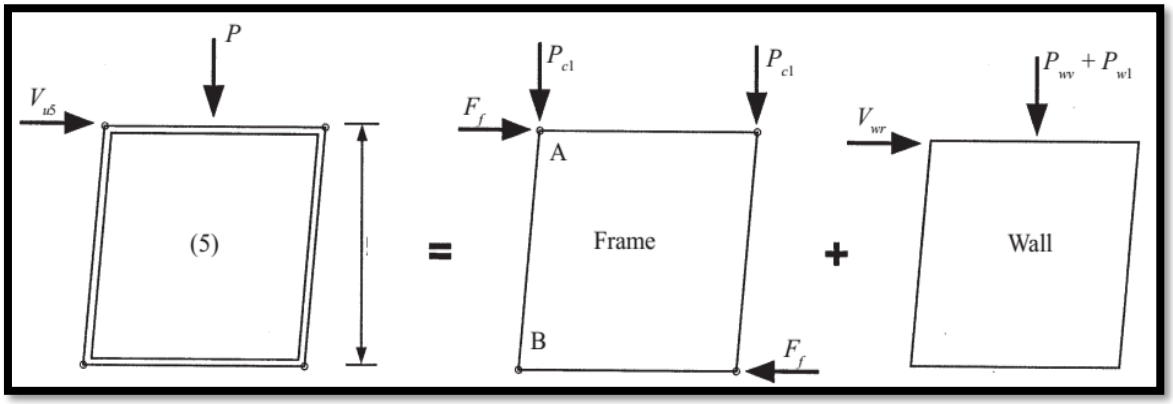

Figure 3.9. Failure mechanism 5 **(Mehrabi & Shing, 2003)**

The flexural resistance of the bare frame, with plastic hinges at the column end sections, is calculated first.

$$F_f = \frac{4M_{pc}}{h} = \frac{4 \cdot 52.34}{3.075} = 68.08\ kN$$

The lateral load resistance due to failure mechanism 5 is now computed.

$$V_{u5} = V_{wr} + F_f = 2.61 + 68.08 = 70.69\ kN$$

A summary of results is presented in Table 3-3.

Summary of results	V_{u1} [kN]	130.23	Lateral resistance for mechanism 1
	V_{u2} [kN]	158.04	Lateral resistance for mechanism 2
	V_{u3} [kN]	70.88	Lateral resistance for mechanism 3
	V_{u4} [kN]	81.56	Lateral resistance for mechanism 4
	V_{u5} [kN]	70.69	Lateral resistance for mechanism 5
	V_u [kN]	70.69	Lateral resistance

Table 3-3. Summary of lateral resistance for the 5 failure mechanisms

It can be seen from Table 3-3 that, as expected, failure mechanism 5 is governing the lateral resistance of the infilled frame.

3.7 SENSITIVITY ANALYSIS

While the geometrical properties of the infilled frame were measured with sufficient accuracy, the mechanical properties could vary to some extent. This is due to the fact that no laboratory tests were carried out in order to determine the mechanical properties of the polystyrene infill, nor of concrete, depicted in Table 3-1. Typical values for concrete class C 20/25 were assumed. In the case of polystyrene, typical values found in the literature were adopted in order to use the analytical equations in section 2.3.4.

A sensitivity analysis was carried out, in order to quantify the possible variation in the failure loads due to variation of the mechanical properties, according to the analytical method. From this analysis it is possible to quantify how each of these parameters will influence the final result, by varying only one parameter at a time, and comparing it to the "reference" case, which is the one depicted in Table 3-3. Several parameters, such as compressive strength, elastic modulus, strut width ratio, and residual friction coefficient were investigated.

3.7.1 Residual friction sensitivity analysis

The residual friction coefficient is a parameter which is used for the determination of the residual shear strength of the cracked wall, as shown in section 2.3.4.1. The residual shear strength is used in failure mechanisms 1, 2 and 5, and therefore will be the only ones affected by the variation of the residual friction coefficient. This parameter cannot be greater than the initial friction coefficient, but must be greater than 0. For this reason, the range of variation for the residual friction coefficient is determined as:

$$0 \leq \mu_r \leq \mu_0 \qquad\qquad \mu_0 = 0.5$$

From *Figure 3.10* it can be observed that failure mechanism 3 and 4 are not affected by the variation of the residual friction coefficient, as they don't depend on it. Failure mechanisms 1 and 2 are affected, but don't govern the lateral load resistance, as failure mechanism 5 is still governing. Failure mechanism 5 shows a considerable range of values due to the variation of this parameter, as shown below.

$$68.1\ kN\ \leq V_{u5} \leq 85.2\ kN$$

Due to the fact that failure mechanism 5 does not govern the lateral load resistance when $\mu_r = 0.5$, the global capacity is governed by failure mechanism 3 when the residual friction coefficient adopts very high values. The range of possible values for the lateral load capacity, due to a variation of the residual friction coefficient, is shown below, which is governed by failure mechanism 5 for low values of residual friction coefficient, and by failure mechanism 3 for high values.

$$68.1\ kN\ \leq V_u \leq 70.9\ kN$$

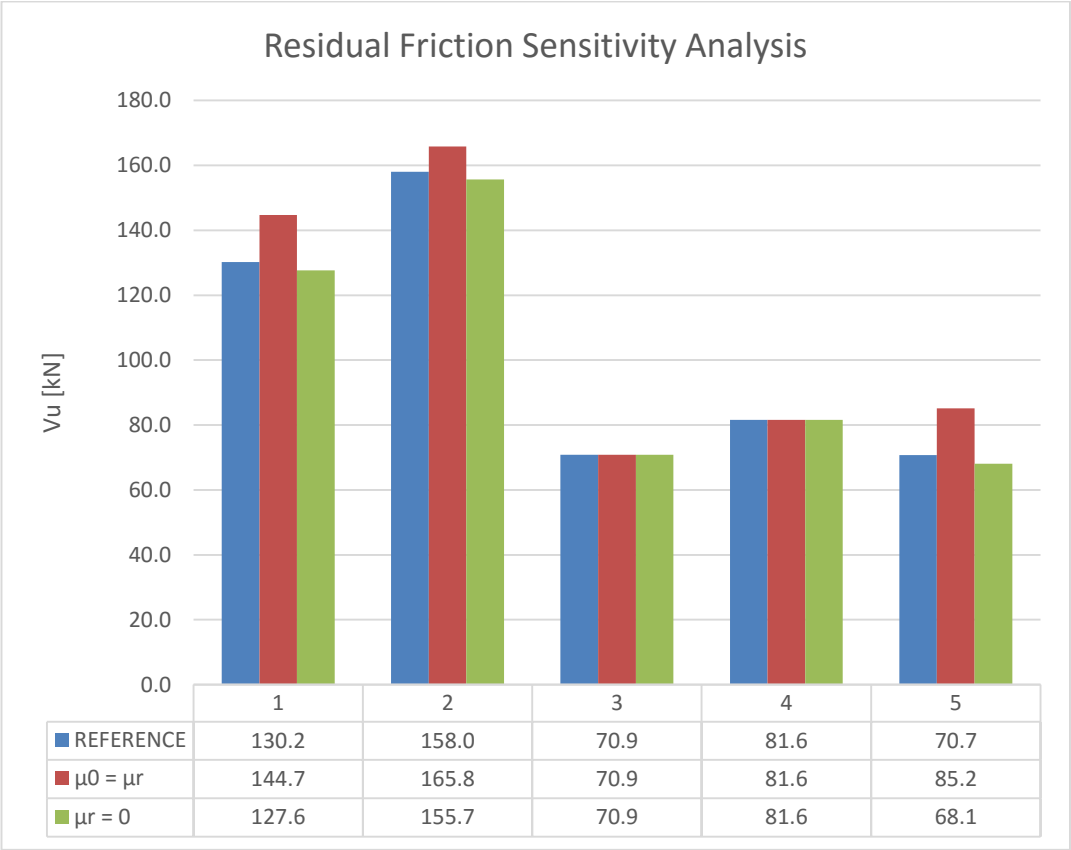

Figure 3.10. Sensitivity analysis for residual friction coefficient

3.7.2 Elastic Modulus sensitivity analysis

A similar analysis as the one performed in section 3.7.1 was carried out for the polystyrene infill elastic modulus (E_p). The range of possible values studied was based on the range of values found in the literature, and is shown below.

$$2.0\ MPa\ \leq E_p \leq 7.0\ MPa$$

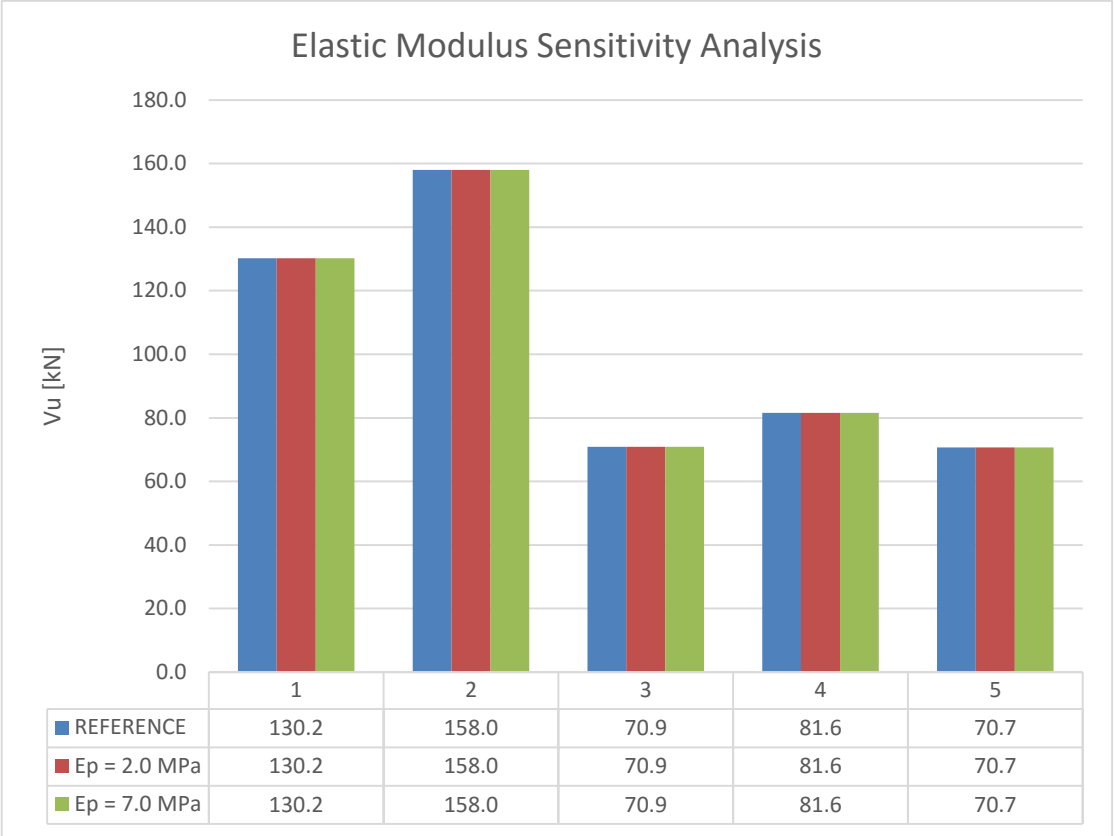

Figure 3.11. Sensitivity analysis for polystyrene elastic modulus

The only failure mechanism affected by this variation is V_{u4}, due to the fact that the contact length between frame and infill depends on the ratio between concrete and polystyrene elastic modulus $\left(\frac{E_c}{E_p}\right)$, as depicted in section 2.3.4.6. However, due to the great flexibility of polystyrene material, the contact length calculated with any of the values in this range exceeds the length of the infill, and therefore the infill length is used instead. For this reason, in the range of interest, polystyrene elastic modulus has no influence in the lateral load resistance of the structure. Having said this, V_{u5} governs the lateral load capacity regardless of the adopted value of E_p, as depicted in *Figure 3.11*.

3.7.3 Concrete compressive strength sensitivity analysis

Variations in the concrete compressive strength are unavoidable, due to the intrinsic nature of the heterogeneous material. The concrete class specification of the frame is C 20/25, and the investigated range of values is shown below.

$$15\ MPa \leq f_{ck} \leq 40\ MPa$$

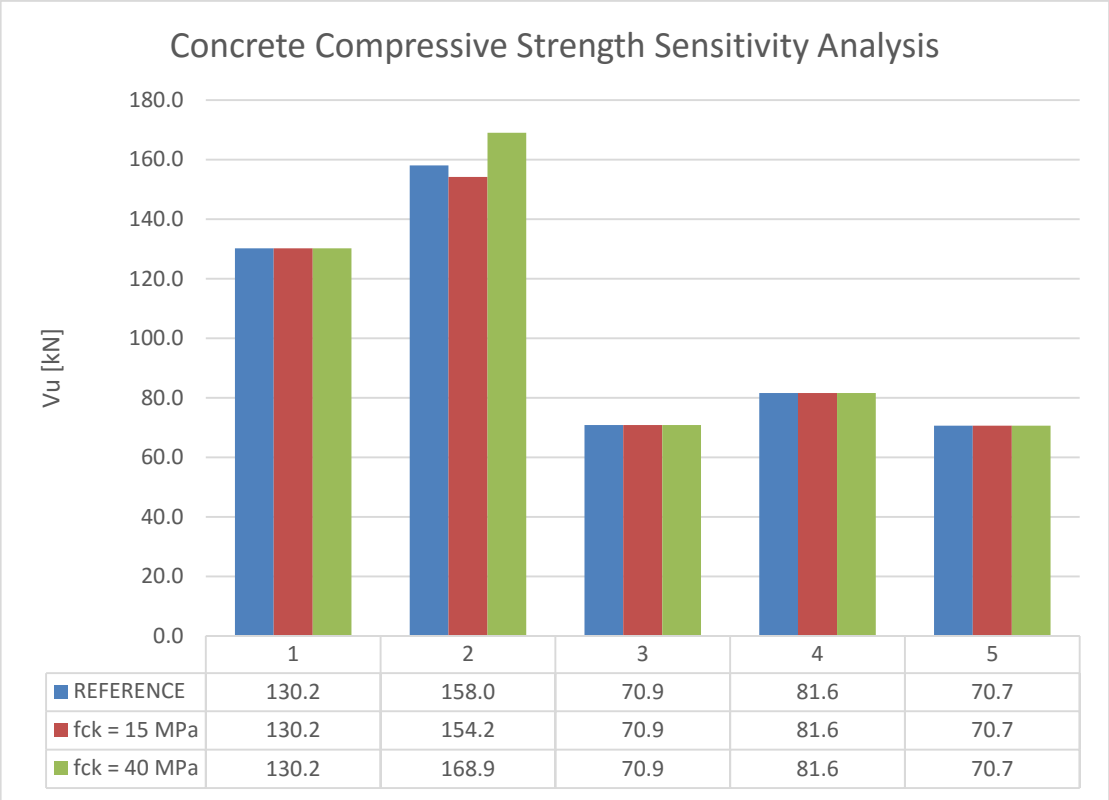

	1	2	3	4	5
REFERENCE	130.2	158.0	70.9	81.6	70.7
fck = 15 MPa	130.2	154.2	70.9	81.6	70.7
fck = 40 MPa	130.2	168.9	70.9	81.6	70.7

Figure 3.12. Sensitivity analysis for concrete compressive strength

From *Figure 3.12* it can be noted that varying the concrete compressive strength only affects V_{u2}, since this mechanism depends on the ultimate shear resistance, which is affected by concrete strength. However, failure mechanism 2 is predominant for very still infills (which is the opposite case from polystyrene infills), and as it can be seen from *Figure 3.12*, the resistance of mechanism 2 is much greater than the rest of the mechanisms, and hence does not govern the global resistance in the range of values here studied. So similarly to the previous case, variation of the concrete compressive strength, although has some influence in V_{u2}, does not have any influence in the final resistance value, since V_{u5} still governs, and does not depend on f_{ck}.

3.7.4 Polystyrene compressive strength sensitivity analysis

Similar to section 3.7.3, the possible variation of polystyrene compressive strength is now studied. The range of values were selected based on the typical values found in the literature, and are presented below.

$$0.1\ MPa \leq f_{pk} \leq 0.2\ MPa$$

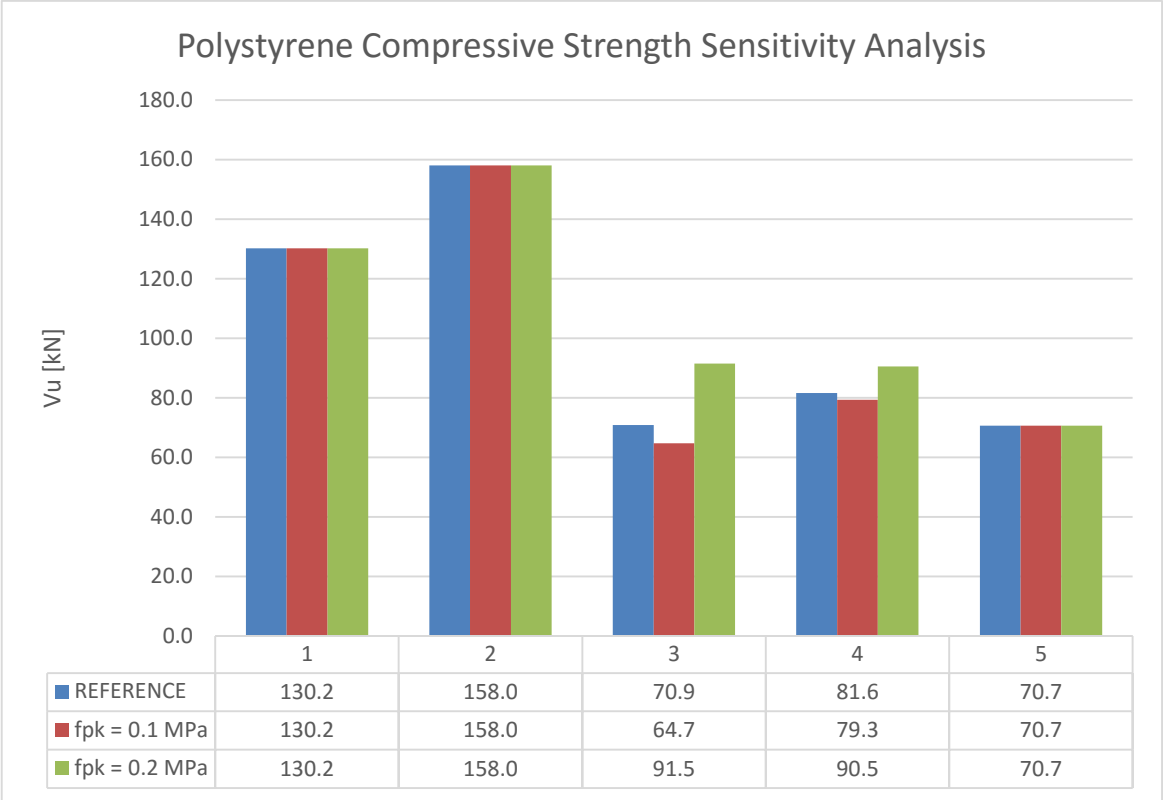

Figure 3.13. Sensitivity analysis for polystyrene compressive strength

From *Figure 3.13*, it's worth pointing out how only failure mechanisms 3 and 4 are influenced by the variation of polystyrene compressive strength. Both these failure mechanisms are very similar, and account for the compressive strength of the infill explicitly, as the infill is assumed to reach the crushing strength along the contact length (*Figure 2.22* and *Figure 2.23*). It is very interesting to see how, for the lower bound values of f_{pk}, failure mechanism V_{u3} starts to govern over V_{u5}. The range of possible values for V_{u3}, V_{u4}, and the global lateral load capacity of the structure (V_u), due to a variation of polystyrene compressive strength, are depicted below.

$$64.7\ kN\ \leq V_{u3} \leq 91.5\ kN$$

$$79.3\ kN\ \leq V_{u4} \leq 90.5\ kN$$

$$64.7\ kN\ \leq V_{u} \leq 70.7\ kN$$

3.7.5 Compressive strut width ratio sensitivity analysis

A similar analysis was carried out in order to determine the influence of the assumed compressive strut width ratio (w/D). From sections 3.2 - 3.6, it can be observed that the compressive strut width is not an explicit input parameter for any of the failure mechanisms

($V_{u,i}$), and therefore V_u does not depend on w/D. The crushing load, however, depends explicitly on w, as depicted in section 2.3.4.2.

$$V_{crush} = wtf_{pk}cos\theta$$

From the above expression, it can be observed that the crushing load has a linear dependence on w. This can also be observed from *Figure 3.14*. The possible range of values investigated is based on previous investigations undergone for masonry infilled walls, as shown in *Figure 2.4*. The extreme values are reported below.

w/D	V_{crush} [kN]
0.05	3.03
0.45	27.3

Table 3-4. Extreme values of the crushing load, according to w/D ratio.

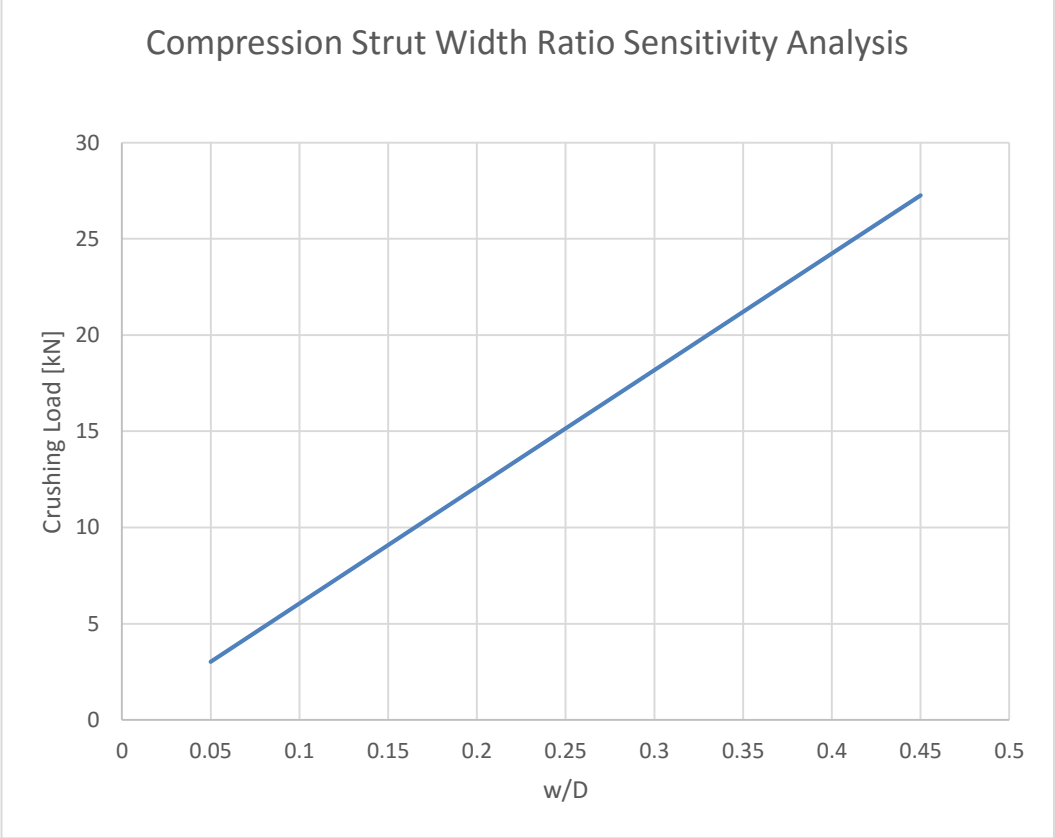

Figure 3.14. Sensitivity analysis for compression strut width ratio on the crushing load

3.7.6 Summary and analysis of results

A summary of the results investigated throughout the current section is proposed below in Table 3-5.

Failure mechanism	REFERENCE	RESIDUAL FRICTION		ELASTIC MODULUS		COMPR. STRENGTH CONC.		COMPR. STRENGTH POLY.	
		$\mu_0 = \mu_r$	$\mu_r = 0$	E_p = 1.9 MPa	E_p = 4.35 MPa	f_{ck} = 15 MPa	f_{ck} = 40 MPa	f_{pk} = 0.1 MPa	f_{pk} = 0.2 MPa
V_{u1} [kN]	130.2	144.7	127.6	130.2	130.2	130.2	130.2	130.2	130.2
V_{u2} [kN]	158.0	165.8	155.7	158.0	158.0	154.2	168.9	158.0	158.0
V_{u3} [kN]	70.9	70.9	70.9	70.9	70.9	70.9	70.9	64.7	91.5
V_{u4} [kN]	81.6	81.6	81.6	81.6	81.6	81.6	81.6	79.3	90.5
V_{u5} [kN]	70.7	85.2	68.1	70.7	70.7	70.7	70.7	70.7	70.7
V_u [kN]	70.7	70.9	68.1	70.7	70.7	70.7	70.7	64.7	70.7

Table 3-5. Sensitivity analysis

From Table 3-5 it is clear to see that, except for high values of the residual friction coefficient, or very low values of polystyrene compressive strength, failure mechanism 5 is always governing the global lateral resistance. As a general statement, the only parameter investigated that affects V_{u5} is the residual friction coefficient, and the only parameter that affects V_{u3} is polystyrene compressive strength. For this reason, these two parameters (μ_r and f_{pk}) are the only mechanical properties which could have some influence on the lateral load resistance of the infilled frame, according to the simplified analytical method proposed in this chapter.

Variation of the Elastic modulus of polystyrene affects only V_{u4}. However, in the range of interest, it has no effect on the final value of this failure mechanism. V_{u4} does not govern the global lateral load resistance of the structure under any of the cases here studied, and therefore, a variation of E_p in the range of interest is not expected to influence the lateral load resistance, according to the simplified analytical method studied in this chapter.

4 FINITE ELEMENT ANALYSIS AND MODELING

Finite element analysis is a very powerful tool for the purpose of structural analysis, broadly used by researchers and designers nowadays, in order to determine stress states, displacements and strains in a very precise way. For this task, MIDAS GEN 2016 (v2.2) was used in order to carry out the pushover analysis of the bare frame and infilled frame. The results obtained from this analysis are meant to be compared with the ones obtained in chapter 3, and ultimately give a reasonable estimate of the failure load, maximum displacement, and expected failure mode of the infilled frame during testing. Finally, SAP2000 was used in order to perform a simple elastic analysis of the frame, and compare these results to the ones obtained with the more refined pushover analysis.

4.1 STARTING ASSUMPTIONS

In order to obtain accurate results, the model must represent the real frame in a precise way. Dimensions of the frame were precisely measured in the lab. Material mechanical properties, as discussed previously, were not precisely measured by tests.

Concrete behavior is built-in to the software, with all the mechanical properties that correspond to the selected concrete class (C 20/25). Reinforcement (longitudinal and transversal) was adequately input to the model as well, in order to carry out the non-linear analysis. Polystyrene, however, is not built-in to the software, and needed to be adequately defined. Due to lack of refined experimental data describing the stress-strain relationship of the material, an initial elastic behavior was assumed, followed by a perfectly plastic relationship.

The supports at the bottom of the columns were modeled as perfectly fixed (zero displacement and rotation at the base). Restraints during the test are such that will ensure this condition not to deviate much from reality.

4.2 RC FRAME

4.2.1 Modeling

First, the reinforced concrete frame was modeled, without any infill, in order to quantify the effect of adding the infill in a latter model. The frame characteristics are depicted in *Figure 4.1* and *Figure 4.2*. The concrete material mechanical properties were assigned in the program, as shown in *Figure 4.3* (a). Once the mechanical properties for the materials have been suitably defined, and the proper dimensions and reinforcement

layout are assigned for beam and columns (*Figure 4.3* (b) and (c)), the frame is then modeled (*Figure 4.4*).

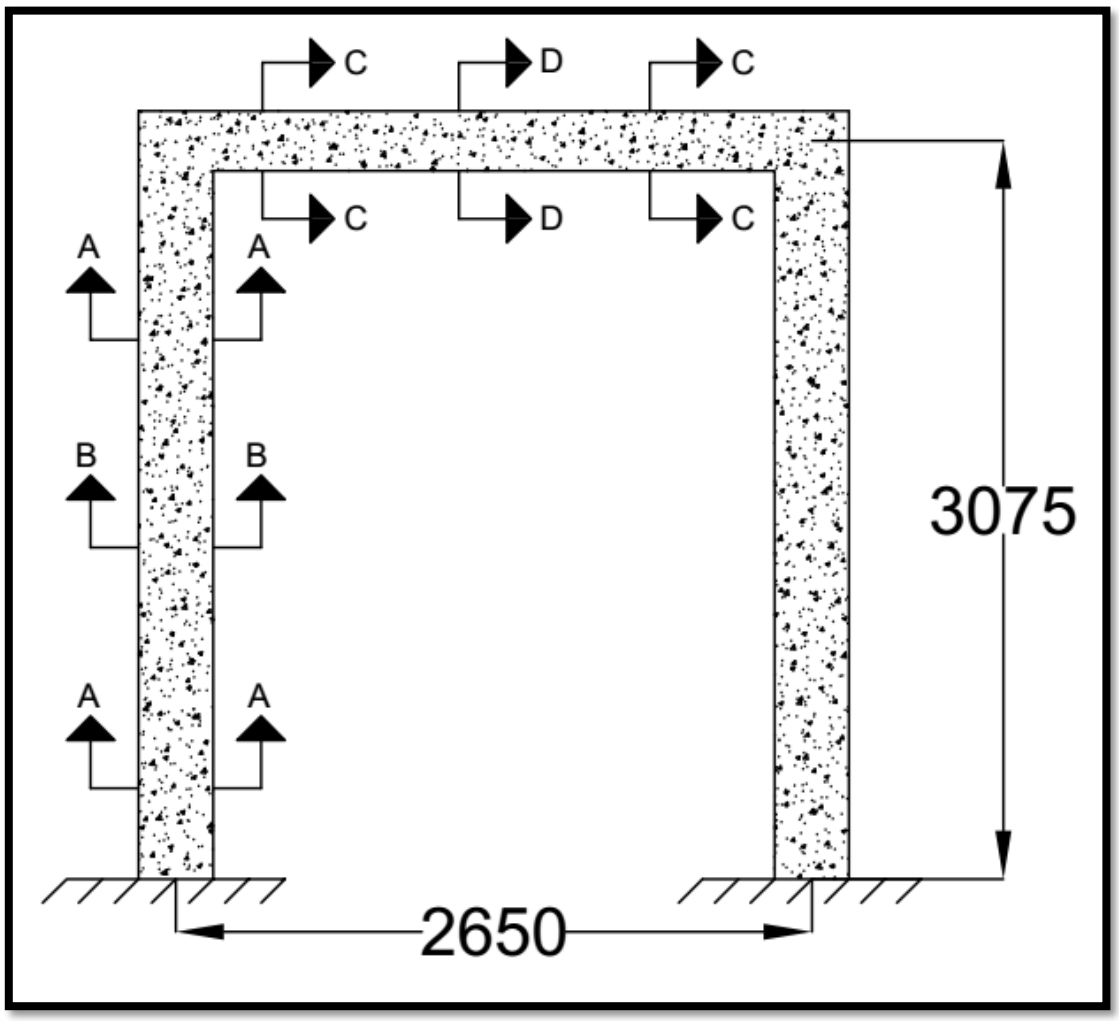

Figure 4.1. Bare frame geometry and layout

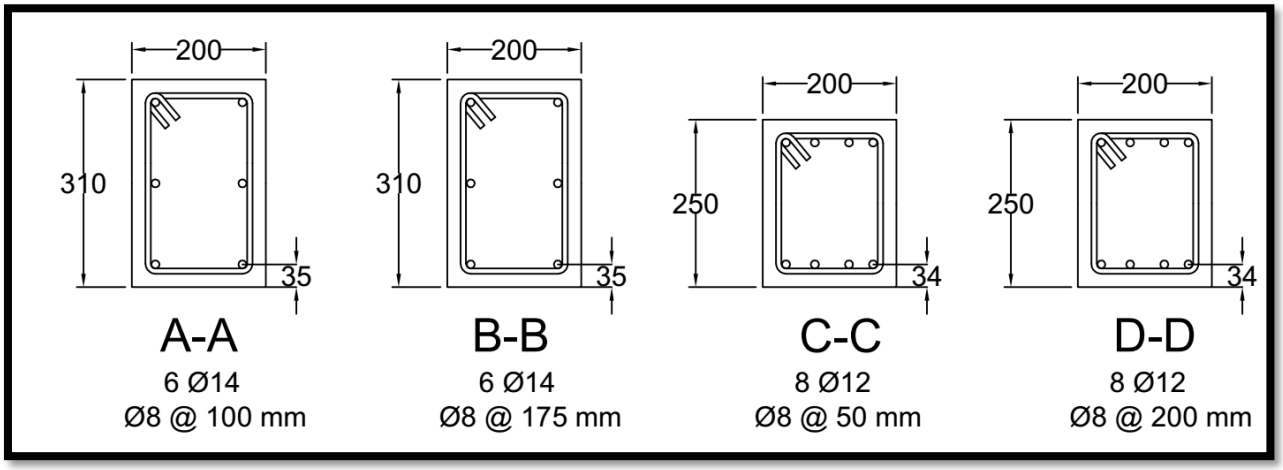

Figure 4.2. Beam and column cross sections and reinforcement layout

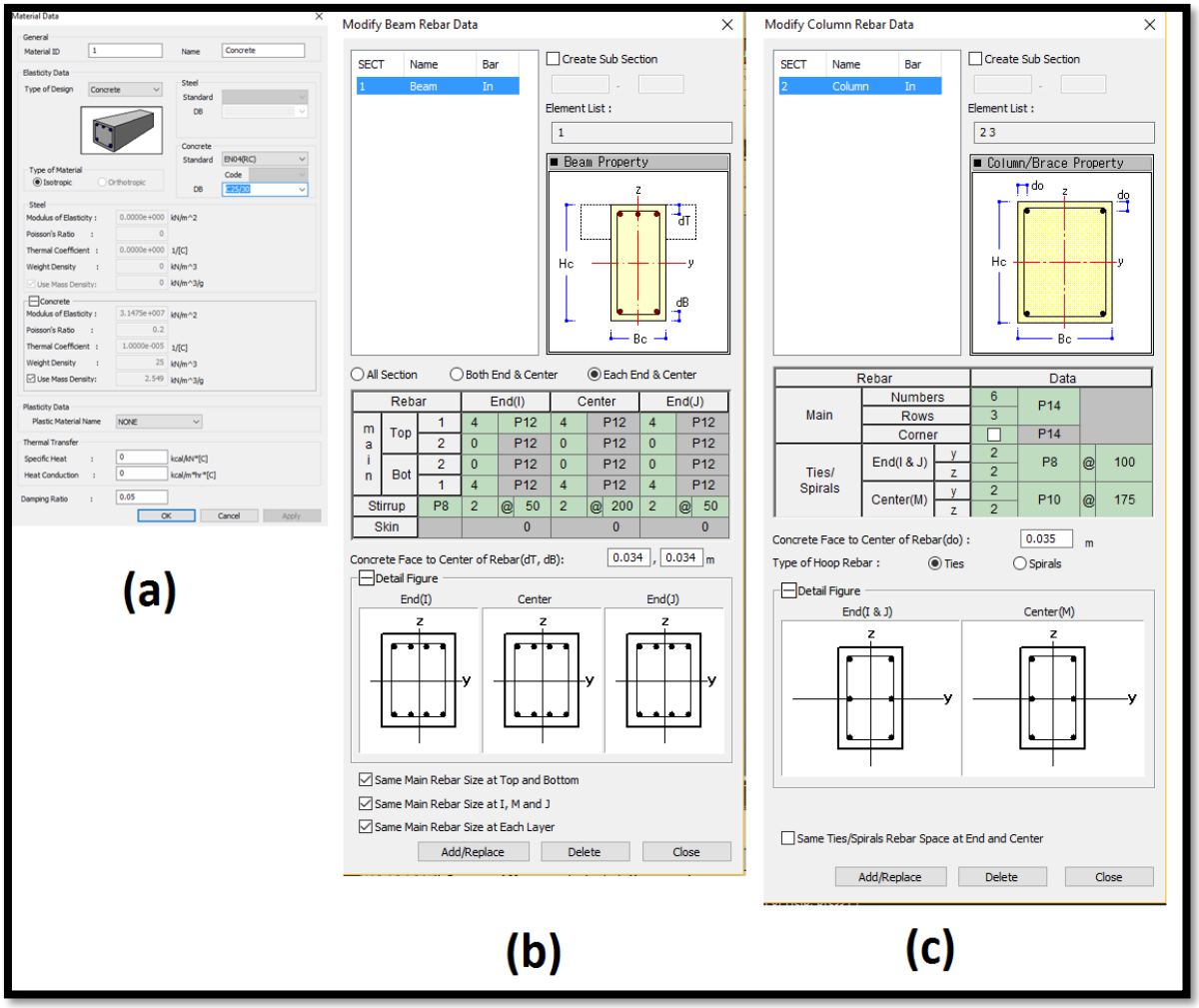

Figure 4.3. Assignment of concrete mechanical properties (a) and steel reinforcement (b) and (c) in MIDAS GEN

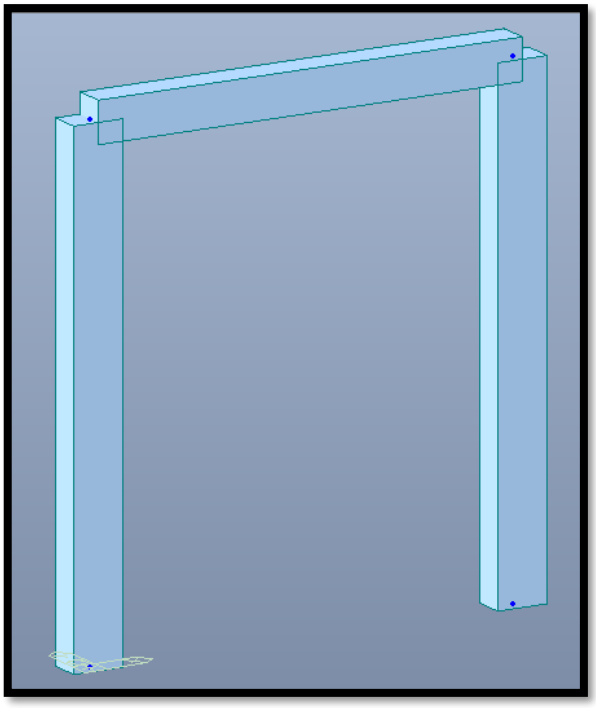

Figure 4.4. Reinforced Concrete Frame model in MIDAS GEN

4.2.2 Pushover Analysis

Once the frame is modeled, a non-linear static analysis (pushover analysis) is performed on the frame structure. A pushover analysis consists basically in subjecting the structure to a monotonically increasing invariant lateral displacement pattern, (displacement of the top left corner of the frame in this case) until an incipient collapse situation is reached. The main output from this analysis is the so called "pushover curve", which describes the load-displacement behavior of the structure under lateral loads, accounting for geometrical and material non-linearities. Midas Gen includes a built-in option which performs this type of analysis, and was used for this research in order to obtain the pushover curve.

Nonlinear behavior is considered in Midas by the lumped plasticity method, which considers two plastic hinges at each end of member (beam or column), where the nonlinear behavior is lumped (1 flexural hinge, and 1 shear hinge, at each end of the member). Due to the nature of the lumped plasticity approach, possible plastic hinge locations must be defined before the pushover analysis is carried out (for this case, possible plastic hinges are defined at both ends of beam and columns), as depicted in *Figure 4.5*.

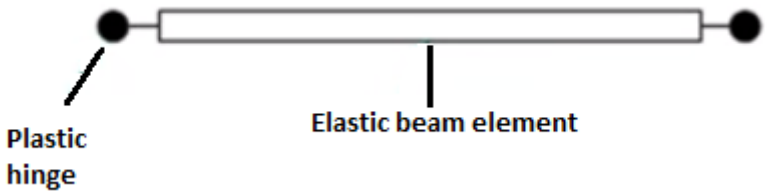

Figure 4.5. Lumped plasticity in beam elements

As mentioned before, each member end has 2 different types of plastic hinges (one for flexure and one for shear). The flexural plastic hinge is described by a moment-rotation behavior, which is elastic up to yielding (A-B branch in *Figure 4.6*), then presents a perfectly plastic behavior (B-C branch in *Figure 4.6*) where it can continue to rotate without taking additional load, until the ultimate rotation, where failure is achieved (point C in *Figure 4.6*). The shear plastic hinge, on the other hand, has a completely different behavior to the flexural hinge, as shear phenomena is brittle by nature, and can't account for any post-elastic resources. Shear hinges are defined by a force-displacement behavior, which is elastic up to failure (*Figure 4.8*). Plastic hinges in columns must account for the interaction between axial force and yield moment (*Figure 4.7*), while axial force interaction is neglected in beam plastic hinges.

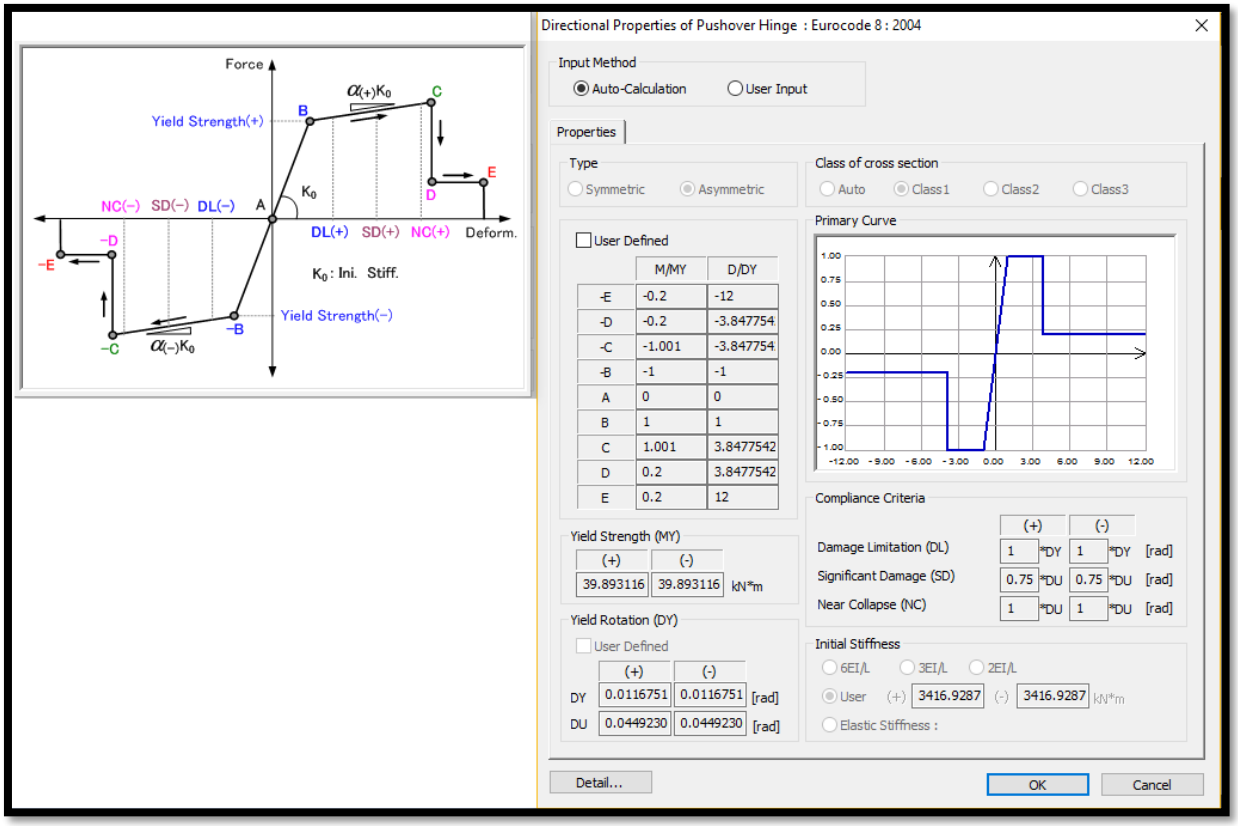

Figure 4.6. Flexural plastic hinge definition for beam in Midas Gen

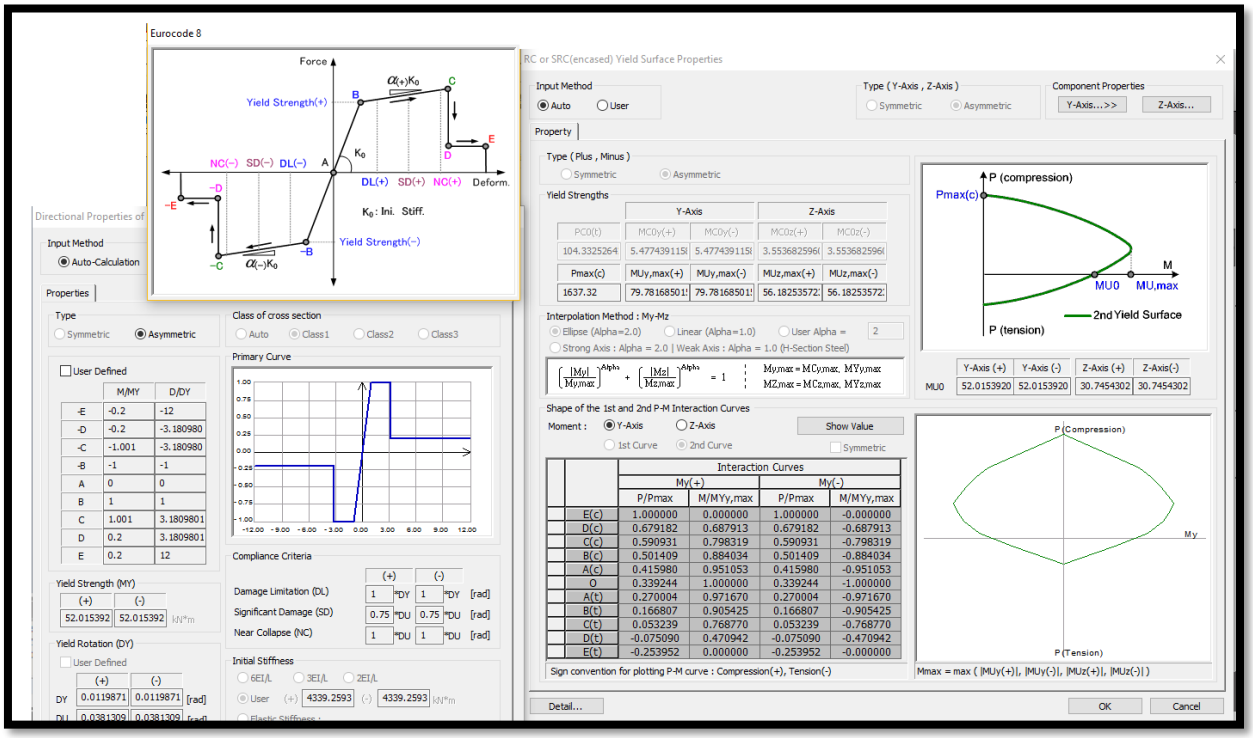

Figure 4.7. Flexural plastic hinge definition for column in Midas Gen

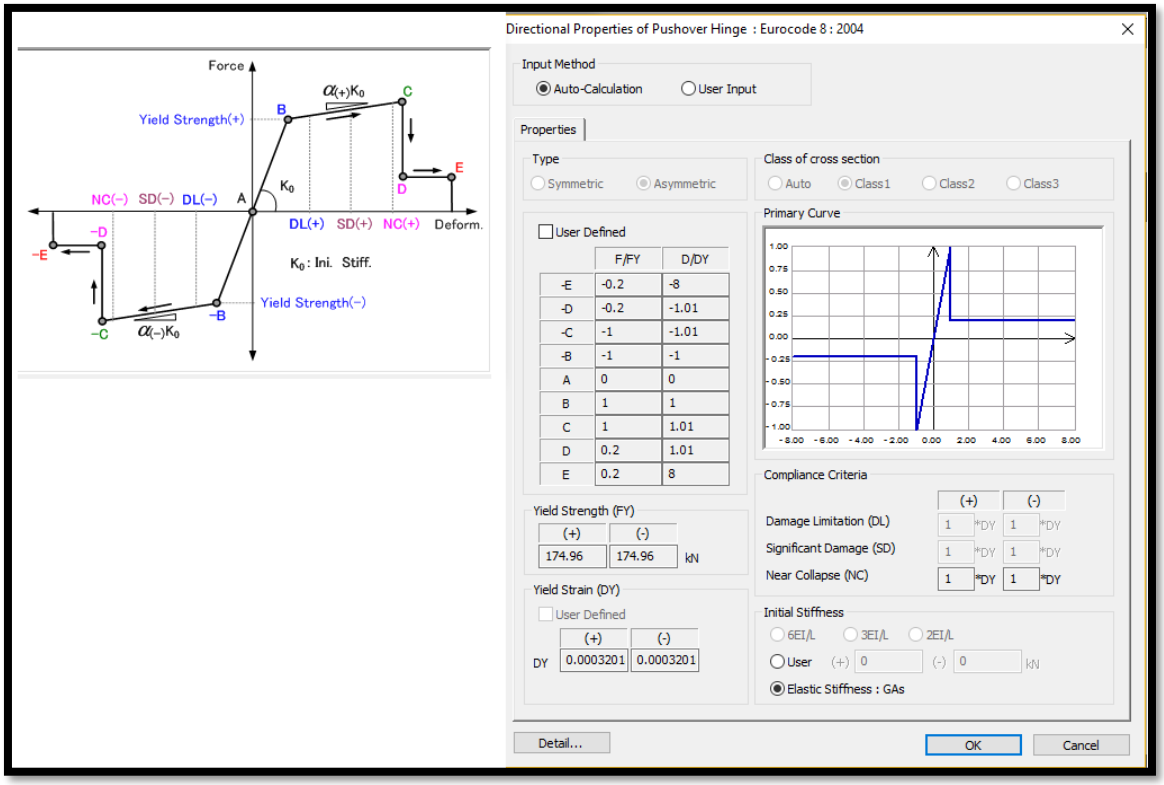

Figure 4.8. Shear plastic hinge definition for beam or column in Midas Gen

Once all the plastic hinge properties have been assigned, the master node is defined (top left corner of the frame). Displacements will be referred to this node, and the load is applied at this location also. Finally, the pushover load case is properly defined, with a maximum displacement of 15cm, and sufficient increment steps in order to ensure convergence (2000 steps were considered for this case). The pushover curve for the bare frame can be seen in *Figure 4.10*. From the curve, a peak load of 59.43 kN is reached at a displacement of 10.80 mm. The maximum displacement, where failure of the structure is achieved, is equal to 119.10 mm.

For a quick check of the cross section capacity, a simple hand calculation was performed on the column and the beam cross sections, neglecting effects of the axial force and compression steel, since they can be considered negligible for this purpose. The calculations are presented below.

1. Column Resisting moment

- Calculation of the neutral axis:

$$A_s \cdot f_y = 0.8 \cdot f_{cd} \cdot b \cdot x$$

$$2 \cdot 308mm^2 \cdot 450MPa = 0.8 \cdot 20MPa \cdot 200mm \cdot x \rightarrow x = 86.63\,mm$$

- Strain at mid layer

Due to the fact that the second layer of the steel is in the middle of the cross section, verification of yielding in steel is performed in this layer.

$$\frac{0.0035}{86.63\ mm} = \frac{0.0035 + y}{155mm} \rightarrow y = 0.00276$$

Where 155mm is the distance from the compressed edge to the mid layer of steel, and "y" is the corresponding strain at that layer.

Since "y" is greater than ε_{sy} = 0.002, the steel at mid layer has yielded.

- Resisting moment:

The resisting moment was calculated about the compressed edge of the cross section as follows:

$$M_{Rd} = 308mm^2 \cdot 450MPa \cdot (275mm + 155mm) - 0.8 \cdot 20MPa \cdot 200mm \cdot 86.63 \cdot \left(\frac{0.8 \cdot 86.63}{2}\right) = 50\ kN \cdot m$$

2. Beam Resisting Moment

- Calculation of the neutral axis:

$$A_s \cdot f_y = 0.8 \cdot f_{cd} \cdot b \cdot x$$

$$4 \cdot 113.1mm^2 \cdot 450MPa = 0.8 \cdot 20MPa \cdot 200mm \cdot x \rightarrow x = 63.62\ mm$$

- Resisting moment:

The resisting moment was calculated about the compressed edge of the cross section as follows:

$$M_{Rd} = 452.39mm^2 \cdot 450MPa \cdot 216mm - 0.8 \cdot 20MPa \cdot 200mm \cdot 63.62mm \cdot \frac{0.8 \cdot 63.62}{2} = 38.79\ kNm$$

After having calculated the capacity of both members, as expected, it can be noted that the column is stronger than the beam in terms of flexural resistance. The flexural capacities obtained by the means of simple hand calculations are in very good agreement with flexural plastic hinge resistance for beams and columns used during pushover analysis, which can be seen in Figure 4.9. The column resistance is also in good agreement with the interaction diagram from *Figure 3.4*, considering no axial load.

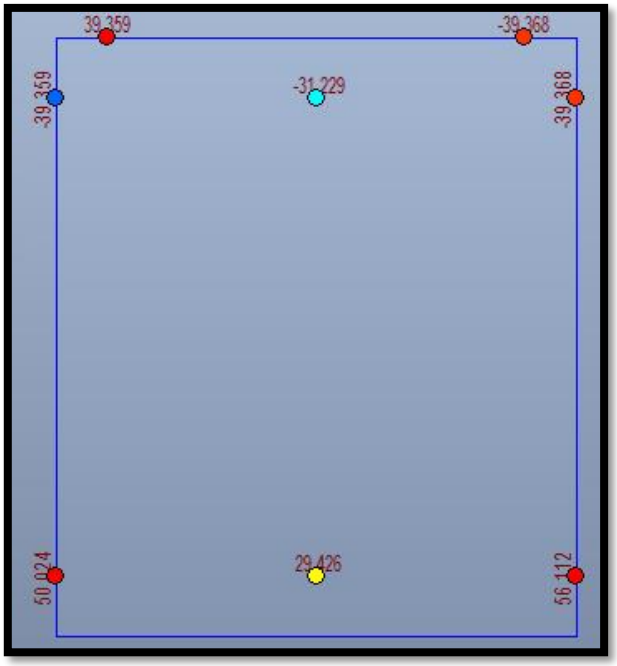

Figure 4.9. Yielding moments at plastic hinges

The pushover curve observed in *Figure 4.10* presents a discontinuous nature. This can be explained by analyzing the failure mode sequence of the frame, which consists of a series of plastic hinge activations, and plastic hinge failures, and are reflected in the curve by the discontinuities in the load-displacement curve, due to the sudden loss of stiffness.

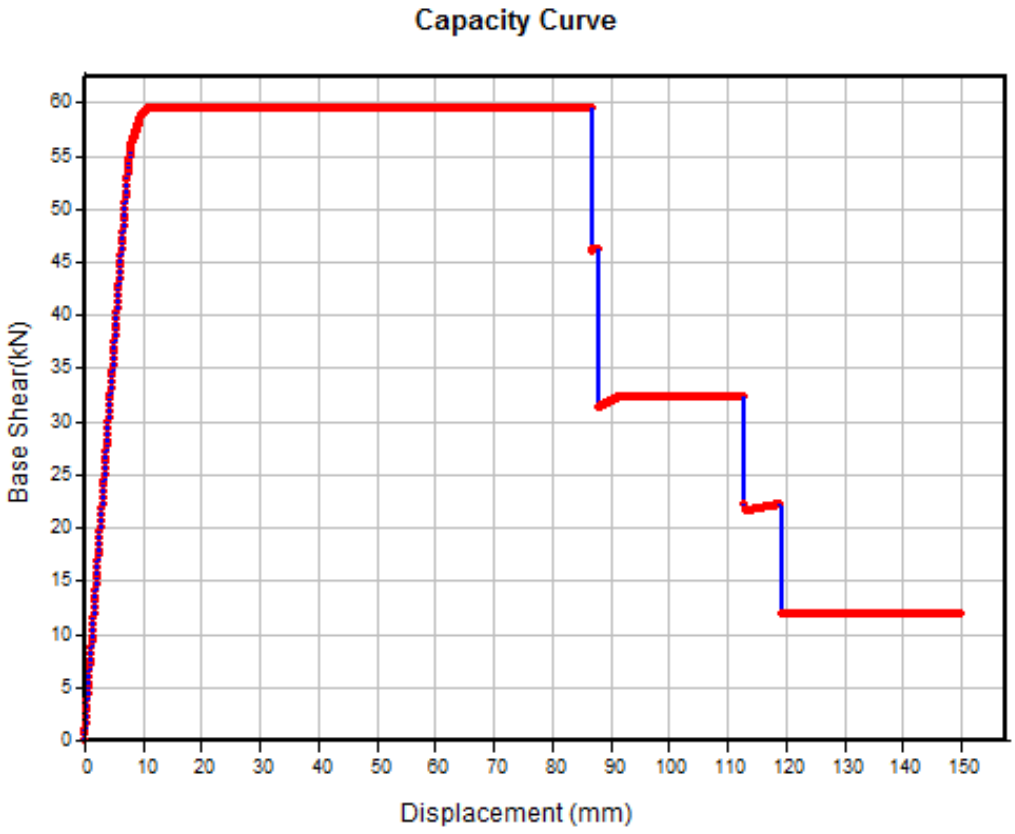

Figure 4.10. Pushover curve for RC Frame Structure

The aforementioned behavior can be understood in a simple way by observing *Figure 4.11* and *Figure 4.12*. In *Figure 4.11* (a) the frame is still within the elastic range (the 6 plastic hinges defined at the ends of beams and columns are blue, which means they are still behaving elastically). The big blue dot in the load-displacement curve below the frame shows the structure's current position, where it can be seen how the frame is still in the elastic range. Then, in *Figure 4.11* (b) the plastic hinge at the base of the windward column has been activated (the plastic hinge has turned green). Similarly, *Figure 4.11* (c) shows the moment when the plastic hinge is activated at the base of the leeward column. *Figure 4.12* (a) and (b) show the moment of activation of plastic hinges on the beam ends. At this point, the frame has yielded and cannot take any more load, but it can still continue to deform, because of the ductile nature of the flexural plastic hinge.

After the long horizontal branch in the load-displacement curve, *Figure 4.12* (c) shows the moment when the first plastic hinge reaches failure (at the base of the windward column), and the plastic hinge has turned red. Finally, *Figure 4.12* (d), (e) and (f) show the moment when the other three plastic hinges reach failure, represented as discontinuities in the load-displacement curve.

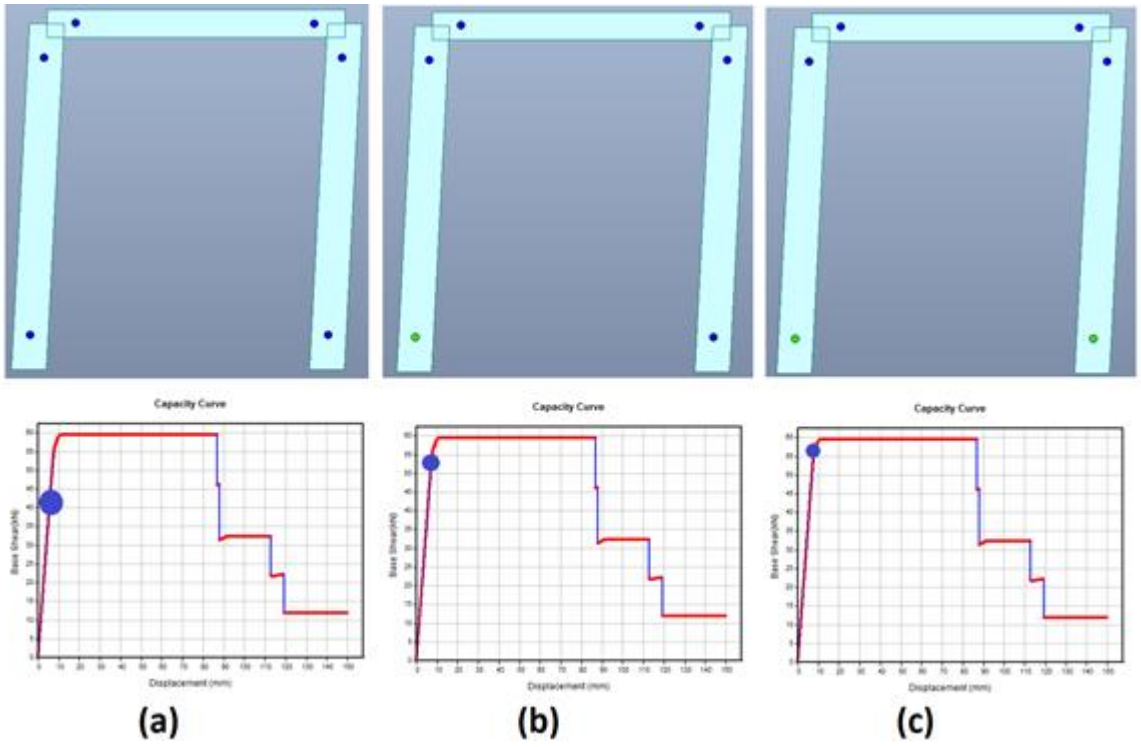

Figure 4.11. Pushover analysis plastic hinge sequence for bare frame

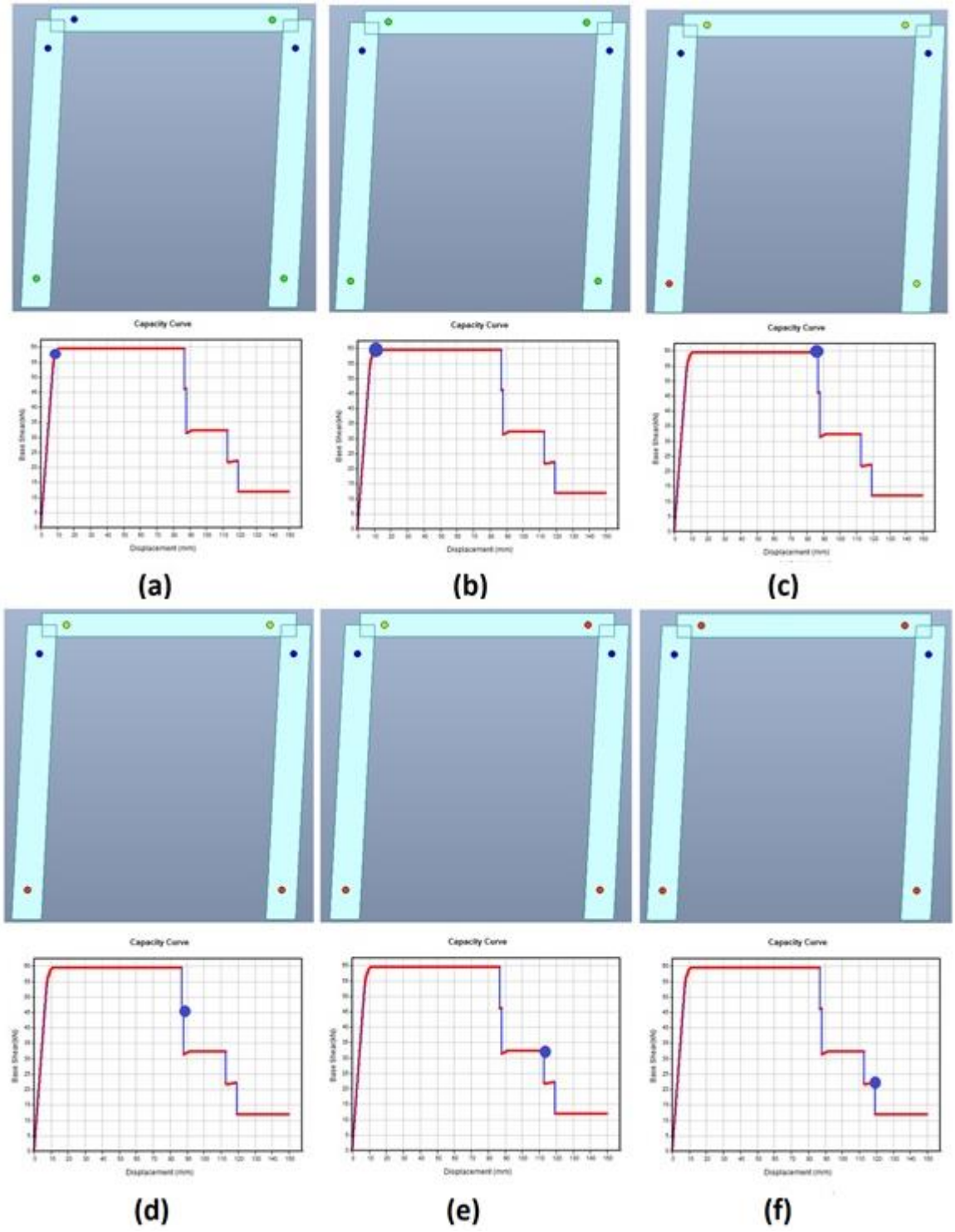

Figure 4.12. Pushover analysis plastic hinge sequence for bare frame

Failure of the structure is achieved when 4 plastic hinges are activated, as depicted in *Figure 4.12* (f). It's worth mentioning that the top sections of the columns are still behaving elastically at the point of failure, and never achieve yielding. The most relevant results from the capacity curve in *Figure 4.10* are presented in Table 4-1

Bare frame	1st yield load [kN]	52.69
	Displacement at 1st yield [mm]	7.28
	2nd yield load [kN]	55.95
	Displacement at 2nd yield [mm]	8.03
	3rd yield load [kN]	58.73
	Displacement at 3rd yield [mm]	9.68
	4th yield load [kN]	59.43
	Displacement at 4th yield [mm]	10.80
	1st hinge failure load [kN]	59.43
	Displacement at 1st hinge failure [mm]	86.70
	2nd hinge failure load [kN]	46.27
	Displacement at 2nd hinge failure [mm]	87.9
	3rd hinge failure load [kN]	32.37
	Displacement at 3rd hinge failure [mm]	112.88
	4th hinge failure load [kN]	22.13
	Displacement at 4th hinge failure [mm]	119.1
	Maximum Load [kN]	59.43
	Maximum Displacement [mm]	119.10
	Ductility $\left(\frac{\delta_y}{\delta_u}\right)$	16.36

Table 4-1. Bare frame capacity curve most relevant results

4.3 POLYSTYRENE INFILL

4.3.1 Modeling

Polystyrene material was defined at this stage, in order to include the infill to the previous model, with the properties reported in Table 4-2 which are the same values used in chapter 3. *Figure 4.13* shows the assignment of polystyrene mechanical properties in MIDAS GEN.

Uniaxial yield strength	0.1 MPa
Initial elastic modulus	4.35 MPa
Poisson's ratio	0.01
Weight density	10.4 MPa

Table 4-2. Polystyrene mechanical properties

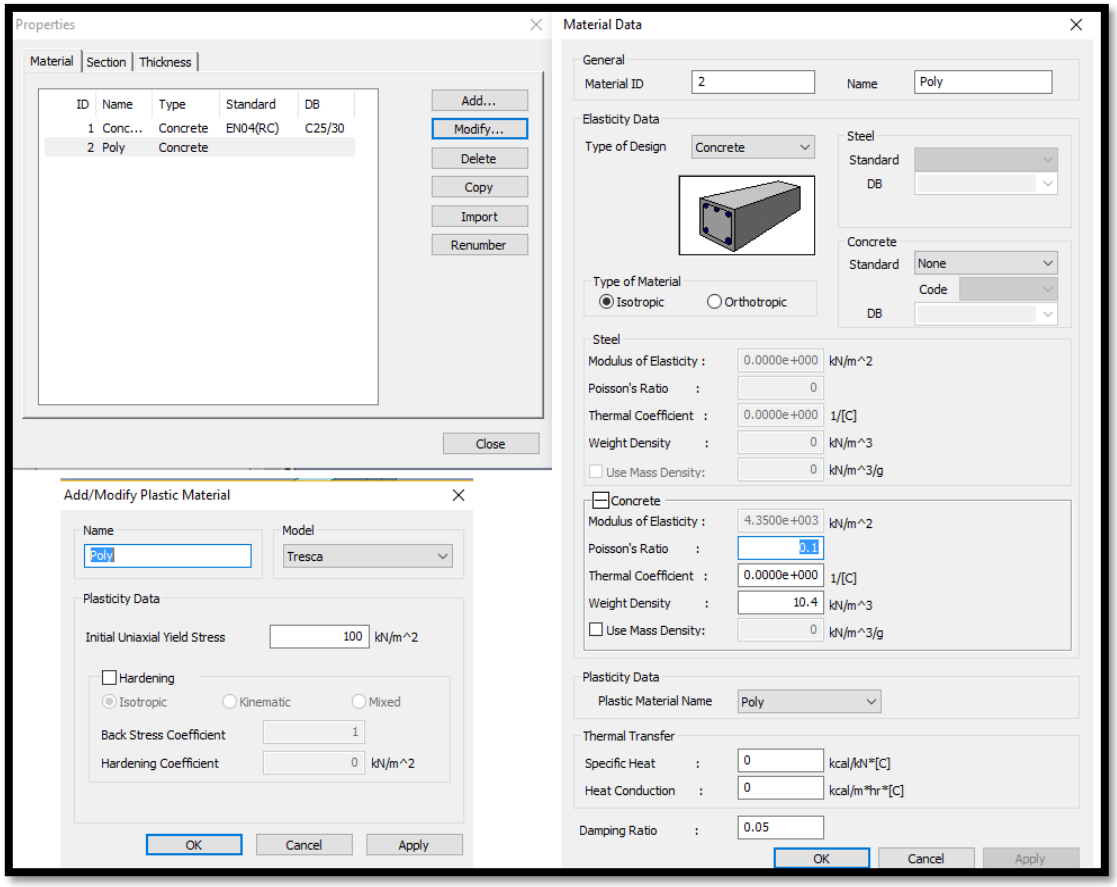

Figure 4.13. Definition of polystyrene material in MIDAS GEN

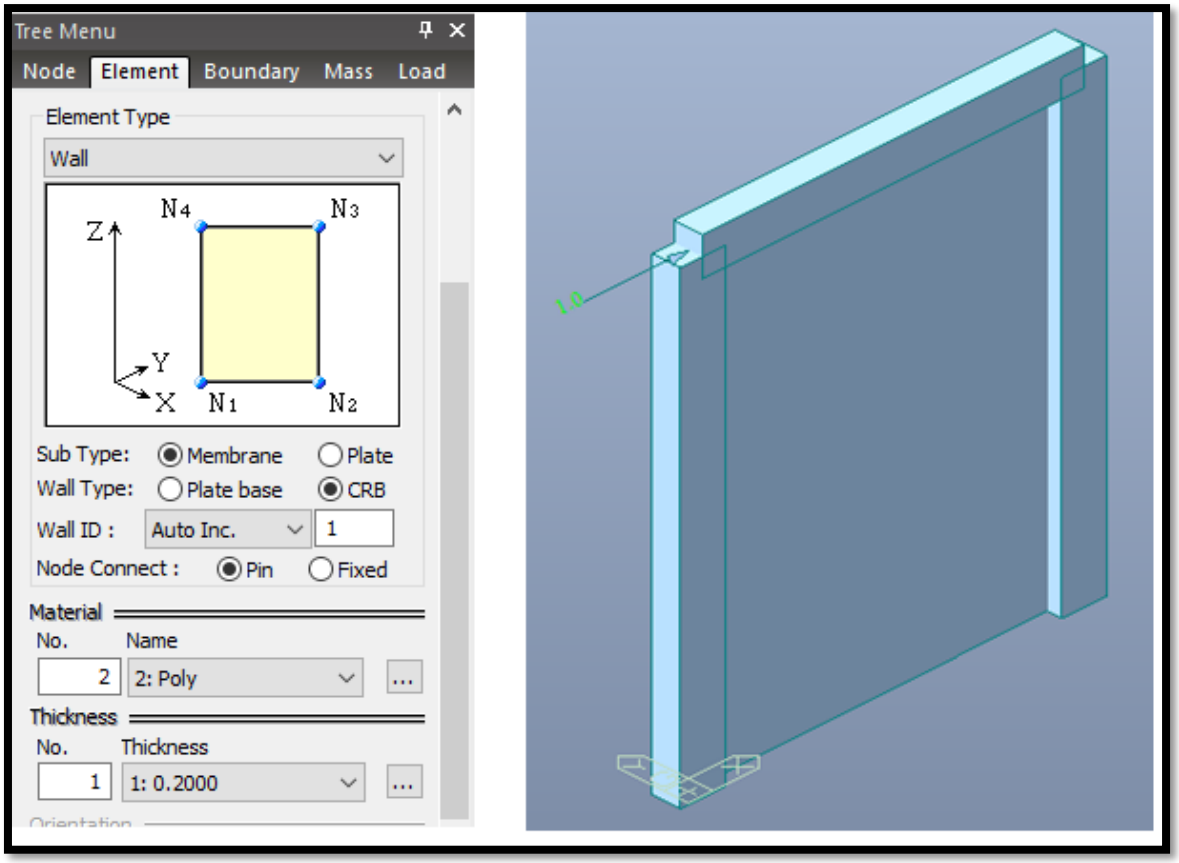

Figure 4.14. Infilled frame model in MIDAS GEN

Once the material has been defined, 0.2m thick Concrete Retaining Block (CRB) wall elements are defined, using membrane sub type elements, which are placed within the frame used in *Figure 4.4*. The new model is shown in *Figure 4.14*. In order to carry out the pushover analysis, reinforcement needs to be assigned to the wall (even though it has none). For this reason, a fictitious reinforcement layout of $2\phi 4 \, @ \, 1000 \, mm$ is chosen is both directions, just in order to be able to carry out the analysis, which corresponds to a reinforcement ratio of 0.0126%, which is extremely low.

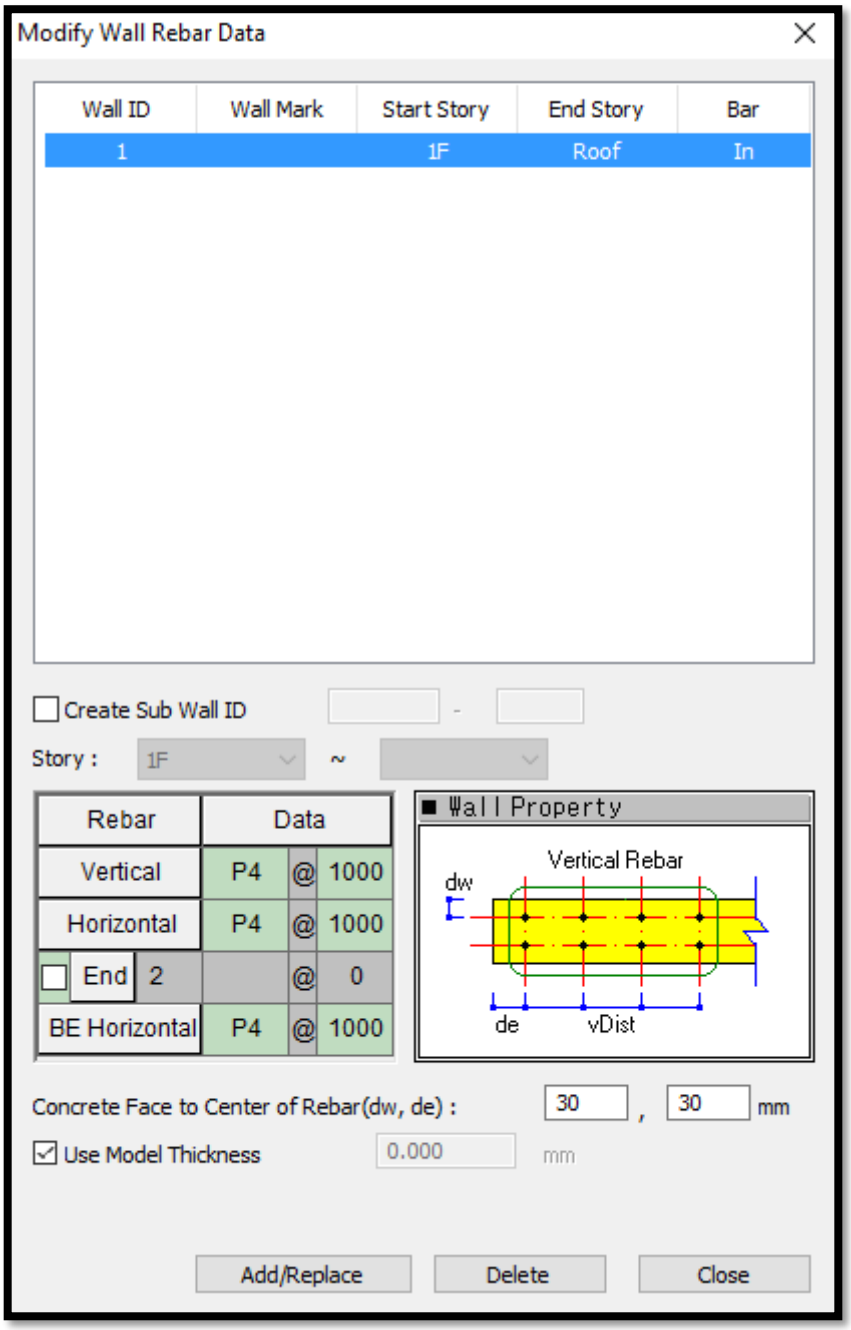

Figure 4.15. Fictitious wall reinforcement layout

4.3.2 Pushover Analysis

A similar analysis to the one performed in section 4.2.2 was carried out for this model, with the only difference that, in this case, the infill is present in the model, instead of performing the pushover analysis on the bare frame. One additional plastic hinge needed to be defined and then assigned to the top and bottom of the infill, as depicted in *Figure 4.16* and *Figure 4.17*. The pushover curve for the infilled frame is shown in *Figure 4.18*.

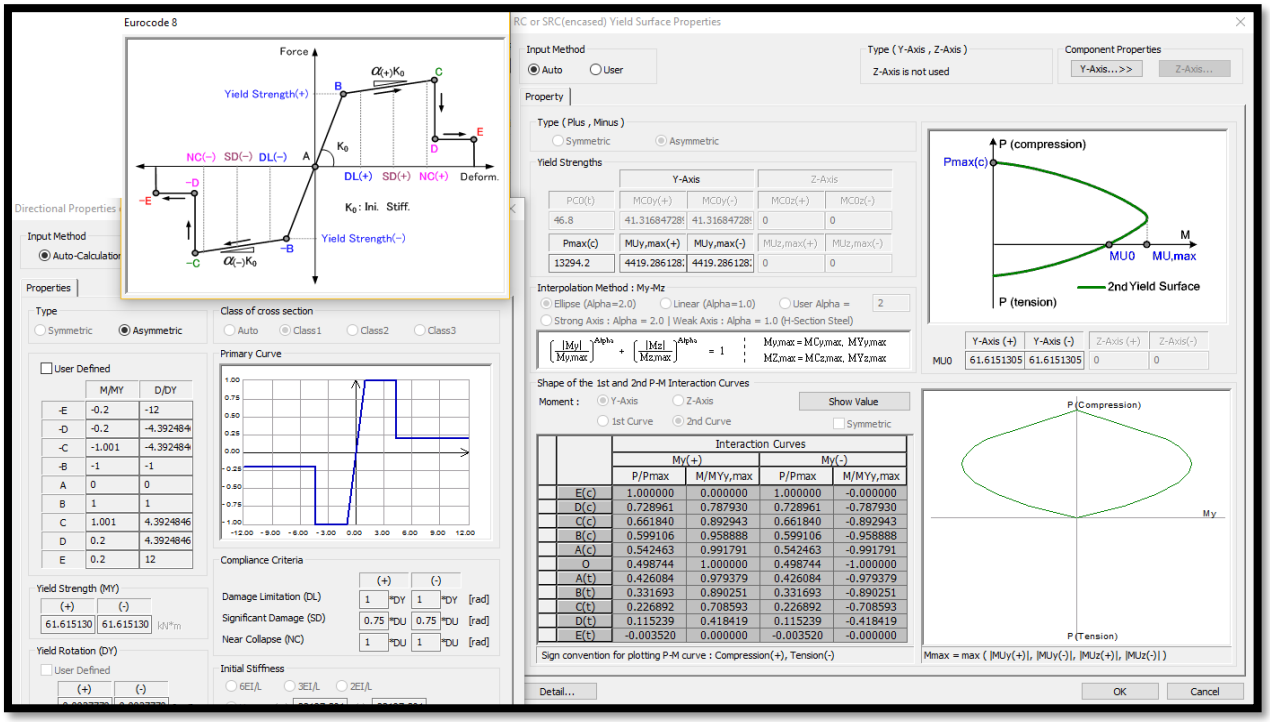

Figure 4.16. Wall flexural plastic hinge definition in Midas Gen

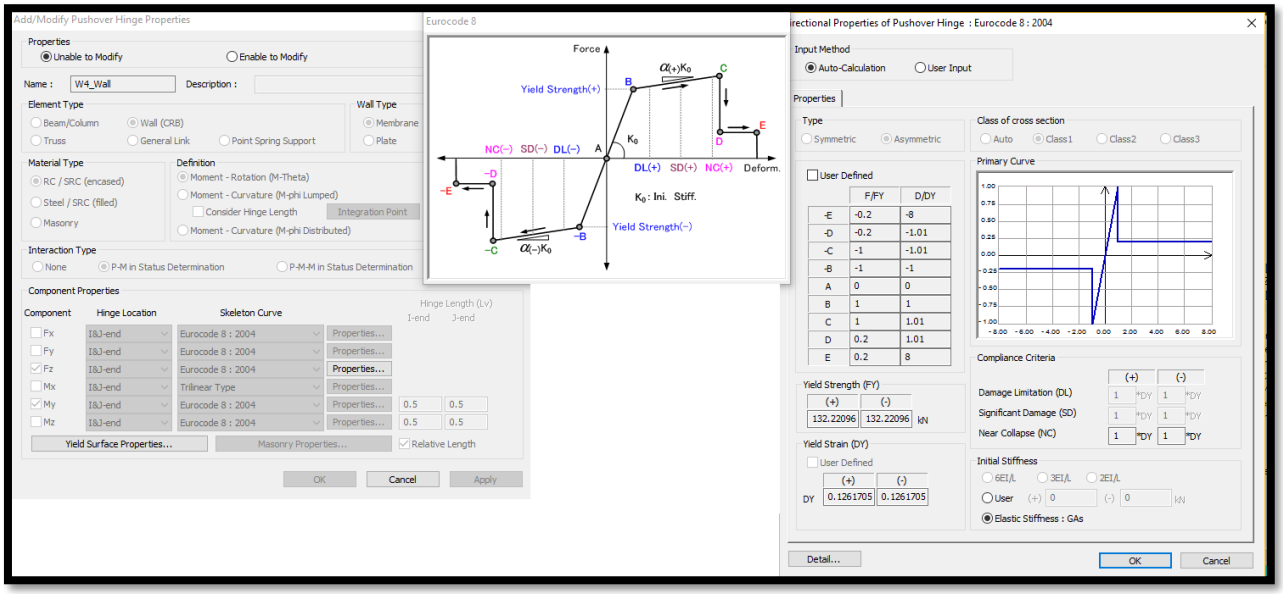

Figure 4.17. Wall shear plastic hinge definition in Midas Gen

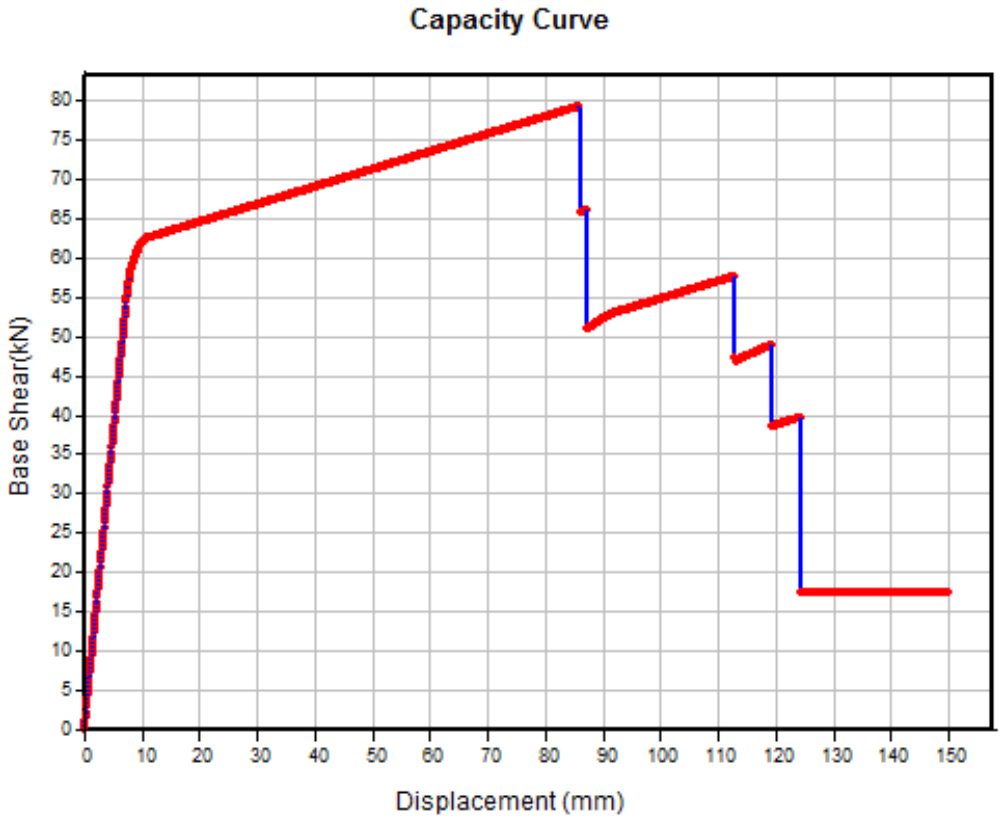

Figure 4.18. Pushover curve for infilled frame structure

From *Figure 4.18* it is worth noticing how the initial behavior of the infilled frame is quite similar to the one in *Figure 4.10*, of the bare frame, with a very similar yield strength, displacement and stiffness. The structure has an initial elastic behavior (*Figure 4.19* (a)). After the first plastic hinge yielding (*Figure 4.19* (b)), the structure continues to take load, with a reduced stiffness. *Figure 4.19* (c), (d) and (e) show the activation of the next 3 plastic hinges. At this point, the frame structure has achieved yielding and cannot continue to take additional load. Therefore, the only component which is still able to take more load is the infill, which is still behaving elastically up to this point.

After activation of the 4 plastic hinges on the frame, the structure continues to take additional load, with a significantly reduced stiffness, up until the first plastic hinge failure on the windward column (*Figure 4.19* (f)), where the maximum load is achieved (79.24 kN). After the sudden drop, the structure continues to take additional load, with a constant stiffness, up until the failure of the second plastic hinge (*Figure 4.20* (a)), where there is a second sudden drop in the load-displacement curve. Similarly, the structure continues to take additional load, with constant stiffness, and sudden drops where plastic hinges achieve failure (*Figure 4.20* (b) and (c)). After the fourth plastic hinge has failed, the infill still

behaves elastically. The structure is able to reload until reaching failure of the top plastic hinge of the infill, in shear, as depicted in *Figure 4.20* (d). Due to the fact that the failure of the last plastic hinge is in shear, there is no ductile behavior at the end, and the failure occurs in a brittle way. At this point, the structure has achieved failure, at a maximum displacement of 119.18 mm. The most relevant results of the capacity curve from *Figure 4.18* are presented in Table 4-3. A comparison of both capacity curves is proposed in *Figure 4.21*.

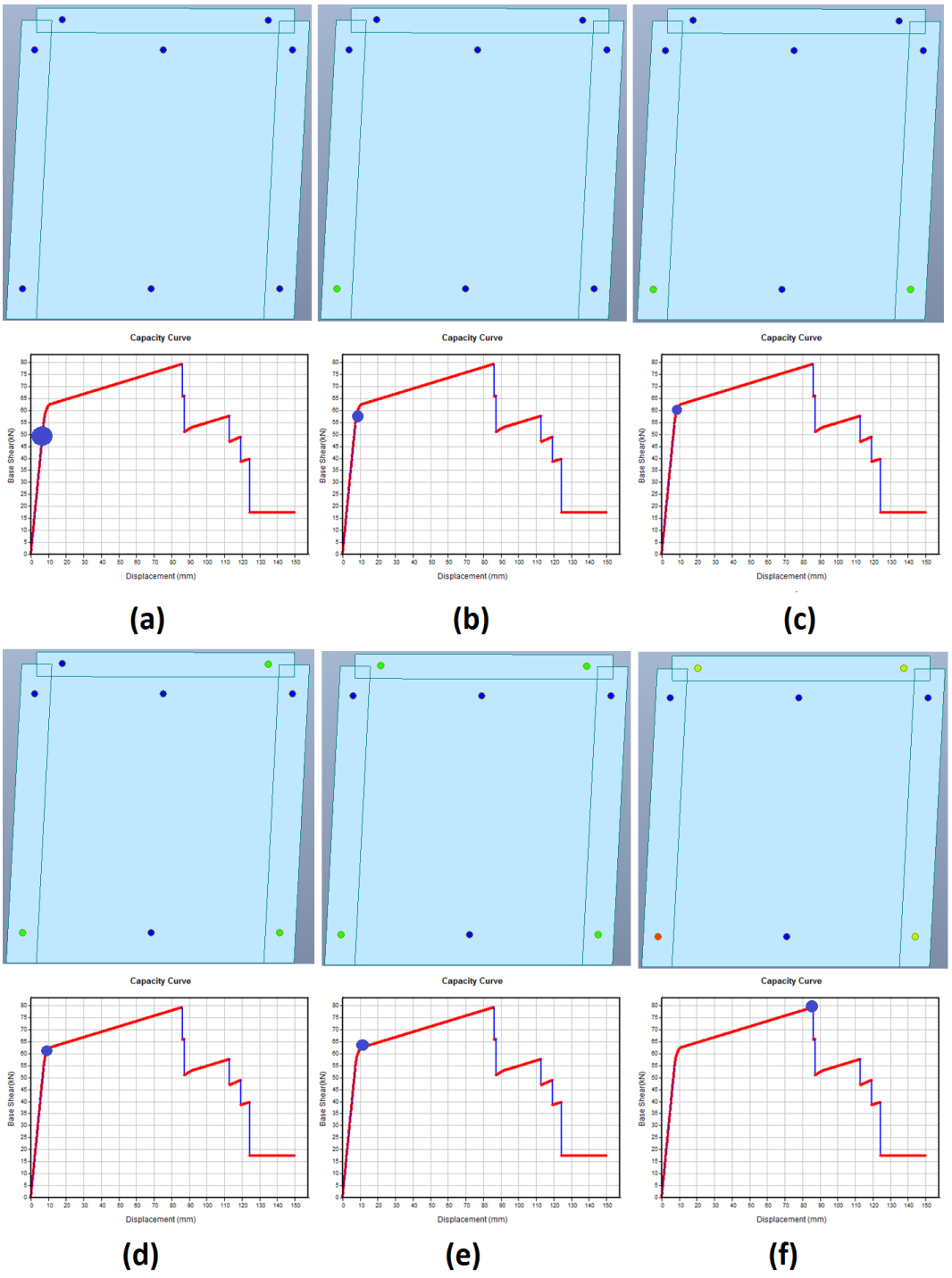

Figure 4.19. Pushover analysis plastic hinge sequence for infilled frame

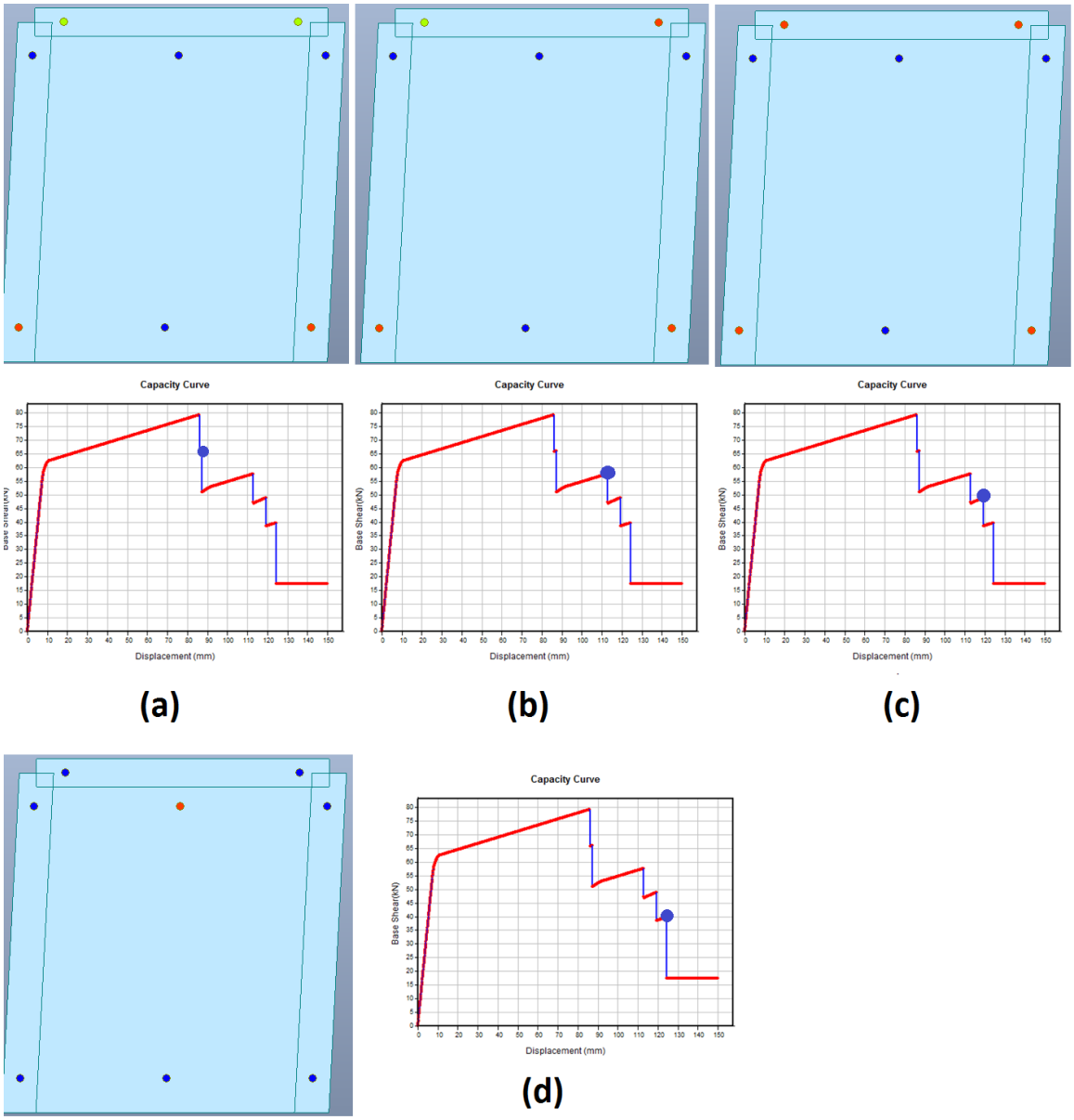

Figure 4.20. Pushover analysis plastic hinge sequence for infilled frame

Infilled frame	1st yield load [kN]	54.85
	Displacement at 1st yield [mm]	7.35
	2nd yield load [kN]	58.75
	Displacement at 2nd yield [mm]	8.18
	3rd yield load [kN]	61.53
	Displacement at 3rd yield [mm]	9.6
	4th yield load [kN]	62.4
	Displacement at 4th yield [mm]	10.65
	1st hinge failure load [kN]	79.24
	Displacement at 1st hinge failure [mm]	85.95
	Load increase [kN]	16.84
	2nd hinge failure load [kN]	66.10
	Displacement at 2nd hinge failure [mm]	87.23
	Load increase [kN]	0.46
	3rd hinge failure load [kN]	57.62
	Displacement at 3rd hinge failure [mm]	112.88
	Load increase [kN]	6.71
	4th hinge failure load [kN]	48.78
	Displacement at 4th hinge failure [mm]	119.18
	Load increase [kN]	1.18
	5th hinge failure load [kN]	39.60
	Displacement at 5th hinge failure [mm]	124.28
	Load increase [kN]	1.04
	Total load absorbed by infill [kN]	26.23
	Maximum Load [kN]	79.24
	Maximum Displacement [mm]	119.18
	Ductility $\left(\frac{\delta_y}{\delta_u}\right)$	16.21

Table 4-3. Infilled frame capacity curve most relevant results

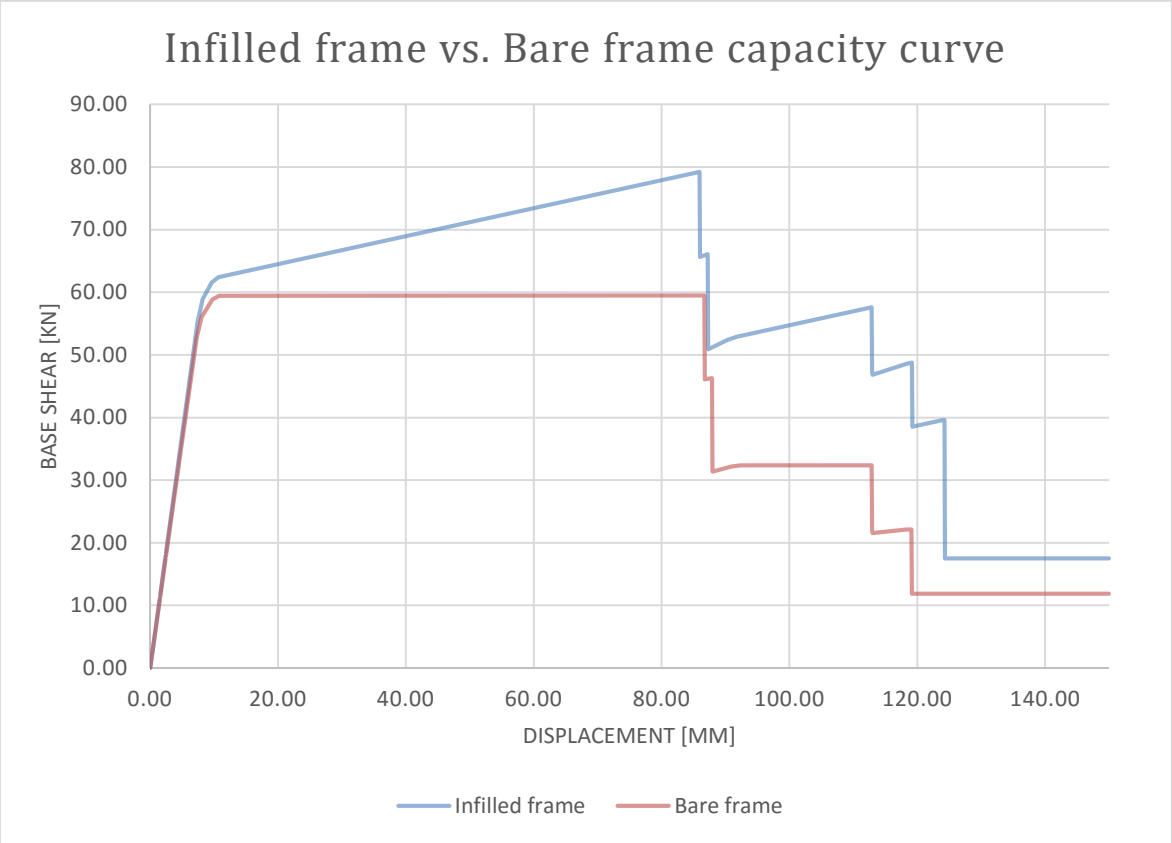

Figure 4.21. Comparison between infilled frame and bare frame capacity curves

4.4 ELASTIC MODEL WITH COMPRESSION STRUT

Another topic of interest for this investigation is the applicability of simplified methods for analysis (macro-models), instead of refined and more advanced approaches such as finite element analysis (micro-models). The use of an equivalent compression strut model for the analysis of masonry infilled RC frames under lateral load has been widely investigated and used in past years. The width of the equivalent strut, however, has been a topic of discussion and has several different approaches, as seen before in *Figure 2.4*. This section is dedicated to the development of a similar approach for polystyrene infilled RC frames under lateral load, using similar width-to-length ratios for the compressive strut, and comparing these results to the ones obtained by finite element analysis.

4.4.1 Modeling

Due to the fact that the purpose of this investigation is focused on simplified tools for analysis, a simple elastic approach is proposed, using 3 frame (Bernoulli beam) elements for the beam and columns, and a truss element for the equivalent compression strut, considering the elastic properties for each material accordingly (Table 4-2 for polystyrene

properties, and the built in properties for C 20/25 concrete in the software). Two elastic models were carried out, in parallel, using the SAP2000 software: one for the frame with equivalent compression strut, and another one for the bare frame, as shown in *Figure 4.22* (a) and *Figure 4.22* (b) respectively. The reason for the latter model, is to use it as reference, in order to quantify the effect of adding the compression strut. It is also useful to compare it to the results obtained in section 4.2 for the bare frame.

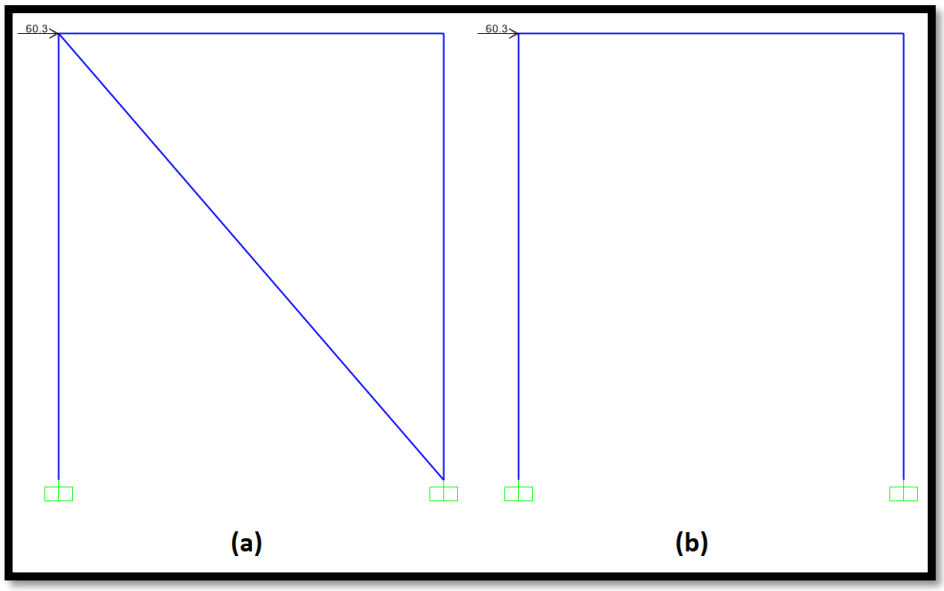

Figure 4.22. Elastic models of infilled frame with equivalent compression strut (a) and bare frame (b) in SAP2000

4.4.1.1 Bare Frame

From Table 4-1, it can be observed that the first yielding, corresponding to the base of the columns, occurs at a load equal to 52.69 kN. The internal actions on the frame, under a horizontal load of 52.69 kN, are depicted in *Figure 4.23*.

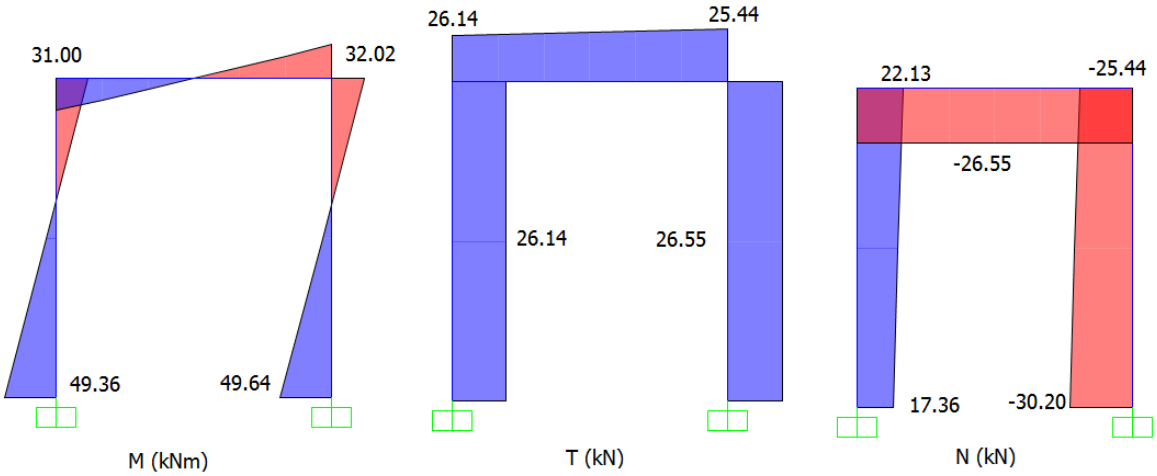

Figure 4.23. Internal actions diagrams for frame under 52.69 kN lateral load

After this first plastic hinge activation, the internal actions are "frozen", and an auxiliary structure is analyzed. This auxiliary structure can be idealized as the same frame having a hinge at the bottom section of the windward column, where the plastic hinge has been activated, and it can keep taking an additional 3.26 kN lateral load under the new structural scheme. Now, a third auxiliary structure is analyzed, with 2 plastic hinges, one at the base of each column, and with a horizontal load equal to 2.78 kN. Finally, a third auxiliary structure is analyzed, with one additional plastic hinge on the right hand side of the beam, and a horizontal load equal to 0.7 kN. At this point, the structure's internal actions are computed for the first model, and the three auxiliary models, and the actions are summed in order to obtain the final internal action diagrams.

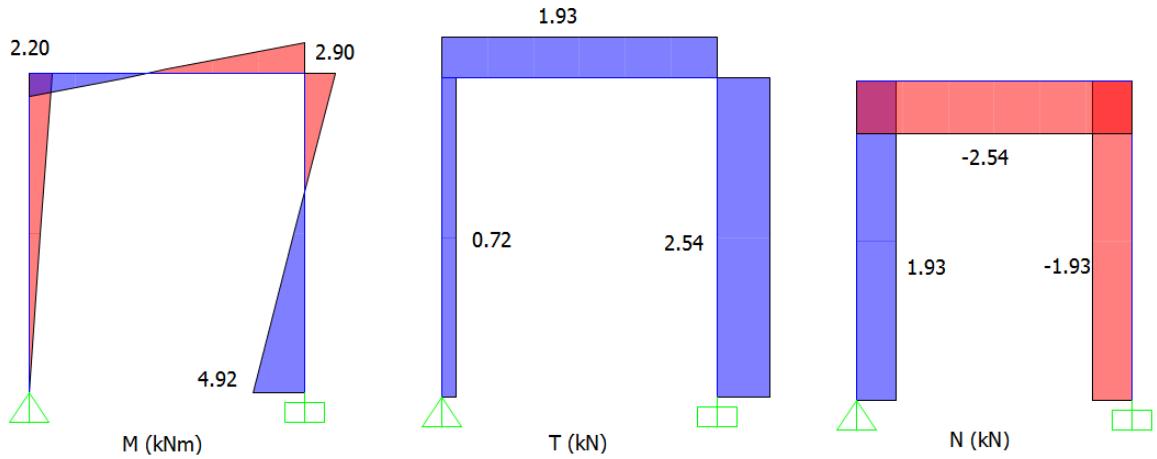

Figure 4.24. Internal actions diagrams for auxiliary structure 1

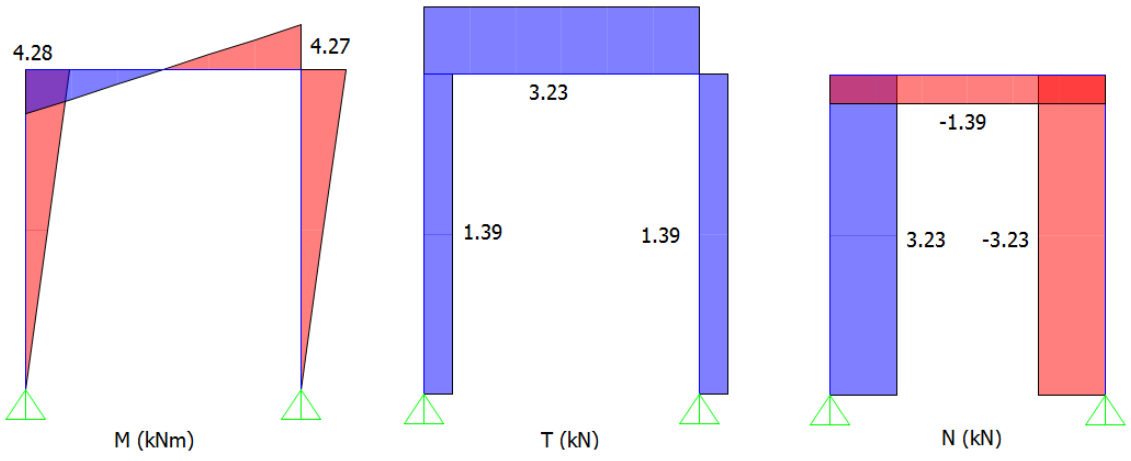

Figure 4.25. Internal actions diagrams for auxiliary structure 2

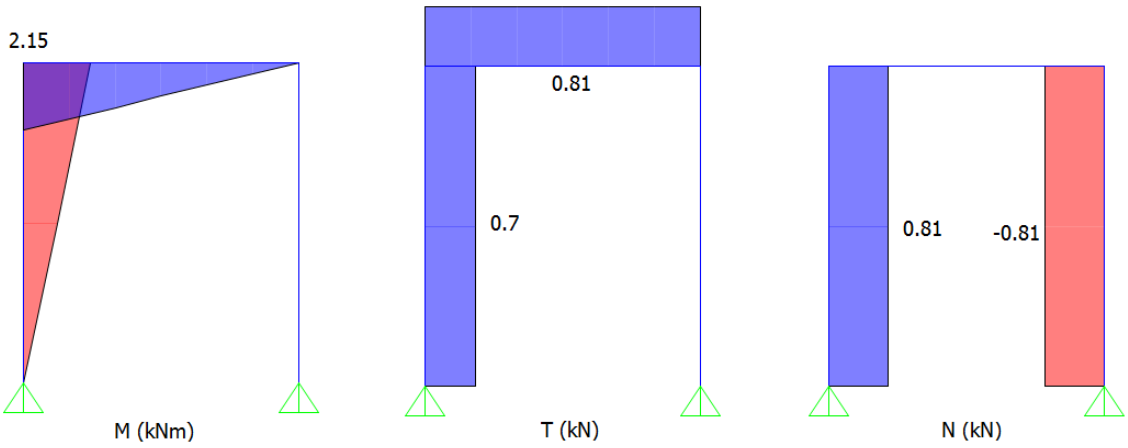

Figure 4.26. Internal actions diagrams for auxiliary structure 3

Finally, by means of the superposition principle, the internal action diagrams from *Figure 4.23*, *Figure 4.24*, *Figure 4.25* and *Figure 4.26* can be simply added to obtain the final diagram on the frame, under a total load of 59.43 kN, as depicted in *Figure 4.27*

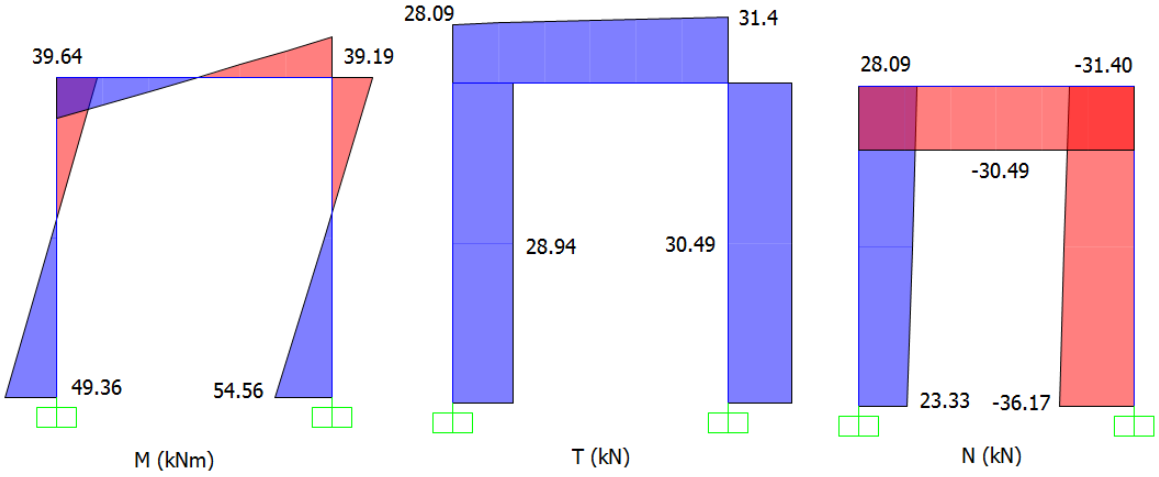

Figure 4.27. Internal actions diagrams for frame at maximum load (59.43 kN) applying super-position principle

Finally, the corresponding horizontal displacements of the structure were computed, immediately before the formation of plastic hinges on columns and beams. The values are depicted in Table 4-4.

Load [kN]	Displacement [mm]
52.69	7.29
55.95	8.04
58.73	9.73
59.43	10.94

Table 4-4. Load-displacement points of frame structure just before activation of plastic hinges

4.4.1.2 Infilled frame

Similarly, an elastic analysis was carried out on the same frame structure, with the addition of a compression strut, as depicted in *Figure 4.22* (a). Initially, a compression strut width/length ratio of w/D = 0.25 was considered, as a first approximation, which was later checked and adjusted. This results in using a strut with dimensions 200 x 1127 mm. From Table 4-3, the relevant points of interest to be analyzed can be determined. Similar to the previous analysis, an incremental elastic analysis was performed. First, a 54.85 kN load was applied on the frame structure with compression strut, fixed at the bottom. Then, incremental loads were applied on the auxiliary models accordingly, in order to follow the plastic hinge activation sequence observed in *Figure 4.19*, similar to the analysis performed in section 4.4.1.1. Results can be seen in *Figure 4.28* - *Figure 4.33*.

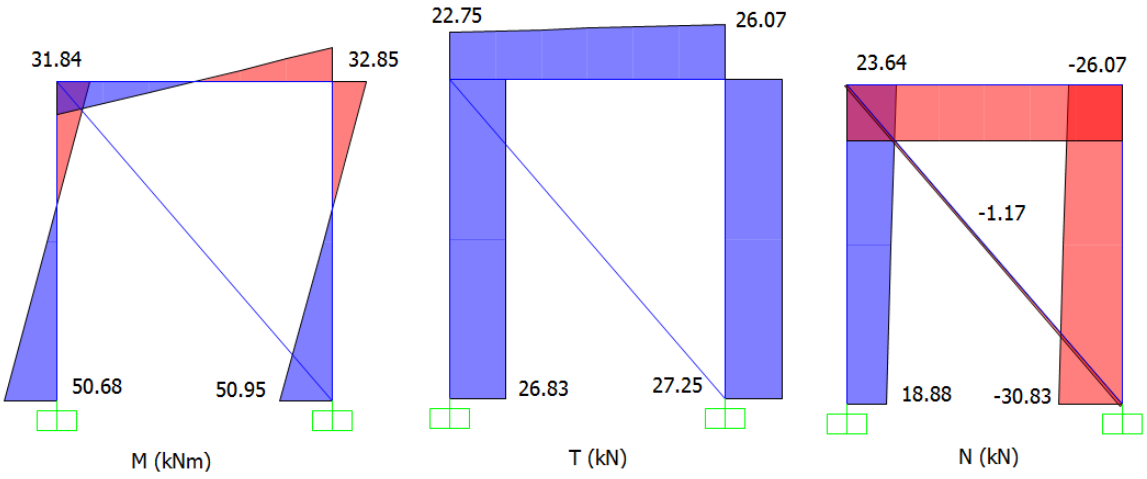

Figure 4.28. Internal actions diagrams for frame with strut under 54.85 kN lateral load

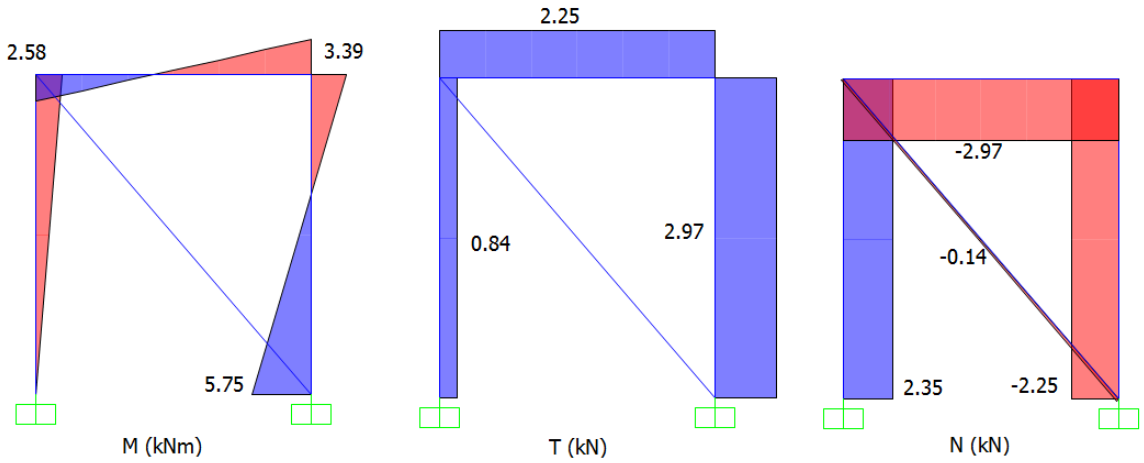

Figure 4.29. Internal actions diagrams for auxiliary structure 1

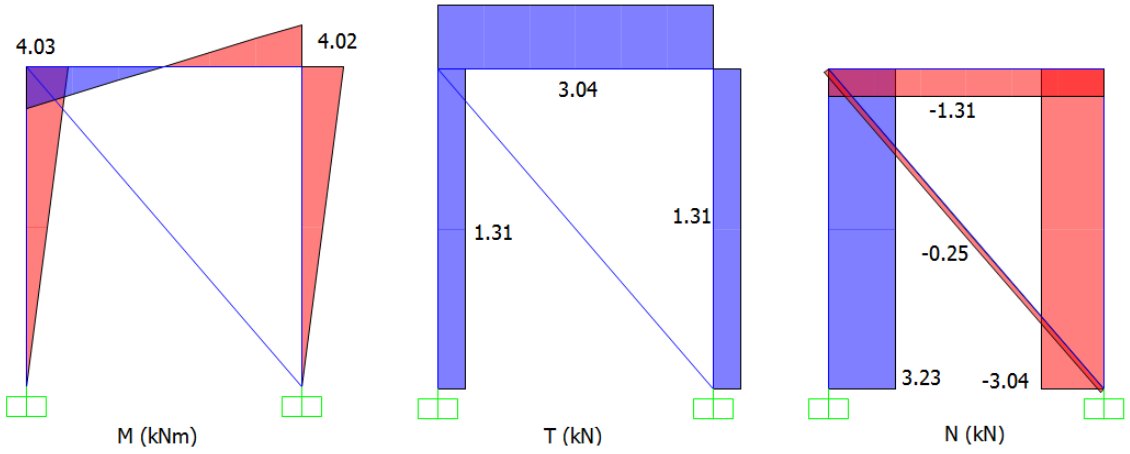

Figure 4.30. Internal actions diagrams for auxiliary structure 2

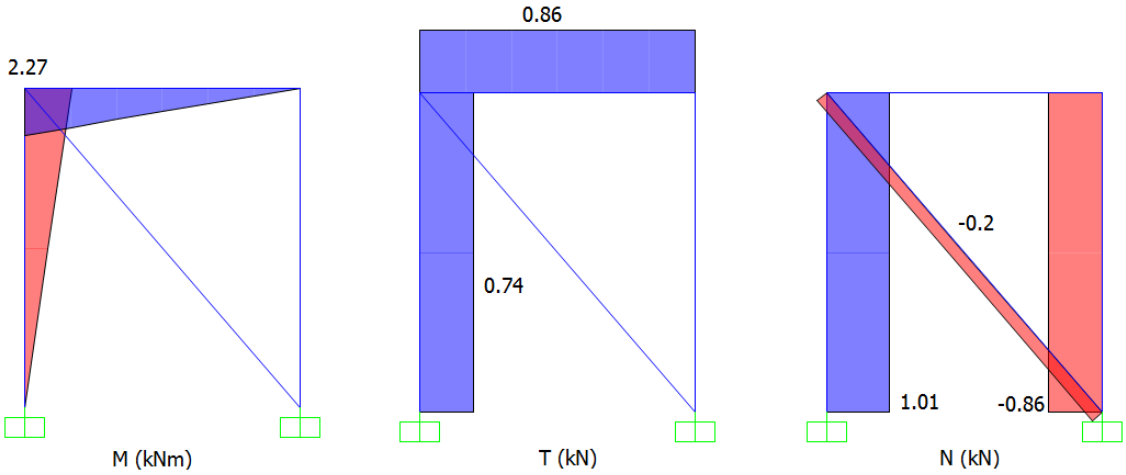

Figure 4.31. Internal actions diagrams for auxiliary structure 3

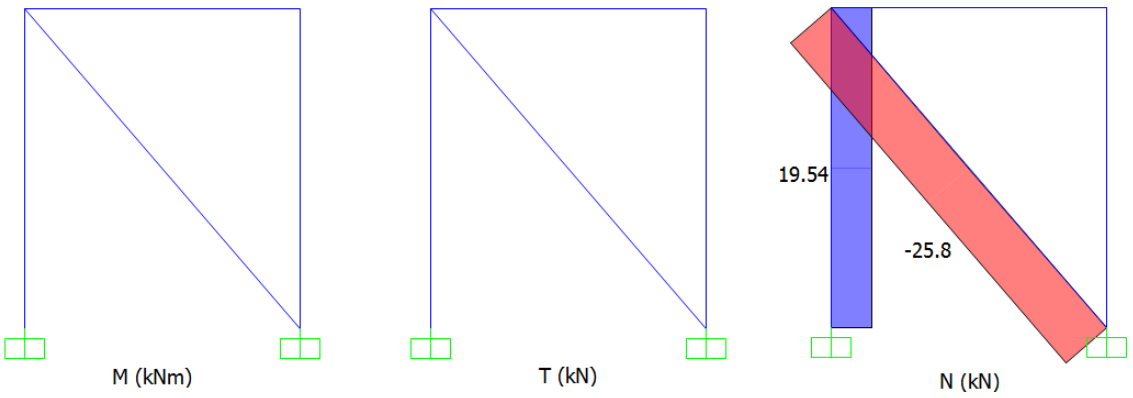

Figure 4.32. Internal actions diagrams for auxiliary structure 4

At this point, plastic hinges are activated at both, the base of the columns, and at the ends of the beams. From this point forward, the only component which is still able to carry additional load is the compression strut, through axial force. The strut carries an additional 16.84 kN before the failure of the first plastic hinge, reaching the maximum load of the capacity curve in *Figure 4.18*. After the sudden drop due to the failure of plastic hinges at the base of the columns, the strut continues to take even more load. As shown in Table 4-3, the infill is able to carry an additional 26.23 kN in total, after the frame structure has completely yielded. The resulting internal actions at this point are depicted in *Figure 4.33*.

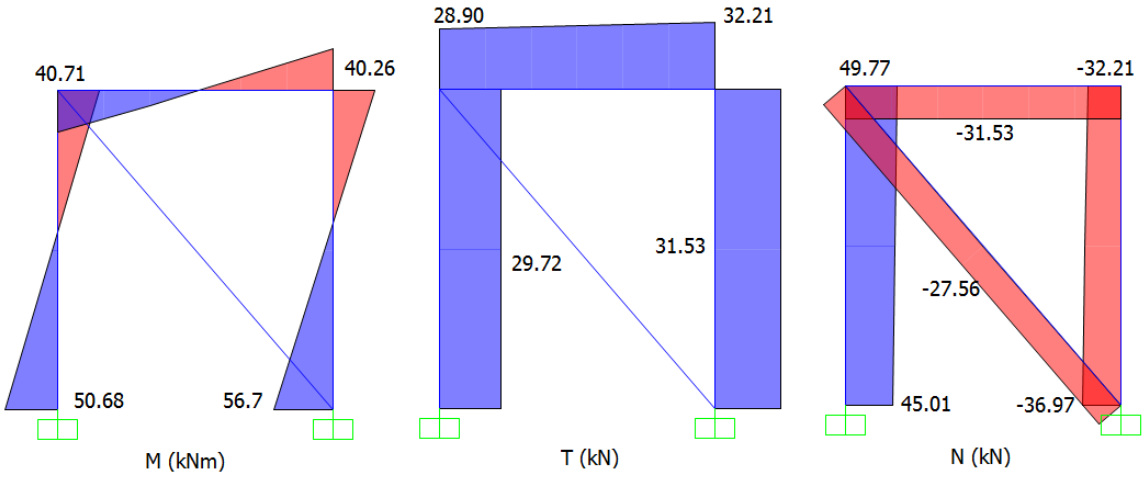

Figure 4.33. Internal actions diagrams for frame with strut at maximum load (79.24 kN) applying super-position principle [kN, m]

Finally, the corresponding horizontal displacements of the structure were computed, immediately before the formation of plastic hinges on columns and beams, and at the moment the structure reaches its maximum load capacity. The values are depicted in Table 4-5.

Load [kN]	Displacement [mm]
54.85	7.48
58.75	8.36
61.53	9.95
62.4	11.23
79.24	174.86

Table 4-5. Load-displacement points of infilled frame structure just before activation of plastic hinges and at maximum load capacity

4.4.2 Elastic analysis and results

Two elastic models were carried out, in parallel, in order to quantify the influence of adding the compression strut, and to compare the results of a simple elastic approach to the pushover analysis from section 4.3. In order to model the post-elastic behavior of the frame (after activation of the first plastic hinge and before collapse), auxiliary models were used with idealized hinges at the sections where plastic hinges have been activated. The internal actions from these auxiliary models were then super imposed to the ones where the structure is still behaving elastically, to obtain the final internal actions (*Figure 4.27* and *Figure 4.33*). It's worth mentioning that, for the purpose of this analysis, the strut was considered weightless, in order to compare the results with the ones of the bare frame adequately.

From *Figure 4.28* - *Figure 4.32*, it is clear that the compressive strut, due to its very low elastic modulus (and hence low axial rigidity), has a negligible contribution on the structure's resisting mechanism against lateral force before activation of all four plastic hinges. It is not until the frame structure has completely yielded that the strut is really activated (*Figure 4.32*), and starts to take load. An additional analysis was performed, in which both, the bare frame and the frame with strut, were subjected to a 100 kN lateral load, during elastic phase, and at each activation of plastic hinge, in order to isolate and quantify the sole effect of adding the compression strut, at each stage. Internal actions at the sections of interest (see *Figure 4.34*) are reported in Table 4-6.

Section	Stage	BARE FRAME				FRAME WITH STRUT			
		M(x) [kN-m]	V(x) [kN]	N(x) [kN]	Top displacement [mm]	M(x) [kN-m]	V(x) [kN]	N(x) [kN]	Top displacement [mm]
A	No plastic hinges	94.2	50.11	45.14	13.83	92.89	49.41	46.12	13.64
B		59.9	50.11	45.14		59.06	49.41	46.12	
C		59.9	45.14	-49.89		59.06	44.5	-49.19	
D		59.71	45.14	-49.89		58.87	44.5	-49.19	
E		59.71	49.89	-45.14		58.87	49.19	-44.5	
F		93.69	49.89	-45.14		92.39	49.19	-44.5	
STRUT		-	-	-		-	-	-2.14	
A	With first plastic hinge	-	21.99	59.06	23.06	-	21.49	60.37	22.53
B		67.63	21.99	59.06		66.07	21.49	60.37	
C		67.63	59.06	-78.01		66.07	57.69	-76.21	
D		88.87	59.06	-78.01		86.82	57.69	-76.21	
E		88.87	78.01	-59.06		86.82	76.21	-57.69	
F		150.99	78.01	-59.06		147.52	76.21	-57.69	
STRUT		-	-	-		-	-	-3.53	
A	With first two plastic hinges	-	50.02	116.04	60.67	-	47.09	116.04	57.13
B		153.81	50.02	116.04		144.8	47.09	116.04	
C		153.81	116.04	-49.98		144.8	109.24	-47.05	
D		153.69	116.04	-49.98		144.69	109.24	-47.05	
E		153.69	49.98	-116.04		144.69	47.05	-109.24	
F		-	49.98	-116.04		-	47.05	-109.24	
STRUT		-	-	-		-	-	-8.97	
A	With three plastic hinges	-	100	116.04	173.58	-	84.86	116.04	147.33
B		307.5	100	116.04		260.93	84.86	116.04	
C		307.5	116.04	-		260.93	98.47	-	
D		-	116.04	-		-	98.47	-	
E		-	-	-116.04		-	-	-98.47	
F		-	-	-116.04		-	-	-98.47	
STRUT		-	-	-		-	-	-23.2	

Table 4-6. Internal actions on the bare frame and frame with strut, under 100 kN horizontal loading

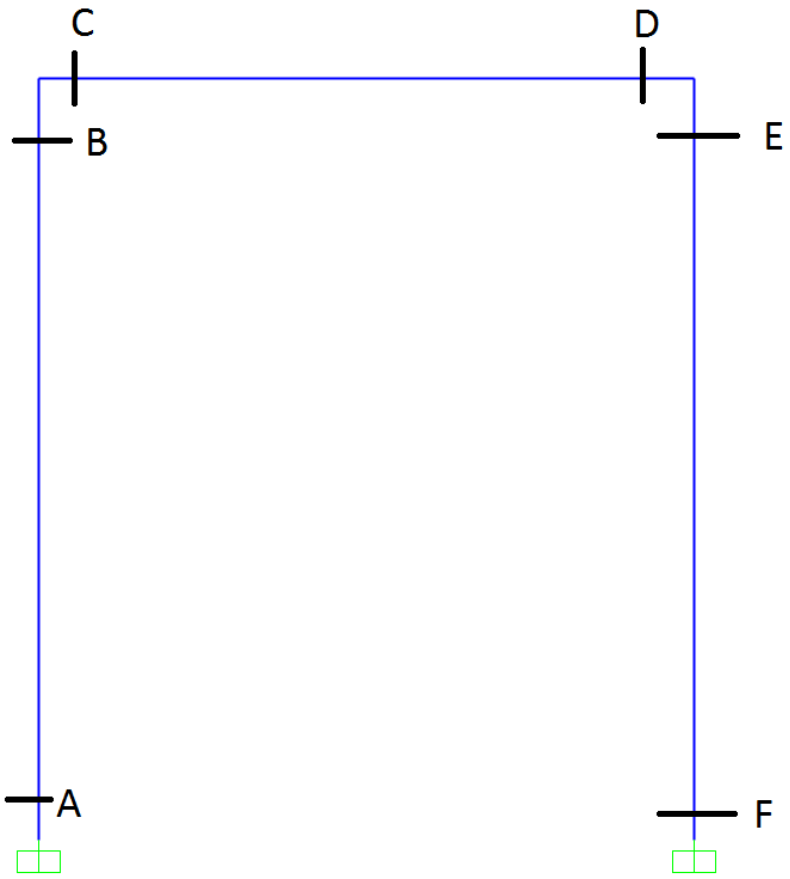

Figure 4.34. Sections of RC frame studied in order to quantify contribution of compression strut

Table 4-7 shows the error made by computing the internal actions and displacements on the bare frame, instead of the frame with the strut, assuming the values of the frame with the strut are the correct ones. As it can be observed, the error is quite negligible at the first three stages (6% difference). Finally, after the formation of the third plastic hinge, results are significantly different (more than 17%). In general, the internal actions on the bare frame are always slightly higher than the ones on the frame with strut. The results confirm once again that, due to the great difference in rigidities to lateral loading between the frame and the strut, the contribution of the strut is negligible before the RC frame has reached at least 3 plastic hinge activations. Due to the fact that the third and fourth plastic hinge yield at practically the same load, for practical purposes, the latter stage has no significant contribution on the response either.

Section	Load	ERROR			
		M(x)	V(x)	N(x)	Top displacement
A	No plastic hinges	1.41%	1.42%	-2.12%	1.39%
B		1.42%	1.42%	-2.12%	
C		1.42%	1.44%	1.42%	
D		1.43%	1.44%	1.42%	
E		1.43%	1.42%	1.44%	
F		1.41%	1.42%	1.44%	
STRUT		-	-	-	
A	With first plastic hinge	-	2.33%	-2.17%	2.35%
B		2.36%	2.33%	-2.17%	
C		2.36%	2.37%	2.36%	
D		2.36%	2.37%	2.36%	
E		2.36%	2.36%	2.37%	
F		2.35%	2.36%	2.37%	
STRUT		-	-	-	
A	With first two plastic hinges	-	6.22%	0.00%	6.20%
B		6.22%	6.22%	0.00%	
C		6.22%	6.22%	6.23%	
D		6.22%	6.22%	6.23%	
E		6.22%	6.23%	6.22%	
F		-	6.23%	6.22%	
STRUT		-	-	-	
A	With three plastic hinges	-	17.84%	0.00%	17.82%
B		17.85%	17.84%	0.00%	
C		17.85%	17.84%	-	
D		-	17.84%	-	
E		-	-	17.84%	
F		-	-	17.84%	
STRUT		-	-	-	

Table 4-7. Difference between internal actions on bare frame and frame with strut

4.5 SUMMARY AND ANALYSIS OF RESULTS

Two pushover analysis were carried out, one for the bare frame, and the other for the infilled frame, in sections 4.2 and 4.3 respectively. Section 4.4 focuses on an elastic analysis for two models separately, one of a bare frame, and one of a frame with a compression strut, which represents the infill contribution to the lateral load response. The purpose of the elastic analysis was to compare the results to the pushover analysis, in order

to predict if simplified tools are appropriate for the task of modeling polystyrene infilled frames.

By comparing the two pushover curves in *Figure 4.21* it can be observed how the initial stiffness is practically identical in both cases. This behavior suggests that the infill is not contributing to the lateral response of the structure in the initial (elastic) branch, since the infilled frame presents the same response as the one of the bare frame, except for a very slight gain of strength (4.76%). After the frame yielding (at about 10.6mm in the load-displacement curve), the bare frame pushover curve (red curve) presents a horizontal branch, since the frame cannot take any more load, while the infilled frame curve (blue curve) continues to take additional load. This means that the moment when the frame yields completely (4 plastic hinges have been activated), the infill begins to get loaded.

The fact that the infill presents a negligible contribution to the lateral load resistance before the frame achieves yielding is also confirmed by the elastic analysis performed in section 4.4.1.2, where the strut is practically unloaded before this point. Additionally, the influence of adding the strut was quantified for each stage of plastic hinge formation, and reported in Table 4-7. It can be noted that, similar to what was observed during the pushover analysis, before the activation of the four plastic hinges, the strut has a negligible contribution on the response to lateral loading.

Next, the load-displacement relationship was investigated and compared between the elastic approach and the pushover analysis. At every activation point of plastic hinges, displacements were computed for each respective load. An additional point was included before failure of the first plastic hinge in the case of the infilled frame. For this purpose, the displacement on the elastic model was constructed by the super position of several auxiliary models, in order to account for the plastic hinge formation at the base of columns and beam ends, as seen in section 4.4. The difference between both approaches was computed assuming the pushover analysis to be the correct one.

STRUCTURE	Load [kN]	Displacement [mm]		DIFFERENCE [%]
		ELASTIC ANALYSIS	PUSHOVER ANALYSIS	
BARE FRAME	52.69	7.29	7.28	0.14
	55.95	8.04	8.03	0.12
	58.73	9.73	9.68	0.52
	59.43	10.94	10.8	1.30
INFILLED FRAME	54.85	7.48	7.35	1.77
	58.75	8.36	8.18	2.20
	61.53	9.95	9.6	3.65
	62.4	11.23	10.65	5.45
	79.24	174.86	85.95	103.44

Table 4-8. Comparison of the load-displacement relation between elastic analysis and pushover analysis

Table 4-8 shows, in general, good agreement between the results of the pushover analysis and elastic approach of the bare frame, even after the activation of three plastic hinges. In the case on the infilled frame, there is also good agreement up until the formation of the third plastic hinge. After this point, and before reaching failure of the first plastic hinge, the results diverge greatly (more than 100%), which makes the elastic approach clearly unreliable after this point. Results can also be seen graphically in *Figure 4.35* and *Figure 4.36*. In general, the elastic analysis leads to greater displacements. The great difference between either analyses at the last stage is partly due to assumptions made during the pushover analysis, such as the plastic hinge length (due to the lumped plasticity approach). Also, the strut width plays an important role at this point, as the axial stiffness of the strut depends on it.

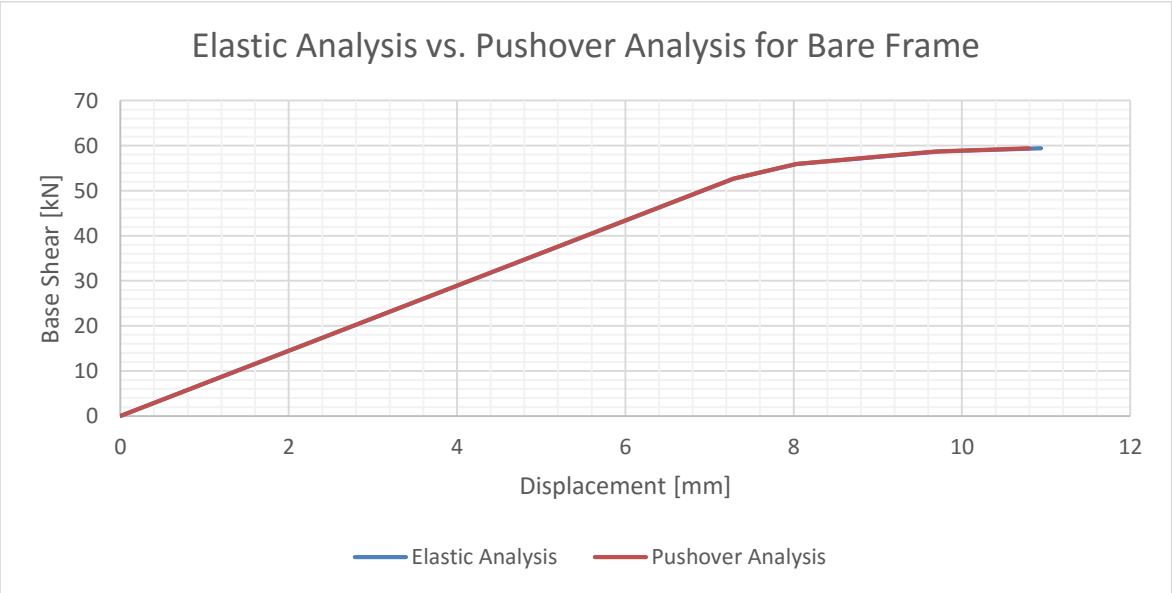

Figure 4.35. Load-displacement relationship of bare frame: Elastic analysis vs. Pushover analysis

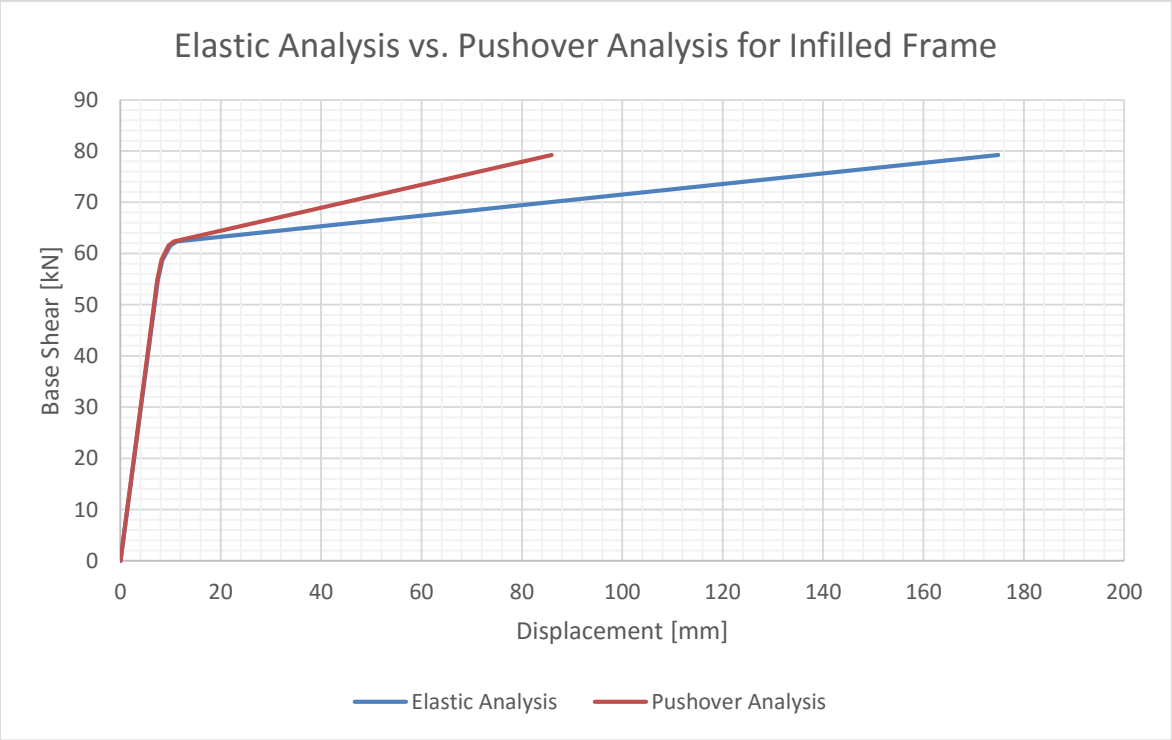

Figure 4.36. Load-displacement relationship of infilled frame: Elastic analysis vs. Pushover analysis

By analyzing the capacity curve in *Figure 4.18*, it can be observed that the plot follows a constant linear stiffness after the frame structure has yielded (after approximately a 10.65 mm displacement). If the hinge failures on the concrete frame were disregarded (plastic hinges with infinite deformation capacity for the RC frame) the curve would follow a straight line from the point where the concrete frame has yielded, up until failure of the plastic hinge of the infill. This is, actually, in line with the fact that the infill is the only component which is still able to carry load after this point, and is behaving elastically, as discussed previously.

By computing the slope of the load-displacement curve in *Figure 4.18*, the elastic stiffness was obtained, as shown in (4-1), which is constant throughout all the "growing" or "loading" segments of the plot after frame has yielded.

$$K = \frac{\Delta V}{\Delta x} = 224\ N/mm \qquad \textbf{(4-1)}$$

Let us now consider the structure in *Figure 4.22* (a). As mentioned before, after the frame structure has yielded, the only element still able to carry load is the compression strut. As it is behaving elastically, the strut, whose load carrying mechanism consists of axial loading only, has the well know elastic stiffness for an element under axial loading:

$$K = \frac{\mathrm{EA}}{\mathrm{L}} \qquad \textbf{(4-2)}$$

Where:

- E = Elastic Modulus of Polystyrene: 4.35 MPa
- A = Cross section area of the strut [mm^2]
- L = Length of the strut: 4059 mm

The only unknown quantity is the cross section area of the strut. By fixing the out of plane thickness equal to 200mm (equal to the thickness of the infill), the only unknown remains the strut width (w). The problem has one equation and one unknown. By equating expressions (4-2) and (4-1), the value for the strut width is determined.

$$K = \frac{\mathrm{EA}}{\mathrm{L}} = \frac{(4.35\ MPa) \cdot (200\ mm) \cdot w}{4509\ mm} = 224 \frac{N}{mm} \quad \textbf{(4-3)}$$

$$w = 1161\ mm \quad \textbf{(4-4)}$$

$$^{w}/_{D} = {}^{1161}/_{4509} = 0.257 \quad \textbf{(4-5)}$$

According to the previous expressions, in order to analyze the structure with an equivalent compression strut, a 200x1161 mm strut should be used. The strut width ratio, in this case, corresponds to w/D = 0.26 (practically identical to the w/D = 0.25 used during the elastic analysis in section 4.4), which is inside the common value range used for masonry infilled frames, as discussed in Chapter 2.

5 CONCLUSIONS AND RECCOMENDATIONS

Previous experimental campaigns with masonry infilled frames have shown that from the five failure mechanisms described in section 2.3.4, failure mechanism 5 is expected to take place for weak infills. Polystyrene is a material which is much weaker than masonry, and therefore, for the purpose of this research it is treated as a "weak masonry infill", in order to use the analytical procedure described in this section, which has been developed for masonry infilled frames. As expected, from Table 3-3 it can be observed that failure mechanism 5 is governing the lateral resistance of the infilled frame, according to the simplified analytical method. However, Failure mechanism 3 delivers a very similar lateral load capacity to the one suggested by failure mechanism 5, and could eventually govern the lateral load capacity. Also, the failure mode could be a combination between the latter two.

Failure mechanisms 1 and 2 seem to be much larger in magnitude than the other 3. For this reason, the infilled frame is not expected to fail in this nature (a crack crossing through the infill, in a horizontal or inclined way). Instead, plastic hinges are expected to form at column and/or beam ends. This failure mode is in agreement with the pushover analysis performed in section 4.3, as depicted in *Figure 4.19* and *Figure 4.20*.

A sensitivity analysis was performed in order to quantify the influence of a possible variation of the mechanical properties of the materials. From Table 3-5 it is clear to see that, except for high values of the residual friction coefficient, or very low values of polystyrene compressive strength, failure mechanism 5 is always governing the global lateral resistance, according to the analytical method studied in chapter 3. As a general statement, the only parameter investigated that affects V_{u5} is the residual friction coefficient, and the only parameter that affects V_{u3} is polystyrene compressive strength. For this reason, these two parameters (μ_r and f_{pk}) are the only mechanical properties which could have some influence on the lateral load resistance of the infilled frame, according to the simplified analytical method presented in chapter 3.

Variation of the Elastic modulus of polystyrene affects only V_{u4}. However, in the range of interest, it has no effect on the final value of this failure mechanism. V_{u4} does not govern the global lateral load resistance of the structure under any of the cases studied, and therefore, a variation of E_p in the range of interest is not expected to influence the lateral load resistance computed via the analytical method studied in chapter 3, according to the sensitivity analysis performed in section 3.7.

A variation of the compressive strut width ratio results in a linear variation of the crushing load, as depicted in *Figure 3.14*. According to the analysis performed in section 4.4, a reasonable value to be assumed for this purpose could be in the vicinity of $^{w}/_{D} = 0.25$, which is a very similar value to those used for masonry infills.

The pushover curves in *Figure 4.21* suggest that the infill has a negligible participation in the lateral load response of the structure before the frame reaches yielding (activation of 4 plastic hinges). This is also confirmed by the results obtained in Table 4-7, where an elastic analysis of the bare frame vs. the frame with strut was performed, for every stage of plastic hinge yielding. Although the response, according to Table 4-7, starts to diverge between the activation of the third and fourth plastic hinge, these occur at almost identical loading, and therefore, it's influence is negligible. For this reason, no significant contribution of the polystyrene infill is expected to occur before yielding of the frame structure.

By comparing the capacity curves in *Figure 4.21*, one can observe how the ductility resources in both cases are quite similar. The values for ductility of the bare frame and the infilled frame are 16.36 and 16.91, respectively, according to Table 4-1 and Table 4-3, which represents a gain of about 3% in the case of the infilled frame. Although this slight increase in ductility is not considered to be significant, there is, however, a considerable 33% increase of strength (from 59.43 kN to 79.24 kN) when adding the infill. For this reason, the use of the bare frame model with added mass could be used, without significant error, during the elastic behavior of the structure. For most practical applications, it is desirable to remain within the elastic response of the structure, and therefore, it could be conceived as just the bare frame, either using an advanced pushover analysis, or a simple elastic analysis, which delivers very similar results.

After analyzing the post elastic behavior of the structure in *Figure 4.18*, the constant stiffness was computed, which corresponds to the contribution of the infill in the response to lateral loading. The stiffness was then used in order to determine the equivalent strut width to be used in a simple elastic analysis, which resulted in using $^{w}/_{D} = 0.257$. This value is practically identical to the assumed one $\left(^{w}/_{D} = 0.25\right)$, which is a typical value used or masonry infilled frames.

When comparing results obtained from chapter 3 (simple analytical method), to the ones obtained in chapter 4 (finite element analysis), some remarks must be made. First, as expected, the simplified approach seems to deliver more conservative results for the lateral load capacity than the more refined finite element approach. The capacity of the infilled

frame, according to the simplified analytical method, delivers an 18% increase of strength with respect to the bare frame, instead of the 33% increase predicted by the pushover analysis. Also, the failure modes predicted by the analytical method (V_{u3} or V_{u5}) are in partial agreement with the one predicted by the finite element method. Both of the latter ones predict a failure mode composed by a flexural contribution of the frame, with plastic hinge formations, and then either crushing of the infill along the contact length, or residual shear resistance of the fractured infill. However, the simplified method predicts plastic hinge formation only in columns, and not in beams, as opposed to the finite element approach.

Similar analysis should be carried out with variation of the overall frame dimensions, cross section geometry and reinforcement, and vertical axial loading, which is out of the scope of this research. By performing more similar analysis, a significant database can be analyzed in order to obtain statistically significant results for design, along with the experimental campaigns.

Laboratory tests are recommended to be carried out, in order to determine the mechanical properties of the materials used for future investigations (concrete, polystyrene, reinforcing steel, etc.) Due to the lack of data, common values found in the literature were adopted, which could have an influence on the results (specially friction coefficients and compressive strength). It is worth mentioning also that the values found in the literature correspond to the characteristic values, which are a lot more conservative than the mean values of mechanical properties, and therefore, experimental failure loads are expected to be greater than the ones computed with characteristic values for mechanical properties.

Following the results obtained in this research project, an experimental campaign will be carried out in order to complement and verify what has been discussed, on an infilled frame with the same geometric and mechanical properties as the one here analyzed. The results obtained from the experimental campaign should be properly compared with the ones obtained during this research, in order to properly validate the numerical results. Special attention should be paid not only to the load-displacement relationship, but also to the expected failure mode vs. the actual failure mode observed during testing.

6 REFERENCES

Calvi, M., Bolognini, D. & Penna, A., 2004. *Seismic Performance of Masonry-Infilled RC Frames - Benefits of slight reinforcements,* Guimarães: SÍSMICA 2004 - 6º Congresso Nacional de Sismologia e Engenharia Sísmica.

Crisafulli, 1997. *Seismic Behaviour of Reinforced Concrete Structures with Masonry Infills,* Christchurch: University of Cantebury.

Decanni, L., Mollaioli, F., Mura, A. & Saragoni, R., 2004. *SEISMIC PERFORMANCE OF MASONRY INFILLED R/C FRAMES,* Vancouver: 13th World Conference on Earthquake Engineering.

Fiorato, A. E., Sozen, M. A. & Gamble, W. L., 1970. *An Investigation of the Interaction of Reinforced Concrete Frames with Masonry Filler Walls,* Champaign: University of Illinois.

Holmes, M., 1961. Steel frames with brickwork and concrete infilling. In: *Proceedings of the Institution of Civil Engineers.* UK: Thomas Telford, pp. 473-478.

Kakaletsis & Karayannis, 2008. Influence of Masonry Strength and Openings on Infilled RC Frames Under Cycling Loading. *Journal of Earthquake Engineering,* 12(2), pp. 197-218.

Liuaw, T. C. & Kwan, K. H., 1985. Unified Plastic Analysis for Infilled Frames. *Journal of Structural Engineering,* 111(7), pp. 1427-1448.

Mehrabi, A. B., Shing, B. P., Schuller, M. P. & Noland, J. L., 1994. *Performance of Masonry-Infilled R/C Frames Under In-Plane Lateral Loads,* Boulder: University Colorado.

Mehrabi, A. B. & Shing, P. B., 2003. Seismic Analysis of Masonry-Infilled Reinforced Concrete Frames. *TMS Journal,* Volume 21, pp. 81-94.

Moretti, M. L., Papatheocharis, T. & Perdikaris, P. C., 2014. Design of Reinforced Concrete Infilled Frames. *Journal of Structural Engineering,* September, 140(9), p. 10.

Stafford, S. B., 1962. Lateral Stiffness of Infilled Frames. *Journal of Structural Division,* 88(ST6), pp. 183-199.

Valiasis, T. & Stylianidis, K., 1989. Masonry Infilled R/C Frames under Horizontal Loading - Experimental Results. *European Earthquake Engineering,* 3(3), pp. 10-20.